UNIVERSITÀ
DEGLI STUDI
DI PADOVA

UNIVERSITY OF PADOVA

Department of Pharmaceutical and Pharmacological Sciences

Ph.D. COURSE IN MOLECULAR SCIENCES

PHARMACEUTICAL SCIENCES CURRICULUM

XXXI CYCLE

BIOCOMPATIBLE MODULAR NANOVECTORS FOR ANTICANCER DRUG DELIVERY AND CONTROLLED RELEASE

Coordinator: Chiar.mo Prof. Leonard Prins

Supervisor: Chiar.mo Prof. Stefano Salmaso

Ph.D. student: Silvia Brunato

UNIVERSITÀ
DEGLI STUDI
DI PADOVA

UNIVERSITA' DEGLI STUDI DI PADOVA

Dipartimento di Scienze del Farmaco

CORSO DI DOTTORATO DI RICERCA IN SCIENZE MOLECOLARI

INDIRIZZO SCIENZE FARMACEUTICHE

CICLO XXXI

NANOVETTORI MODULARI BIOCOMPATIBILI PER IL TRASPORTO E RILASCIO CONTROLLATO DI FARMACI ANTITUMORALI

Coordinator: Chiar.mo Prof. Leonard Prins

Supervisor: Chiar.mo Prof. Stefano Salmaso

Dottoranda: Silvia Brunato

Alla mia famiglia.

“Happiness is real only when shared”

Christopher McCandless

TABLE OF CONTENTS

1. ABBREVIATIONS

4T1	Murine mammary carcinoma cell line
Ar	Argon
$CDCl_3$	Deuterochloroform
$CHCl_3$	Chloroform
CH_2Cl_2	Dichloromethane
CMC	Critical Micellar Concentration
CO_2	Carbon Dioxide
CT26	Murine colorectal carcinoma
Đ	Polydispersion Index
DDs	Drug Delivery System
DLS	Dynamic Light Scattering
DMF	Dimethyl formamide
DMSO	Dimethyl sulfoxide
DMSO-d_6	Hexadeuterodimethylsulfoxide
Doxo	Doxorubicin
Doxo HCl	Doxorubicin hydrochloride
DoxoMC-E_6L_{10}	$mPEG_{5kDa}$-*b*-(γ-hyd[Doxo]-Glu_6-*r*-Leu_{10}) micelles
DoxoMC-E_8L_8	$mPEG_{5kDa}$-*b*-(γ-hyd[Doxo]-Glu_8-*r*-Leu_8) micelles
DoxoMC-E_{16}	$mPEG_{5kDa}$-*b*-(γ-hyd[Doxo]-Glu_{16}) micelles
DPAP	2,2'-dimethoxy-2-phenylacetophenone
D_2O	Deuterium oxide
EMT	Epidermal-to-Mesenchymal Transition program
EPR	Enhanced permeability and retention
EtOAc	Ethyl Acetate
Et_2O	Diethyl ether
FBS	Fetal bovine serum
FDA	Food and Drug Administration
Glu	Glutamic Acid
Glu-NCA	γ-benzyl-glutamic N-carboxy anhydride

GSH	Glutathione
HCl	Hydrochloric Acid
HER2	Human Epidermal Growth Factor receptor
HydGlu	γ-hydrazinamide glutamic acid
IC_{50}	Half maximal inhibitory concentration
IPA	Isopropyl alcohol
IT	Intratumoral Injection
IV	Intravenous Injection
LAMP-1	Lysosomal-associated membrane protein 1
LCST	Low Critical Solution Temperature
Leu	Leucine
Leu-NCA	Leucine N-carboxyanhydride
MALDI	Matrix-Assisted Laser Desorption Ionization
MC-E_4L_{12}	$mPEG_{5kDa}$-*b*-(γ-hyd-Glu_4-*r*-Leu_{12}) micelles
MC-E_6L_{10}	$mPEG_{5kDa}$-*b*-(γ-hyd-Glu_6-*r*-Leu_{10}) micelles
MC-E_8L_8	$mPEG_{5kDa}$-*b*-(γ-hyd-Glu_8-*r*-Leu_8) micelles
MDR	Multidrug Resistance
mPEG	Methoxy-Polyethylene glycol
$mPEG_{5kDa}$	Methoxy-Polyethylene $glycol_{5kDa}$
$mPEG_{5kDa}$-NH_2	$mPEG_{5kDa}$-cysteamine
MeOH	Methanol
MTT	3-(4,5-dimethylthiazol-2-yl)-2,5-diphenyltetrazolium bromide
MW	Molecular weight
MWCO	Molecular weight cut-off
M_n	Number Average Molecular Weight
NCA	N-carboxy-anhydride
PB	Phosphate buffer
PBS	Phosphate buffer saline
PCL	Poly(caprolactone)
PDI	Polydispersity index
PEG	Polyethylene glycol
PEO	Poly(ethylene oxide)
PFA	Paraformaldehyde
PGA	Poly(glycolic acid)

PLA	Poly(lactic acid)
PLGA	Poly(lactic-*co*-glycolic acid)
PPMA	Poly(methyl methacrylate)
PPO	Poly(propylene oxide)
RES	Reticuloendothelial system
ROP	Ring opening polymerization
ROS	Reactive Oxygen Species
RPM	Revolutions per minute
RPMI 1640	Roswell Park Memorial Institute Medium 1640 culture medium
RT	Room Temperature
SLS	Static Light Scattering
TEA	Triethylamine
TEM	Transmission Electron Microscopy
TFA	Trifluoroacetic acid
TGF-β	Transforming Growth Factor-β
THF	Tetrahydrofuran
TLC	Thin layer chromatography
TNBS	2,4,6-trinitrobenzenesulfonic acid
US	Ultrasound
UV	Ultraviolet

2. ABSTRACT

The research project of this PhD thesis was focused on the design and development of innovative "smart" nanosystems for a controlled anticancer drug delivery.
Smart drug delivery systems have emerged as a strategy to achieve enhanced site-specific drug accumulation and control release within the desired tissue, thus offering the opportunity to reduce systemic side effects caused by an unspecific drug biodistribution.

Among the several colloidal systems available, polymeric micelles formed by amphiphilic polyaminoacidic block copolymers are gaining relevance for therapeutic application as they offer significant advantages such as improved water solubility of lipophilic drugs, enhanced drug bioavailability, high biocompatibility and versatility.
For this purpose, a library of amphiphilic di-block copolymers able to self-assemble in colloidal systems for the intracellular delivery of doxorubicin was designed. The copolymer composition was engineered in order to include aminoacids with peculiar function yielding a smart material. The di-block copolymer backbone was composed by a hydrophilic block of polyethylene glycol and an amino acid-based block including different ratios of γ-hydrazinamide-glutamic acid (hydGlu) and leucine (Leu).
In particular, hydGlu was selected for the conjugation of doxorubicin through a pH-cleavable hydrazone bond endowing the system a controlled drug release in the intracellular acidic compartments upon cancer cell uptake. Leucine was used as a spacer between the glutamic units to minimize the steric hindrance of the conjugated anticancer drug and promote the polymer self-assembly, in virtue of its hydrophobicity. Doxorubicin was selected for a double purpose: firstly, for its well-known anticancer activity and, secondly, together with Leucine, to to actively contribute to the block copolymer self-assembling process.

The library of amphiphilic di-block copolymers was synthetized through Ring Opening Polymerization using a polyethylene glycol bearing a terminal reactive amino group ($mPEG_{5kDa}$-NH_2) as macroinitiator and *N*-carboxy anhydride aminoacids as monomers. The library was characterized by an increased leucine content with respect to glutamic acid in order to understand the effect of different aminoacid ratios in terms of doxorubicin conjugation efficiency and particle stability and select the best candidate for *in vitro* and *in vivo* studies.

At first, $mPEG_{5kDa}$-OH was converted in $mPEG_{5kDa}$-NH_2 through a radical addiction of cysteamine. *N*-carboxy Anhydride analogues (NCA) of γ-benzyl glutamic acid and leucine were synthetized by reaction with triphosgene. Consequently, $mPEG_{5kDa}$-NH_2 was used as macroinitiator for the polymerization of NCA monomers, yielding four $mPEG_{5kDa}$-*b*-(γ-benzyl-Glu_n-*r*-Leu_m) polymers with γ-benzyl glutamic acid:leucine ratios of 16:0, 8:8, 6:10, 4:12. Afterwards, the γ-benzyl ester protecting group of glutamic acid of the copolymers library was removed by direct reaction with hydrazine hydrate, leading to the formation of γ-hydrazide glutamic acid moieties with a 99% conversion yield. This procedure provided four $mPEG_{5kDa}$-*b*-(γ-hyd-Glu_n-*r*-Leu_m) derivatives. Finally, the conjugation of doxorubicin through the pH-sensitive hydrazone bond formation was performed for the four di-block copolymers, obtaining a high drug conjugation yield for the di-block copolymers bearing leucine as a spacer along the polyaminoacidic block.

The self-assembling of the drug conjugated copolymers was achieved by a dialysis process, and the generated colloidal systems were characterized by dynamic light scattering, zeta potential, transmission electron microscopy and critical micelle concentration. The analyses revealed that the doxorubicin-conjugated copolymers assembled in spherical shape and neutral charged systems with a size of nearly 20 nm, highlighting the important role of doxorubicin and leucine as driving forces for the hydrophobic core formation. Furthermore, these analyses confirmed that the nanovectors possessed suitable features for the selective tumor accumulation exploiting the EPR effect. The low CMC values obtained for the colloidal systems would provide a remarkable stability and prevent the dissociation of the nanosystems upon injection in the bloodstream. Doxorubicin conjugation increased the polyaminoacidic block hydrophobicity leading to a stronger micelles cohesion and a reduction of copolymers concentration required for the self-assembling process.

In virtue of the pH-cleavable hydrazone bond between doxorubicin and the copolymers backbone, the nanosystems were expected to selectively release the drug at acidic condition. In fact, the nanocarriers showed a faster release at pH 5.5 with respect to the blood mimicking condition, leading to a sustained and controlled release of doxorubicin from the nanocarriers in acidic intracellular compartments while preventing drug dissociation in the bloodstream.

The cytotoxicity of the colloidal formulations was tested on two cancer cell lines, CT26 murine colorectal carcinoma and 4T1 murine mammary carcinoma. The doxorubicin conjugated colloidal formulations showed a dose dependent cytotoxicity on both cell lines, revealing IC_{50} values comparable with the ones obtained by incubation with the free doxorubicin.

Furthermore, confocal analyses on CT26 cell lines were performed to assess the intracellular fate of the drug loaded formulations, and the results confirmed the lysosomal entrapment and the selective intracellular release of doxorubicin.

Based on these evidence, the antitumor efficacy of the system was evaluated *in vivo* on CT26 and 4T1 subcutaneous tumor model. The studies were performed evaluating both the intratumoral and the intravenous administration routes. The drug-conjugated formulation bearing the 6:10 glutamate:leucine ratio was selected for this purpose since it was the most performing in terms of drug release and cytotoxic activity.

When administered *in vivo* to CT26 and 4T1 tumor bearing mice, the drug loaded nanovectors displayed an excellent safety profile and efficient tumor volume reduction activity, leading to prolonged survival rates of the animals.

3. RIASSUNTO

Il presente progetto di ricerca si è focalizzato sulla progettazione e lo sviluppo di un nanosistema innovativo ed intelligente per il rilascio direzionato e controllato di farmaci antitumorali. In quest'ottica, i nanosistemi "*smart"* per il direzionamento di farmaci possono rivestire un ruolo fondamentale grazie al loro accumulo sito-specifico ed il rilascio controllato di molecole attive, offrendo così la possibilità di ridurre gli effetti collaterali causati da una biodistribuzione incontrollata del farmaco e di migliorare la qualità di vita del paziente.

Tra i vari sistemi colloidali disponibili in campo farmaceutico, le micelle polimeriche formate da copolimeri anfifilici poliaminoacidici offrono peculiari vantaggi come un aumento della solubilità di farmaci lipofili in acqua, una maggiore biodisponibilità, un'elevata biocompatibilità e versatilità.

A tale scopo è stata progettata una libreria di copolimeri anfifilici per il *delivery* intracellulare di Doxorubicina (Doxo) in grado di auto-assemblarsi in sistemi colloidali. Il *backbone* polimerico è composto da un blocco idrofilico di polietilenglicole (PEG) e un blocco poliaminoacidico costituito dal derivato γ-idrazinico dell'acido-glutammico (hydGlu) e da Leucina in diversi rapporti molari.
In particolare, hydGlu è stato selezionato per la coniugazione di Doxo attraverso la formazione di un legame idrazonico pH-sensibile, che permette un rilascio specifico del farmaco nei compartimenti acidi intracellulari. L'aminoacido Leucina è stato utilizzato non solo come *spacer* tra i monomeri di acido glutammico per minimizzare l'ingombro sterico del farmaco, ma anche per promuovere l'autoassemblaggio del polimero grazie al suo carattere idrofobico. Il farmaco Doxo è stato scelto per un duplice scopo: in primo luogo, per la sua ben nota attività antitumorale e, in secondo luogo, per promuovere il *self-assembling* del nanosistema.
La libreria di copolimeri anfifilici è stata sintetizzata attraverso la metodica di polimerizzazione "Ring Opening Polymerization" (ROP) usando un polietilenglicole funzionalizzato con un gruppo amminico terminale reattivo ($mPEG_{5kDa}$-NH_2) come macroiniziatore e amminoacidi in forma *N*- carbossi anidridica (NCA) come monomeri.

Inizialmente, $mPEG_{5kDa}$-OH è stato convertito in $mPEG_{5kDa}$-NH_2 attraverso l'addizione radicalica di cisteamina. Gli analoghi NCA degli aminoacidi γ-benzil-glutammico e Leucina

sono stati sintetizzati mediante reazione con trifosgene. Successivamente, $mPEG_{5kDa}$-NH_2 è stato utilizzato come macroiniziatore per la reazione di polimerizzazione dei monomeri NCA, portando alla sintesi di quattro polimeri $mPEG_{5kDa}$-*b*- (γ-benzil-Glu_n-*r*-Leu_m) con rapporti molari di acido γ-benzil-glutammico:Leucina di 16: 0, 8: 8, 6:10, 4:12. Successivamente, il gruppo protettore γ-benzil estereo dell'acido glutammico è stato rimosso per reazione diretta con idrazina idrata, portando alla formazione del derivato γ-idrazidico dell'acido glutammico con una resa di conversione del 99%. Pertanto, l'intera libreria di copolimeri è stata convertita nei derivati γ-idrazidici $mPEG_{5kDa}$-*b*- (γ-hyd-Glu_n-*r*-Leu_m). Infine, Doxo è stata coniugata al *backbone* polimerico attraverso la formazione del legame idrazonico pH-sensibile, ottenendo una elevata resa di coniugazione del farmaco per i copolimeri funzionalizzati con Leucina nel blocco poliaminoacidico.

I sistemi colloidali ottenuti mediante dialisi sono stati caratterizzati attraverso DLS; TEM, Potenziale Zeta, e determinazione della concentrazione micellare critica (CMC). Le analisi hanno dimostrato che i polimeri coniugati con Doxo assemblano assumendo una forma sferica con dimensione di circa 20 nm, caratteristiche ottimali per l'accumulo selettivo nel tessuto tumorale sfruttando l'effetto EPR, ed evidenziando l'importante ruolo di Doxo e Leucina nel promuovere la formazione del *core* idrofobico. La bassa concentrazione di CMC ottenuta per i sistemi colloidali può essere indice di una notevole stabilità del sistema e impedire la loro dissociazione nel circolo sanguigno. La coniugazione di Doxo ha apportato un aumento di idrofobicità del blocco poliaminoacidico determinando una maggiore coesione delle micelle e una riduzione della concentrazione di polimero richiesta per il s*elf-assembling*.

I sistemi colloidali hanno rilasciato selettivamente il farmaco in ambiente acido, mostrando un l'idrosili del legame idrazonico più rapida a pH 5.5 rispetto alle condizioni fisiologiche. Questo si traduce in un rilascio controllato e selettivo di Doxo in compartimenti intracellulari acidi, evitando la dissociazione farmacologica nel sangue.

La citotossicità delle formulazioni colloidali è stata testata sulle linee cellulari tumorali murine CT26 e 4T1, rispettivamente carcinoma del colon-retto e carcinoma mammario. Le formulazioni colloidali hanno riportato una citotossicità dose-dipendente su entrambe le linee cellulari, con valori di IC_{50} paragonabili a quelli ottenuti mediante incubazione con il solo farmaco di riferimento. Inoltre, sono state eseguite analisi di microscopia confocale sulla linea cellulare CT26 per valutare il destino intracellulare del sistema micellare, confermando l'accumulo lisosomiale e il rilascio selettivo intracellulare di Doxo.

Sulla base di queste evidenze, l'efficacia antitumorale del sistema è stata valutata *in vivo* su modelli animali di tumore sottocutaneo. Gli studi sono stati condotti valutando sia la via di somministrazione intratumorale che quella endovenosa. La formulazione contenente il farmaco caratterizzata dal rapporto molare Glutammato:Leucina di 6:10 è stata selezionata per questo scopo poiché si è rivelata la più performante in termini di rilascio di farmaco ed attività citotossica. Gli studi *in vivo* hanno confermato l'efficienza del sistema micellare in termini di riduzione del volume della massa tumorale, un prolungamento della sopravvivenza degli animali trattati e una tossicità trascurabile sia conseguente a trattamento locale che sistemico.

4. INTRODUCTION

Over the years, nanocarriers have been deeply investigated as potential drug delivery systems for the treatments of several diseases, mainly focusing on anticancer therapy[1] as they represent a promising strategy to overcome the conventional therapies limitations. The development process of a new drug entity is expensive and time consuming and, although its potency, the therapeutic effect could be reduced by unfavourable pharmacokinetics, low aqueous solubility, poor biodistribution, untimely drug degradation and lack of selectively for the desired tissue. Accordingly, new drug administration technologies are needed in the pharmaceutical area.

Drug Delivery Systems (DDs) are non-conventional systems suitable for a controlled and site specific drug release. Indeed, DDs overcome the limitations of poorly water soluble drugs or unfavourable pharmacokinetics profile, and they can also protect drugs affected by premature degradation before reaching the desired site. DDs offers advantages in term of providing for a site-selective and controlled drug release, reducing systemic side effects and improving patient compliance[2].

Nanosystems exhibit peculiar physical-chemical properties which significantly differ from the conventional bulk systems, hence the nanometric scale process has gained attention in many scientific fields, including chemistry to physics, to pharmaceutical and biomedical field. As a consequence, biomedical research focused on the design of nanocarriers as nanoparticles, micelles, liposomes, dendrimers, polymersomes and several others, to be employed for the treatment of severe diseases and in diagnosis field. Natural components or synthetic polymers can be used for the assembling of nanocarriers[3]. The nanocarriers physical-chemical properties are affected by the components features and the assembling strategies.

To pursue an *in vivo* application of these nano-sized drug carriers, key features as biocompatibility, shape, size, hydrophilic/hydrophobic balance, drug release profile, complement activation, bioelimination and other need to be deeply studied. Moreover, as requested for anticancer therapy, DDs need to protected drugs from the external environment and should possess a suitable size to allow the extravasation through the fenestrated tumour capillaries while avoiding the glomerular filtration in the kidneys, leading to a prolonged circulation time and an increased accumulation within the tumor mass. In addition, both tolerability and safety are ameliorated by the prolonged drug lifetime and the selective extravasation. A well-known example is Doxil®, the liposomal Doxorubicin formulation, which

showed a reduced cardiotoxicity with respect to the free drug[4], approved for the treatment of Kaposi's sarcoma in 1995 by the US Food and Drug Administration (FDA).

Although these advantages, the drug nanocarriers need to overcome different biological barriers and obstacles which could limit the site-specific accumulation, namely endosomal and lysosomal escape, pressure gradients, opsonisation process, phagocytes sequestration and drug efflux pumps[5].

As a consequence of their size, nanocarriers require internalization pathways not occurring for small molecules[6], such as endocytosis, and the consequent trafficking to lysosomes, where the drug can be released or degraded[7]. Many efforts are dedicated to design innovative multifunctional nanocarriers owing to limit the macrophages sequestration and to overcome the biological barriers. The use of targeting agents to chemically modify the surface of nanocarriers enables the selective distribution in tissues where the specific receptors for the ligand are overexpressed, improving the treatment therapeutic efficacy. Regrettably, the opsonisation process could occur, causing the formation of a protein corona that covers the nanocarrier surface and masks the targeting ligands, resulting in a decreased selective accumulation. Opsonisation is affected by nanocarrier size, hydrophobicity, surface charge and decoration. In particular, hydrophobic and charged particles are more frequently involved in the opsonisation process, compared to the hydrophilic and neutral ones[8–10]. In light of this observation, the surface decoration with hydrophilic polymers as polyethylene glycol (PEG) has become a widely used strategy to protect nanocarriers and limit the protein adsorption. Creating an elastic and hydrophilic corona on nanocarrier surface, PEG prevents the interactions with Opsonins[11] and the possible aggregation in plasma due to the high ionic content.

Over the years, several technologically advanced systems have been designed owing to a controlled drug release in terms of drug distribution and release. Stimuli-responsive nanocarriers represent a promising strategy to reach a targeted drug delivery, as drug release can be specifically triggered by different external stimuli, that could be chemical, physical or biological.

Nowadays, among the variety of drug delivery systems developed, polymeric micelles have emerged as versatile carriers thanks to their biocompatibility, the prolonged circulation time, the ability to specifically accumulate in solid tumors and the possibility to host several active molecules due to their unique core-shell structures (Figure 1.).

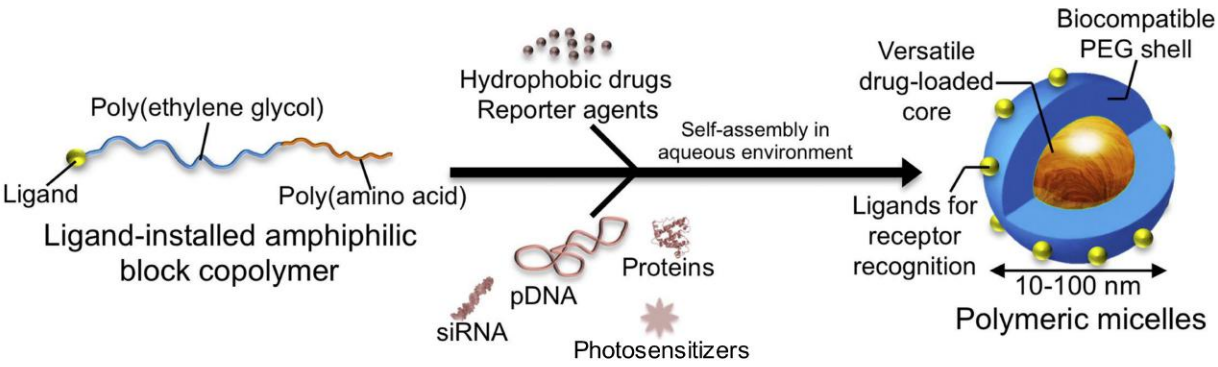

Figure 1. *Representation of self-assembled polymeric micelles from amphiphilic block copolymers, as versatile platform for incorporating different bioactive molecules*[12].

4.1. OVERVIEW ON CANCER

Cancer is currently one of the major causes of death worldwide, responsible for nearly one quarter of all death in UK and USA[13]. Approximately the 70% of cancer deaths occurred in low and middle developed countries, and a remarkably rise to19.3 million of new cases per year by 2025 is estimated[14].

4.1.1. Carcinogenesis and Cancer Hallmarks

Cancer is provoked by an uncontrolled cell replication, starting from a single cell or from a cells group. A malignant cancer acquires the ability to invade other tissues and organs, while a benign one is not invasive, remaining in the original site without compromising the functionality of the organs. Due to a fast growing of blood and lymphatic systems, cancer cells can easily spread from their original tissue to others, eluding the immune system recognition. Many types of cancers exist, and they are named by the site or the type of cells from which they originate, for instance lymphoma, sarcoma, melanoma. Physiologically, the cell replicative cycle is carefully controlled by a fine equilibrium of pro-proliferative and anti-proliferative biochemical mediators[15]. This balance ensures cell growth and replication when it is required, such as for tissue regeneration after injuries and during child growth, and contributes to the organs and tissues homeostasis maintenance. Moreover, cancer cells can further develop other peculiar tumor features as drug resistance and angiogenic ability.

DNA alterations or damages are frequently the cause of cancer genesis. Among time, DNA can accumulate alterations which are normally fixed by the DNA repair mechanisms, namely homologous recombination, nucleotide and base-excision repair, end joining, mismatch repair and telomere metabolism. These mechanisms lead to the proto-oncogenes activation and tumor-

suppressor genes inactivation[16]. In normal condition, proto-oncogenes encode proteins for mitosis activation, while, when mutated, they become oncogenes causing replication signals overexpression and excessive mitosis. By contrast, tumour-suppressor genes encode proteins able to block cell replication and when altered by genetic mutations, mitosis is not blocked, hence causing an uncontrolled proliferation.

DNA alteration causes are related with different environmental agents, such as ionizing radiations, ultraviolet (UV) sunlight component, several genotoxic chemicals, hormonal and viral agents.

In the carcinogenesis process four main phases can be identified:

- Initiation: Exogenous or endogenous factors provoke irreversible DNA damages, with a rapid progression.
- Promotion: DNA synthesis increases to support the rapid proliferation of mutated cells. Promotors do not change non-initiated cells and the induced changes are still reversible.
- Malignant conversion: benign cells are transformed into malignant ones, genetic and epigenetic changes occur leading to the invasion and metastasis phases.
- Progression: manifestation of malignant neoplasms followed by genetic alterations and karyotype change. Additionally, a continuous evolution of abnormalities at the chromosomal level occurs, providing the ability of invasion and anaplasia.

During its onset and progression, cancer gains different abilities enabling its growth and metastatic dissemination, named cancer hallmarks (Figure 2.):

- Inducing and sustaining proliferative signaling: the growth-promoting production and release in deregulated, and cancer cells even stimulate neighbour normal cells to supply growth factors. Specific receptors are overexpressed in tumor cells in order to become hyper-responsive to otherwise-limited quantity of growth factors. Furthermore, the alteration of some homeostasis regulation pathways can lead to an increase in proliferation signaling.
- Evading growth suppression and malignancy promotion: tumor cells could lack in tumor suppressors expression, as RB and p53 proteins, leading to a continuous proliferation. In addition, the contact inhibition mechanisms, which normally counterbalance the proliferative signals, are defective. Despite Transforming Growth Factor-β (TGF-β) is known as an anti-proliferating factor, recent studies highlighted its role in the epithelial-to-mesenchymal transition (EMT) program activation, promoting the high grade malignancy in cancer cells[17].

- Resisting Cell Death: cell death can occur with three different processes: apoptosis, autophagy and necrosis. Apoptotic cells shrink in small apoptotic corpses being endocytosed by neighbour cells. Several physiological stresses can activate the apoptotic mechanism, such as DNA damage, high levels of oncogene signals, etc., and apoptosis is finely regulated by the equilibrium between pro- and anti- apoptotic proteins, mainly from Bcl-2 family. High-grade tumour malignancy is often caused by an imbalance between the downregulation of pro-apoptotic agents and the overexpression of anti-apoptotic agents. Similar to apoptosis, autophagy operates in normal cells at the basal level, but this mechanism can be induced in the case of strong cellular stress. Either combined or not with apoptosis, the autophagy mechanism can prevent carcinogenesis. Nevertheless, in analogy with TGF-β, autophagy presents contrasting effects on tumor cells and their progression[18]. Necrosis consists in cells explosion and the consequent release of the cytoplasmic contents and proinflammatory signals in the surrounding environment, which attracts inflammatory cells from the immune systems leading to cancer promotion.
- Enabling replicative immortality: Senescence is a viable but irreversible state in which cells are unable to proliferate. Cells which circumvent this state encounter a crisis phase and die. Rarely, several cells could overcome this crisis statement, developing the ability of unlimited replication. The DNA polymerase Telomerase is responsible for telomeres synthesis, which are the shielding ends of chromosomes. Many researches revealed that the telomere shortening is a sort of clock device which regulate cell proliferation. In tumor cells, the telomerase activation process is related to cell death resistance and senescence, hence promoting the uncontrolled cell proliferation. On the contrary, a telomerase lack could generate tumor promoting mutations, whereas consequent telomerase activation could stabilize the mutant genome causing an unlimited proliferation[19].
- Inducing angiogenesis: in adults, the angiogenetic process is quiescent, and it is activated only when required. The “angiogenic switch” occurs in the cancer progression phase, leading to the formation of new vessels to endorse the fast replication.
- Activating invasion and metastasis: this phenomenon begins with a local invasion, followed by the intravasation of the cancer cells in the bloodstream and lymphatic system, then the extravasation in the parenchyma of distant tissues creating micro-metastatic lesions, and finally it concludes with the development of macroscopic tumors.

- Inflammatory microenvironment: The correlation between inflammation and tumor development occurs though two pathways: the intrinsic and the extrinsic pathways. Considering the intrinsic one, the oncogenes activation leads to an expression of mediators connected with inflammation, promoting the development of an inflammatory environment. In the extrinsic pathway, the generated inflammatory environment promotes the tumor progression facilitating the accumulation of further genetic mutations[20].

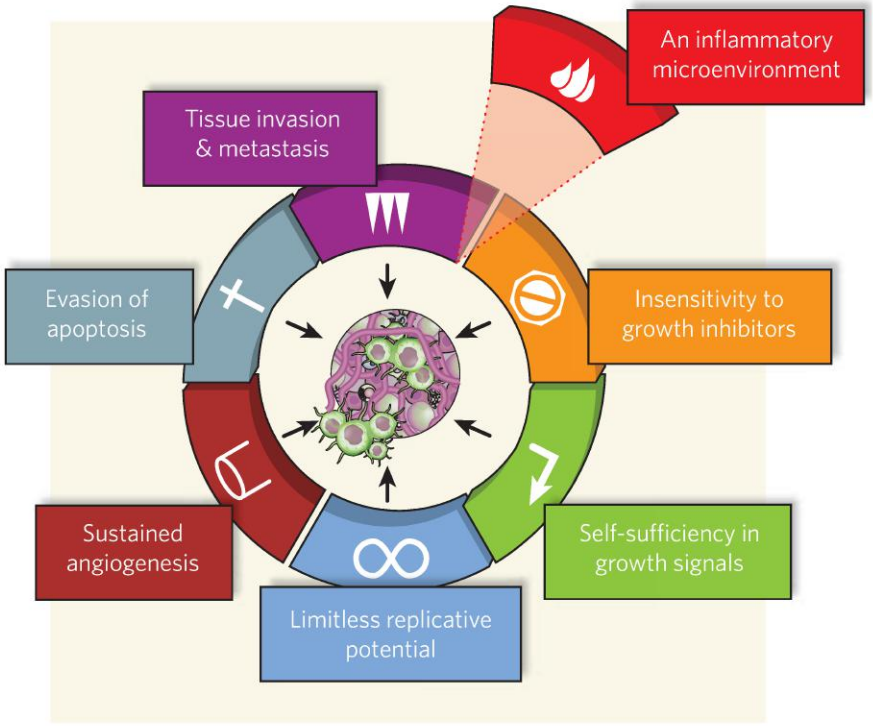

Figure 2. *Representation of cancer hallmarks*[21].

4.1.2. Pathophysiology of the tumor tissue

The principal targets for anticancer drug development are overexpressed receptors, mutated proteins and other molecules involved in specific pathways since only mutated tumor cells can be eliminated. Although this approach can be successful at first, multidrug resistance can occur, leading to a disease relapse.

Recent studies reported that the tumor microenvironment is one of the key feature contributing to the cancer progression, invasion and metastasis[22]. Cancer tissue exhibit peculiar characteristic which distinguish itself from the healthy tissues, thus targeted therapies have been designed to exploit these differences in order to improve the treatment efficacy. Tumor tissues

displays alterations at a cellular, molecular and metabolic level, as a consequence of different genetic alterations.

- Hypoxia: the rapid proliferation of the tumoral mass, caused by the uncontrolled cell replication, requires a relevant amount of oxygen. As a result of the irregular and poor capillary development, oxygen pressure decreases, causing hypoxic condition[23]. It has been demonstrated that oxygen depletion is related with malignant tumor development, since it can affect some pathways regulations connected to angiogenesis and necrosis. Furthermore, Reactive Oxygen Species (ROS) production and reoxygenation of tumor tissues after hypoxia further promote the ROS formation[24]. The generation of more aggressive phenotypes is a general consequence of hypoxia, being resistant to the conventional chemotherapy and radiotherapy and promoting tumor development[25].
- Acidic pH: generally, tumor tissues present an acidic environment which arises from the high metabolic activity. This is due to the high quantity of energy required to support the fast cell replication, but while healthy cells produce energy exploiting aerobic glycolysis within mitochondria, cancer cells exploit the anaerobic pathway. A mitochondria damage or an inadequate oxygen supply increases the glucose consumption, leading to a switch in the metabolism mechanism, from aerobic to anaerobic. As a consequence, the massive lactic acid production by lactate dehydrogenase generates the acidic environment and the activation of proton pumps[26]. Furthermore, high lactate levels can facilitate cancer cells evasiveness towards the immune system resulting in a chronical inflammation condition[27]. Another major cause of pH changes originates from mutations of genes involved in the cancer cell metabolism[28], such as gene encoding for membrane ion transporters. The enhanced metabolic activity leads also to CO_2 accumulation and its rapid conversion in carbonic acid by carbonic anhydrase enzyme, which contributes to the acidic environment formation. Therefore, the tumor microenvironment pH is nearly 6.4-6.8, with respect to the 6.9-7.4 value of the normal tissues[29,30]. This pH variation can be exploited for the design of pH sensitive nanocarriers owing to a selective delivery and drug release in cancer cells.
- Redox equilibrium: tumor cells produce a large amount of hydrogen peroxide, since proto-oncogene Ras activates GTPase Rac1 regulating NADPH-oxidase enzyme. This production leads to ROS formation, which can damage nucleic acids causing mutation in thymine and guanine bases, sister chromatid exchanges and strands breaks[24]. The

consequent result is a deregulation of body's cellular defence system and genomic instability[31].

- Tumor vasculature architecture: originating form a single mutated cell, cancer grows to a 1-2 mm mass exploiting the existing blood vessels[32]. Due to the further increase in dimension, a condition of hypoxia in the mass inner area is generated provoked by the limited oxygen diffusion. Hence, to guarantee an adequate oxygen and nutrients amount and the waste removal, the tumor mass promptly develops its own vascular network, characterized by a peculiar architecture that significantly differs from the physiological one. The tumor vascular networks displays loops, shunts, tortuous vessels, large avascular areas and variable distances between vessels normally absent in normal tissues[33]. The up-regulation of pro-angiogenetic factors and the down-regulation of vessels growth inhibitors triggers the activation of the new vessels formation[34]. In physiological condition, the equilibrium between anti- and pro- angiogenetic factors leads to the generation of well-structured and organized vessels with the presence of the basal membrane to support the endothelium[35]. The tumor tissue lacks this equilibrium, causing the formation of a leaky vasculature with wide fenestration of 100-800 nm[36] and the presence of an incomplete endothelium. Hence, tumor vessels prove to be permeable to macromolecules as plasma proteins or therapeutic agents. On the other hand, this leaky vasculature contributes to the formation of interstitial hypertension, limiting the macromolecules distribution within the tumor[37].
- Enhanced permeability and retention effect (EPR): the peculiar tumor vasculature architecture allowed the discovery of the well-known Enhanced Permeability and Retention Effect, firstly described by Mastumura and Maeda[38]. They reported that molecules possessing a high hydrodynamic size accumulate more efficiently in tumor tissues with respect to the healthy ones[38], and this behaviour arises from two reasons. Firstly, the tumor vasculature presents disorganization and lack of conventional organization. In addition, vessels display gaps between endothelial cells, leading to the *fenestrae* formation, and smooth muscle and a proper basal membrane are frequently missing. These features enable macromolecules which cannot penetrate healthy tissues to permeate within the tumor mass and reach cancer cells. Secondly, tumor tissues present a dysfunctional lymphatic drainage system, which allows for an entrapment and accumulation of macromolecules within the tissue, while small molecules diffuse back to the bloodstream due to their small hydrodynamic size (Figure 3.).

Several pathophysiological factors can affect and promote the EPR effect, such as prostaglandins, bradykinin, nitric oxide, vascular endothelial growth factor (VEGF) and tumor necrosis factor-α (TNF-α), since they trigger peculiar signaling pathways connected to the increase in blood supply.

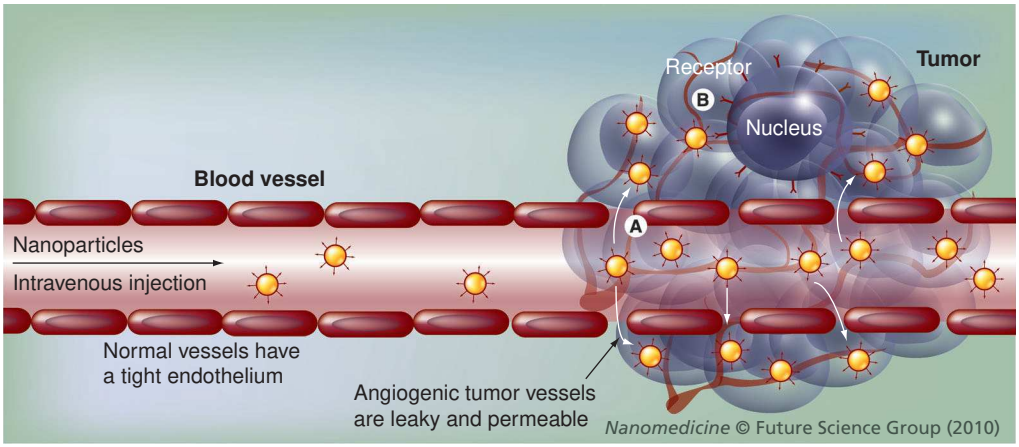

Figure 3. *Representation of the EPR effect in cancer tissues. Tumor vessels present large fenestrations due to the defective angiogenesis process, leading to the nanocarriers extravasation*[39].

4.2. Anticancer Therapies

Cancer remains one of the leading cause of death worldwide and the cancer therapy ambition is to reach selective and efficient treatments limiting or even avoiding the damage of healthy tissues. Among the possible approaches available, the choice depends upon the disease stage, its localisation and the patient condition.

The possible strategies for the treatment of solid tumors are:

- Surgical resection, including hyperthermia, cryosurgery and the local treatment photodynamic therapy;
- Radiation therapy, concerning the use of high doses of radiation to destroy cancer cells and shrink tumours;
- Chemotherapy, a pharmacological systemic treatment;
- Hormone therapy, involving the use of interferons or monoclonal antibodies to slow or block the cancer growth hormone-dependent;
- Immunotherapy, concerning cancer vaccines, a biological treatment based on the use of antibodies and cytokines to support the immune systems against cancer;
- Gene therapy, consisting in the insertion of functional genes into cancer cells in order to correct a metabolic disorder, to modify or repair a genetic dysfunction;

- Angiogenesis inhibitors, involving the administration of interfering agents to block specific mediators and receptor which trigger the angiogenetic process;
- Targeted Therapies, exploited to avoid possible side effects by a specific drug delivery toward cancer cells;
- Stem cells transplant, concerning the administration of stem cells to replace those suppressed by chemotherapy or radiotherapy.

Chemotherapy represents one of the main exploited approach even in combination with other therapies. It involves the use of small molecules able to reduce the replication of cancer cells or to promote apoptosis in rapid proliferating cells, namely chemotherapeutic agents.

One of the limitation related with the use of chemotherapeutics is that they indiscriminately destroy cancerous and fast replicating healthy cells, thus damaging bone marrow cells, hair follicles, and cells located in the digestive tract. The drug concentration in the tumour site is lowered due to the uncontrolled systemic distribution, therefore the drug dose required to fight cancer is higher than necessary, leading to serious side effects as anaemia, myelosuppression and gastrointestinal distress.

In addition, the administration of a high dosage of a specific drug for a prolonged time could lead to Multidrug resistance (MDR), reducing its therapeutic effect. This phenomenon is triggered by the overexpression of specific efflux pumps on the cell membrane, which are responsible of drug discharge and of the upregulation of genes encoding for the reparation of drug damages[40].

Frequently, chemotherapy resorts to the use of drug cocktails, but it could lead to drug interactions and issues related to the patient therapeutic response and toxicity[41]. Furthermore, traditional anticancer molecules suffer from poor water-solubility, requiring other solvents or surfactants to be administered, increasing the treatment toxicity.

Some examples of anticancer drugs available on the market are anthracyclines, fluorouracil, cyclophosphamides, taxanes, showing a wide therapeutic spectrum against haematological and solid cancers[41,42]. The main drawback of these agents is the lack of selectivity between healthy and tumor cells. To overcome this limitation, new therapeutic approaches are gaining interest such as antisense therapy and gene therapy, cellular screening for anticancer drug using combinatorial libraries or in silico research, DDs for the administration of anticancer drugs to enhance the therapy selectivity, new target moieties for DDs, namely specific biomolecules, antigens and receptors overexpressed in certain tumor types.

New powerful strategies can be obtained by the combination between different treatments, such as the use of chemical and physical approaches in order to improve the efficacy and the

selectivity. Therefore, a multidisciplinary approach could become the standard strategy to ameliorate clinical outcomes and life quality reducing systemic side effects.

4.3. Fundamentals for nanocarrier design

Despite current discoveries and developments, drugs released from conventional formulations are unable to reach the specific sites of interest. As a consequence, the application of nanotechnology has increasingly acquired importance in the pharmaceutical field.

Nanotechnology has emerged as a convenient vehicle for anticancer agents since it increases the solubility of hydrophobic drugs, exceeding the pharmacokinetic constraints of traditional formulations. Furthermore, nanocarriers endorse a selective treatment of a desired diseased site, due to the application of different targeting strategies. Concerning all these advantages, nanotechnology allows the increase in treatment efficiency and selectivity, along with a toxicity reduction, similarly to the magic bullet concept of Paul Ehrlich[43,44]. Nonetheless, although these potential improvements, only few nanotechnology-based medicines with clinical purpose have been approved by the regulatory entities[45], due to various obstacles and challenges faced at different development stages. The major cause for approval failure is the lack of efficacy and safety during late-stage clinical trials[46]. However, other concerns need to be considered. The achievement of a nanometric system, which is intended as a three dimensional complex entity with peculiar physicochemical features, requires a well-defined design and a controllable production to reach a reproducible scale-up process[46].

In addition, different biological barriers need to be crossed by nanotherapeutics before reaching the target sites. Concerning the several obstacles limiting the treatment efficacy, the uncontrolled drug distribution within the body plays an important role, hence it leads to insufficient accumulation of the therapeutic agent in the desired site, impeding the achievement of the effective dose. As a consequence, the control of drug distribution is one of the major aim of drug delivery systems to reach better therapeutic efficiency[47,48]. Accordingly, in order to achieve a specific delivery to a desired site of action, the design of nanosystems must consider the peculiar characteristics of the different biological barriers and microenvironments encountered upon administration. Generally, nanotherapeutics are administered though intravenous injection, and the circulation time upon the bloodstream needs to be sufficient to reach the target site[49], avoiding kidneys glomerular excretion and recognition by the reticuloendothelial system in spleen, lungs and liver[47].

Passive targeting: extravasation from the bloodstream

As reported by Maeda and his collaborators, the vasculature of solid tumors is characterized by the presence of wide fenestrations due to an incomplete endothelium formation. This feature leads to the nanoparticle extravasation from the bloodstream and the accumulation in the tumor mass[38] (Figure 4.).

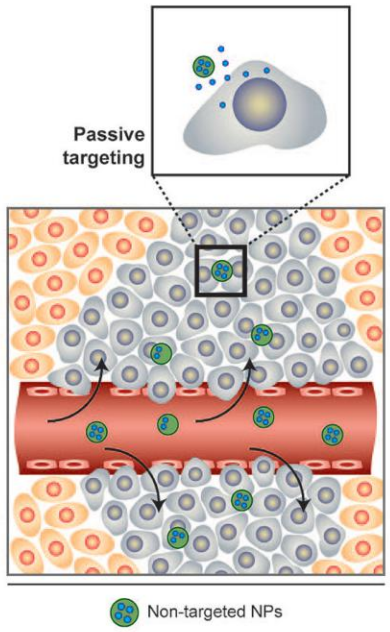

Figure 4. *Representation of passive drug targeting mechanism. (Adapted from Farokhzad et al.*[50]*)*

Additionally, the high interstitial pressure combined with an inefficient lymphatic drainage retains the macromolecules promoting their accumulation in the tumor site. The EPR effect depends on several criteria:

- Size: nanoparticle size affects different biological phenomena, such as biodistribution, circulation half-life, extravasation through the leaky vessels, macrophage recognition and mechanism of cellular uptake. Healthy tissues display a vascular endothelium with junctions of different size, concerning the type of tissue. Generally, the pore size of normal tissues is lower than 6 nm, being too small to permit the extravasation of colloidal systems. Vessels endothelia of kidney glomerulus and liver are non-contiguous, presenting fenestrations of 40-150 nm, bringing to non-specific accumulation of larger particles[51]. Moreover, spleen endothelium exhibit openings between 200 and 500 nm, allowing retention of particle above 200 nm, while kidneys can filter and rapidly eliminate particles below 5 nm with urine[52]. Micrometric sized particles (2-5 μM) can be exploited to target lung cancer since they displayed selective

accumulation in this tissue[5]. Accordingly, nanoparticles in the range of 80-150 nm enable for an optimal circulation time and for an increased extravasation capacity in the tumoral sites[53].

- Shape: particle geometries are involved in dynamics, cellular uptake and *in vivo* outcome[5]. Discoidal particles possess an increased interaction with vessels walls with respect to spherical shaped particles[54], while particles characterized by a high aspect ratio revealed a prolonged half-life and an increased change to accumulate within tumors[55].
- Surface charge: the surface charge of particles can influence the circulation time, the opsonisation process and the interaction with macrophages. Particularly, cationic particles display an increased rate of non-specific uptake, probably caused by interactions with sialic acids, which are components of the cell membranes. Differently, they can promote the endosomal release through mechanisms like the "proton sponge effect", preventing the degradation in the intracellular compartments. Slightly negative charged or neutral particles display longer circulation time due to the reduced adsorption of protein in the bloodstream.
- Stealth-like Behaviour: the functionalization of particle surface with flexible hydrophilic polymers hampers the opsonisation process, increasing the circulation life time. Polyethylene glycol (PEG) is the conventional polymer to obtain stealth nanocarriers[11]. The prolonged circulation time and the extravasation ability into disease sites largely ameliorate the tolerability and safety of nanocarrier-formulated drugs. The PEGylated liposomal formulation of Doxorubicin, well-known as Doxil®, for instance, displayed an improved stability and reduced cardiotoxicity side effect compared to the free drug.

Despite EPR effect in tumors has promoted the use of drug delivery systems, it has been proved to vary dramatically concerning cancer type, degree of tumor vascularization and expression of permeable factors. As a consequence, size, drug properties and anatomical features play a crucial role to define a specific targeting of the tumor[38].

Evasion of macrophage sequestration

Through the activation of the complement, the reticuloendothelial system (RES) is able to recognize non-biocompatible nanocarriers. Upon systemic administration, nanocarriers are covered by a plasma protein layer, namely Opsonin proteins, which are specifically recognized by phagocytes. This recognition leads to the removal of the opsonized nanocarriers from the

bloodstream, lowering or even preventing the drug delivery to the desired site[56]. Hydrophobicity, size, surface charge and surface chemistry affect the opsonisation process[57]. Hence, the nanoparticle surface decoration is a strategy to limit or avoid RES recognition using biocompatible hydrophilic polymers, such as PEG. The steric hindrance promoted by the coating with hydrated and flexible polymer chains makes the nanocarriers invisible to the immune system, increasing the stability[58].

Active targeting

While small hydrophobic molecules can easily diffuse through the cell membrane, a supramolecular system needs to be taken up through an active mechanism. Molecules and macromolecules, such as anticancer drug delivery systems, with a molecular weight greater than 1 kDa cannot diffuse though cell membranes by simple diffusion[6], requiring the endocytosis process.

To obtain an active targeting, nanocarriers need to be modified on the surface using specific ligands, which are designed to bind precisely to a receptor expressed on tumor cells. This binding induces a subcellular internalization *via* receptor-mediated endocytosis[59].

Hence, to obtain an efficient drug delivery into cancer cells, nanocarriers need, firstly, to accumulate in tumor tissue exploiting the EPR effect - passive targeting. Secondly, the biorecognition between the ligand-coated nanocarrier surface and the cell membrane receptors occurs – active targeting (Figure 5.). The active targeting process is a crucial step to promote the nanocarrier access to the cancer cell cytosol, where the targeted drug can be released and exploit its action. This process involves specific ligand-receptor interactions, which can occur after circulation in the bloodstream and extravasation. As already mentioned, prolonged circulation time might ameliorate drug accumulation into tumor site. Consequently, active targeting does not automatically mean an efficient delivery to the tumor, however the combination between the two mechanisms, active and passive targeting, could lead to an improved drug accumulation.

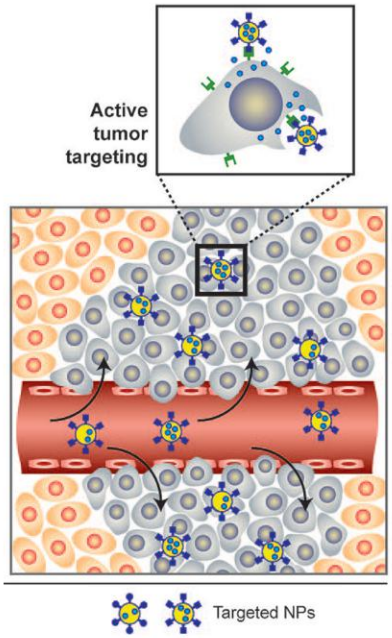

Figure 5. *Representation of active drug targeting mechanism. (Adapted from Farokhzad et al.*[50]*)*

Specific ligands need to be chosen for the functionalization of the nanocarrier surfaces to efficiently achieve a specific cancer cells recognition, such as proteins, sugars, vitamins, peptides, nucleic acids, antibodies and many others[60]. The choice is driven by the fact that cancer cells need an increased amount of oxygen and nutrients to support the rapid proliferation, therefore an overexpression of different receptors occur. For instance, Transferrin receptor, Galactosamine receptor, Human Epidermal Growth Factor receptor (HER2) and Folate receptor are overexpressed in different types of cancer cells[61–63].

Several factors affect the ligand-receptor interaction, including the target receptor expression in tumor tissue with respect to the normal one, receptor availability on the cell membrane, receptor internalization rate, targeting agent density on the nanocarrier surface and others[64–66]. The ligand-receptor interaction provokes a slight invagination on the cell membrane, causing the assembling of clathrins, which are specific molecules involved in the endocytosis process. This process leads to the complete invagination of the cell membrane and the formation of a vesicle containing the nanosystems. Progressively, the vesicle is fused with endosomes, which are intracellular cytosolic organelles where the pH gradually decreases from pH 6.8, typical of primary endosomes, to pH 6.0-5.0 of secondary endosomes[7,67]. This ATP-dependent acidification could be exploited to promote the ligand-receptor dissociation[7] and to recycle the freed receptors. Successively, the endosomal content can be transferred to other intracellular compartments, namely lysosomes, in which the acidic pH of 5.5-4.5[67] and the presence of

several digestive enzymes can degrade the material or promote the drug release from the carrier in the presence of pH-sensitive bonds between the drug and the carrier[7].

Additionally, the internalization process can be clathrins-indipendent, avoiding the lysosomal uptake (8E). Hence, the targeting agent choice is a crucial step because it has consequence on the mechanism of cell internalization, even directing or preventing the lysosomal trafficking[6].

The stability of the targeting agent along the bloodstream is a further key point to define[66]. Therefore, the ligand functionalization on the nanocarrier surface should occur through stable interactions, such as covalent bonds or physical absorption[66], evaluating the possible alterations in properties of both drug and nanocarrier after the process.

Hence, while designing a complex drug delivery system, an accurate analysis of the target tissue, drug, nanocarrier and ligand is necessary to optimize the formulation and the possible applications[59].

Drug release

When the interaction between receptor and nanocarrier occurs, the formulated drug can have two possible fates:

a) it can be released from the carrier into the extracellular space and consequently diffuses into cells;

b) formerly the whole carrier is internalized, then the physical entrapped drug can diffuse out of the nanocarrier, or it can ben release after bond cleavage in the endosomal compartment, if it has been chemically conjugated to the carrier. Upon endosomal escape, a certain quantity of encapsulated material can traffic to the intracellular action site.

Several stimuli can trigger the release mechanism:

- Temperature: thermoresponsive polymers present a phase transition at a specific temperature, namely Low Critical Solution Temperature (LCST), which leads to changes in hydrophilic-hydrophobic balance, solubility and conformation. The drug release could occur due to an increase in endogenous temperature or in an externally applied temperature, causing the collapse of the thermoresponsive polymer[68].
- pH: a shift in pH value can induce the polymer hydrolysis and the consequent vesicles disruption, owing to the drug release[69]. The use of pH-sensitive bond, such as hydrazone, acetal or cys-aconityl bond, is another strategy to obtain a controlled release upon variation of the pH[70].
- Oxidation / Reduction: polymers bearing disulphide bonds between hydrophilic and hydrophobic blocks display stability in the oxidizing extracellular compartment, while

being susceptible to reduction once within the intracellular environments. Particularly, the elevated glutathione (GSH) levels found in different tumors can be exploited to obtain redox-sensitive systems characterized by the selective release of the content within the cytosol[71].

- Light: the use of irradiations with a specific wavelength can induce the drug release. Mabrouk *et al.*[72] reported an interesting system based on azobenzene-loaded polymersomes sensible to UV light. The illumination process induced a conformational change causing the polymersomes disruption.
- Ultrasound: Ultrasounds (US) are a harmless and effective technique allowing for a spatiotemporal controlled release of drugs. This method is non-invasive since it is possible to easily control the tissue penetration depth by changing the frequency, time of exposure and duty cycles. The drug release can be achieved by mechanical or thermal effects produced by radiation forces or cavitation phenomena.

4.4. Polymer-based nanovectors

Concerning the anticancer context, one of the main goals remains the delivery of active compounds to the tumoral tissues, minimizing or avoiding the non-specific distribution of drugs in healthy tissues. Generally, drugs can be covalently linked to different natural or synthetic scaffolds, such as polymers and peptides, ensuring the active molecule delivery. In the case of a polymeric carrier, specific criteria are required[73]:

- The polymer molecular weight should be high enough to prevent a fast elimination from the bloodstream;
- It should bear functional group exploitable for the conjugation of drug or other molecules;
- It should be water soluble of in a stable colloidal suspension;
- It should be biocompatible, non-immunogenic, and biodegradable.

The first polymer-drug conjugate was realized in 1955 by Jatzkewitz *et al.*, using poly-vinylpyrrolidon as polymeric backbone[74]. Formerly, in 1975 Ringsdorf proposed a generic model for the polymer-drug conjugates design, outlining the importance of a suitable number of reactive side chains along the polymeric backbone to allow the binding of functional molecules as drugs[75] (Figure 6.). These reactive groups are introduced during the polymer synthesis, by choosing monomers with specific chemical functionalities[75]. Furthermore, for the drug conjugation, the use of a peculiar chemical spacer between the polymeric backbone and

the active molecule can decide the rate and the site of drug release from the scaffold[76]. A targeting agent can be attached to deliver the polymer-drug conjugate or the delivery system to specific tissues (see paragraph 4.3., active targeting).

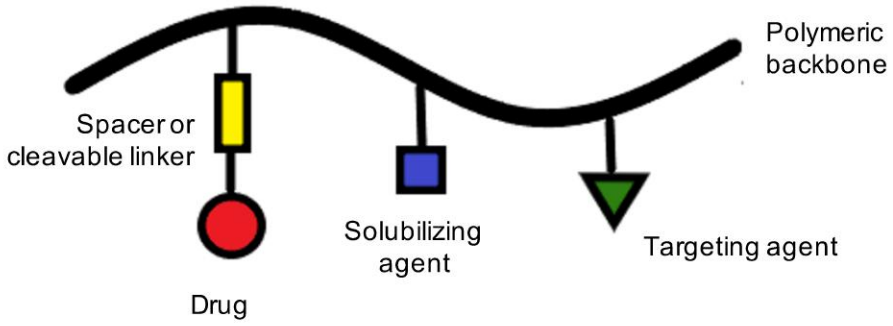

Figure 6. *Ringsdorf's model for drug delivery system.*

Accordingly, polymeric delivery systems possess multiple characteristics affecting the delivery itself and the drug release.

Over the years, several polymeric nanocarriers have been designed and synthetized, based on various scaffolds. Among natural polymers, polysaccharides as pullulan, dextran, inulin and chitosan, polypeptides and polyaminoacids have found extensive applications, including drug delivery, catalysis and tissue engineering, due to their biocompatibility and biodegradability[77–79]. For instance, Li *et al.*[80] synthetized the paclitaxel-poly(L-glutamic acid) derivative, improving the drug solubility and avoiding the toxicity related to the administration of the free drug or in the formulated version Taxol® caused by the use of Cremophor as solubilizing agent[80].

In addition, synthetic polymers have been extensively investigated as well, since they have revealed appropriate structure variability, reproducible synthesis and suitable modification strategies[76]. Concerning synthetic biomaterials, polyesters as poly(lactic acid) (PLA), poly(glycolic acid) (PGA) and poly(lactic-*co*-glycolic acid) (PLGA) were among the first synthetic scaffolds investigated thanks to their availability, revealing several advantages in their use[81]. As an example, the Doxorubicin-PLGA drug conjugated obtained by Yoo *et al.* exhibited a sustained doxorubicin release and an increased HepG2 cellular uptake of the conjugates[82].

Another well-know and versatile synthetic polymer is polyethylene glycol (PEG), which has been widely applied in several kinds of nanovector, such as polymer therapeutics, dendrimers, micelles or polymersomes. As an example, Chen *et al.* conjugated doxorubicin to PEG chain

though a pH sensitive hydrazone bond, to obtain a selective release in the intracellular environment[83].

Hence, the use of natural or synthetic polymeric scaffolds provide the opportunity to obtain versatile and easily modifiable structures allowing a controlled and selective release essential for anticancer purposes.

4.4.1. Polymeric Micelles

The nanovector polymeric backbone can be designed in order to endorse specific physical features. For instance, amphiphilic block copolymers self-assemble in aqueous environment forming micelles, in which the hydrophobic blocks stack together in a core structure, while the hydrophilic blocks protract toward the aqueous media lowering the interfacial free energy of the polymer-water system[84,85]. The hydrophobic core can be exploited as a pharmaceutical reservoir thus it can improve the solubility of hydrophobic drugs in aqueous environment[86]. Furthermore, polymeric micelles analogues, named reverse micelles, have been deeply studied in virtue of their ability in permitting the solubilisation of hydrophilic molecules in a lipophilic medium[87].

Recently, the design of amphiphilic copolymers has gained much attention in the research field, based on the use of polyesters of poly(aminoacids) as hydrophobic portion[88]. As examples, PLA, poly(caprolactone) (PCL), poly(β-benzyl L-aspartate), poly(γ -benzyl L-glutammate), poly(L-lysine) are commonly used for this purpose[88], while the hydrophilic portion often consists in PEG[84].

The nature of the block copolymers affects important features of the micelles formulation, such as stability, size, drug loading capacity, release kinetics, biodistribution and circulation time[84]. More in detail, the composition, the molecular weight and the chemical structure of polymers have been reported to significantly affect the final properties of the micellar nanocarriers[84].

The critical micelle concentration (CMC) is the minimum amphiphile concentration needed for micelles formation. A suitable CMC value for clinical applications should be in the range of 10^{-6}-10^{-7} M or even lower, in order to ensure stability of the nanocarriers after significant dilution, as upon intravenous administration, owning to a prolonged circulation in the bloodstream and consequent accumulation in the desired tissue[89,90]. The polymer micellization process is entropy-driven and it is directly related to the standard free energy (AG_{mic}). The interfacial tension has an enthalphic contribution, while the chain stretching has an entropic contribution, resulting in the equation: $-AG_{mic}=RTln(CMC)$[91]. In aqueous media, the micellization process is driven by the hydrophobic interactions between hydrophobic blocks

and by variations in the water structures in proximity of the polymer chains[92]. A lower CMC value could be due to an increase in the lipophilicity of the copolymer hydrophobic blocks, as a consequence of an increased cohesion of the hydrophobic core *via* stacking interactions[85]. Additionally, hydrophilic blocks can also vary the micelle stability, thus they interact though hydrophilic forces, as hydrogen bonds, dipole-dipole and van der Waals forces, between each other's and with the solvent. Nevertheless, the presence of the hydrophilic corona on the micelles surface reduces the hydrophobic blocks exposure to the aqueous environment, which is one of the leading causes of micelles destabilization[85].

Dynamic Light Scattering (DLS) and Static Light Scattering (SLS) techniques provide a rapid and reliable approach to determine CMC, size and polydispersity of the micellar formulations. (64E). Regarding DLS technique, light hits the colloidal suspension and scatters in all directions. The time related intensity of the scattered light is used to determine the micelles size and distribution in solution[85]. Moreover, the CMC value can be measured using the pyrene molecule as fluorescent probe. The technique is based on the excitation of pyrene at 334 nm and the resulting emission spectrum is recorded from 350 to 450 nm. The ratio between the fluorescence intensity at 383 nm and 372 nm, corresponding to the third peak. The ratio between the emission intensities at 384 nm (I_3) and 373 nm (I_1), I_3/I_1, is plotted against the logarithmic copolymer concentration, considering the inflection point as CMC value[93].

Micelle assembling is usually obtained by the use of different solvents. Generally, the copolymer is dissolved in a solvent able to solubilize both blocks, named as "good solvent". Subsequently, a "bad solvent", which dissolves only one of the blocks, is added gradually. A dialysis process is required finally to slowly replace the "bad solvent" with the "good" one, resulting in the formation of the colloidal suspension while avoiding the formation of large aggregates[92].

The common micelle morphology is the spherical shape and the size ranges between 10 and 200 nm. Nonetheless, micelles can acquire several morphologies, such as rod-like, slightly elliptic, flower-like and crew-cut micelles, due to the nature and length of both hydrophobic and hydrophilic blocks of the copolymers as well as the assembly procedure[85,92]. Since the micellar size range is 10-200 nm, RES recognition and entrapment in the hepatic sinusoidal capillaries can be often avoided[47] (see paragraph 4.3.). Consequently, assuming a sufficiently low CMC value and an appropriate shielded surface, polymeric micelles result in long plasma half-lives[88]. Moreover, the micelle size range allows for a selective extravasation from the fenestrated tumoral vessels, and, combined with the typical inefficient lymphatic drainage,

endorse this colloidal system to accumulate in solid tumors among time, in other words exploiting the EPR effect (see paragraph 4.1.2.).

Thanks to this significant tumor-infiltrating ability, several polymeric micelles have been studying in clinical trials. NK911 is a doxorubicin micellar formulation currently in phase I at the National Cancer Centre Hospital in Tokyo for the treatment of metastatic or recurrent solid tumors refractory to conventional chemotherapeutic agents[94]. NK911 includes drug conjugated poly(aspartic acid) as hydrophobic block and PEG as hydrophilic block. Specifically, doxorubicin is both covalently bound to the polymeric backbone, and even physically entrapped in the micellar core through hydrophobic interactions[95]. NK911 possess a narrow size of 40 nm, owing a good and uniform distribution in tumoral tissues[95].

Recently, micelles based on poly(ethylene glycol)-*b*-poly(aspartic acid) as polymeric scaffold have been functionalized for Cisplatin delivery, a neurotoxic and nephrotoxic agent, creating a metal-polymer chelate complex between the carboxylic pendant group of the aspartic acid and the platinum atom[96]. This formulation revealed a tumor-selective distribution and reduction of drug-related side effects[96].

Actually, the development of smart polymeric micelles is gaining attention, thus they possess the ability to target specific tissues and responding to physical or chemical stimuli with structural changes[97]. The use of pH-sensitive bond, which covalently link the drug to the polymeric scaffold, as hydrazone bond, is a common strategy to design polymeric smart micelles. Bae *et al.*[98] developed in 2005 a pH sensitive system based on poly(ethylene glycol)-*b*-poly(aspartate hydrazone-Adryamicin), in which the acid-sensitive hydrazone bond was used as linker for the covalent conjugation of the anthracycline agent to the poly(aspartic) block. The research proved that the micellar nanocarrier was internalized in small cell lung carcinoma cell line (SBC-3) *via* pinocytosis[98]. The drug release occurred in specific intracellular compartment, namely endosome and lysosomes, due to an acid-catalysed hydrolysis of the pH-sensitive bond[98]. Moreover, the formulation revealed the drug release *in vivo* with extremely low toxicity, as demonstrated by non-altered mice body weight values[98]. Subsequently, the folate targeting agent was selected for the surface functionalization in order to obtain a selective cell internalization in KB cell line[99].

As well as di-block copolymers, tri-block copolymers, as Pluronic, self-assemble in micelles. Pluronic is formed by an ABA structure, where poly(ethylene oxide) (PEO) represents the A side blocks and poly(propylene oxide) (PPO) the central block B. In aqueous environment, the copolymer chains arrange in micelle structures characterized by a PPO core and a PEO corona.

The molar ratio between PO/EO and the Pluronic molecular weight define the physical-chemical characteristics of the resulting formulation[100].

To conclude, nanomedicine depicts micelles as a versatile and functional drug nanocarriers, able to encapsulate drugs as hydrophobic active molecules, gene, siRNA or metals. The unique core-shell architecture endows a prolonged circulation half-time in the bloodstream and a selective accumulation in solid tumors, highlighting their potential as promising drug delivery system in the anticancer research.

4.5. Environmentally sensitive carriers for cancer therapy

Several *in vivo* studies revealed that a selective anticancer drugs delivery can be achieved by the incorporation of targeting moieties which bind to overexpressed receptors or antigens in the desired cells. Despite the advantages related to the use of drug delivery systems, such as the increased drug half-lives, stability and drug accumulation, nanocarriers have to overcome different sequential biological barriers that limit their site-specific bioavailability and so the therapeutic performance[5]. For this reason, drug delivery research is nowadays focusing the attention on the development of multifunctional nanocarriers able to exploit the tumor structural peculiarities, such as pH, temperature, vascular endothelium and others, to overcome the previous limitations and control the drug delivery in specific intracellular compartments, tissues or organs. Stimuli-responsive vectors are gaining importance in the anticancer field, since it is possible to control and trigger their properties by applying external stimuli.

This strategy requires the use of specific biocompatible materials able to undergo a hydrolytic cleavage, specific protonation, or conformational changes at supramolecular or molecular level in response to a desired stimulus[101].

Among stimuli-responsive nanocarriers, pH responsive systems have been deeply investigated (Figure 7.).

Subcellular compartments and different tissues display a wide range of pH gradients in physiological and pathological condition, that can be exploited to reach an accurate nanocarrier response. Several pH moieties are employed, such as hydrazones[102], acetals[103], polyesters[104], polyketals[105], electron-rich trityls[106]. Hydrazone bonds are frequently used as pH sensitive linker between drugs and the polymeric backbone of nanocarriers, as it can release the drug by acidic hydrolysis, namely when the nanocarrier is internalized in endosomes and lysosomes (see paragraph 4.3.).

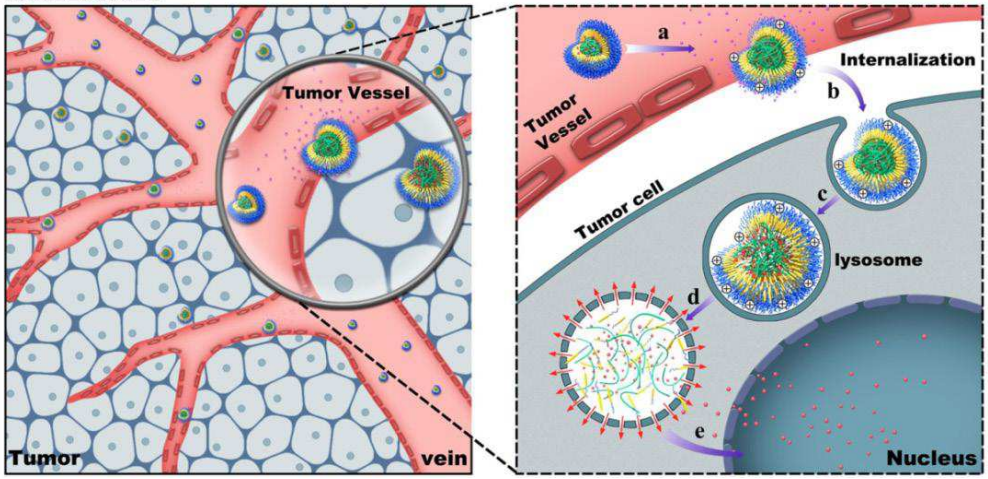

Figure 7. *Schematic interpretation of the pH-sensitive DDs transport from tumor vessels into tumor cells and the drug releasing process in lysosomes.*

Furthermore, pH sensitive systems can be obtained with materials possessing different behaviours in response to pH variations, for instance exploiting the differences in solubility of polymers bearing acidic functional groups. At physiological pH, these peculiar polymers are negatively charged and in an extended conformation, while at lower pH the acidic functions become protonated and the chains hydrophobic, leading to the polymer collapse. This pH related swelling give the change to tune the release of active molecules depending on the microenvironmental pH.

Therefore, the application of different external stimuli allows to a desired release profile at the tumor site having a temporal, spatial and dosage control.

4.6. Ring Opening Polymerization reaction

The aminoacidic di-block copolymers designed in this work with the aim of creating self-assembling nanovectors were synthetized by the Ring Opening Polymerization reaction (ROP), a versatile method to produce polypeptide based polymers[107]. Normally, three phases constitute polymerization reactions: initiation, propagation and termination. ROP reaction are amine-initiated involving the use of N-carboxy-anhydride (NCA) monomers[108]. Three strategies can be exploited to synthesize functional polymer-polypeptides[109]:

1) NCA monomers polymerization with protected pendant group;

2) the use of functional initiator to combine other type of polymerization with ROP;

3) post-polymerization modification of functional polymers bearing aminoacid mimicking pendant groups.

4.6.1. *N*-carboxy Anhydride (NCA) monomers

Synthesis and ROP polymerization reactions of α-aminoacid NCAs were firstly described by Hermann Leuchs in 1906[110]. Successively, the synthetic approach reported by Fuchs-Farthing has gained success due to its pure NCA monomers synthesis with good yields[109]. This procedure involves the direct phosgenation of α-aminoacids with diphosgene or triphosgene in inert polar solvents, such as tetrahydrofuran or ethyl acetate[109] (Scheme 1).

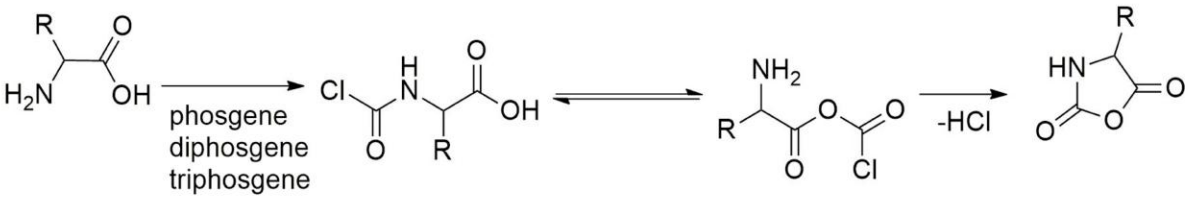

Scheme 1. *NCA synthesis via Fuchs-Farthing method.*

Generally, the NCA product is purified using crystallization, since high purity of NCA derivatives is an essential condition for the following polymerization reaction[111]. As reported that moisture could initiate the polymerization step, dry conditions are needed for NCA storage[111].

4.6.2. Ring Opening Polymerization

ROP reactions are normally initiated by a base or a nucleophile, since the basicity or the nucleophilicity of the initiator could affect the first step of polymerization[109].

As a consequence, two possible mechanisms can be exploited to start the reaction, the Normal Amine Mechanism (NAM) and the Activated Monomer Mechanism (AMM).

The NAM mechanism (Scheme 2) consists in a nucleophilic attack at the C5 carbonyl atom of the NCA cycle by a primary amine initiator[107]. Then, a C5-O1 cleavage occurs followed by decarboxylation, leading to the NCA ring opening and the generation of another primary amine, which can initiate the propagation process[107]. To allow a good polymerization propagation, pure NCA monomers need to be used and moisture avoided, as it causes the NCAs hydrolysis.

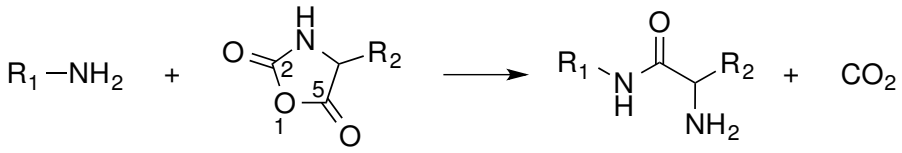

Scheme 2. *Normal Amine Mechanism.*

Conversely, in the AMM reaction (Scheme 3), the initiator acts as a base removing the proton in the N3 position of the NCA monomer, leading to the formation of the corresponding anion. As a consequence, the NCA anion can react with the C5 of another NCA monomer, resulting in a new anion formation and the release of carbon dioxide (CO_2)[111]. The slower is the propagation process in the polymerization, the greater is the contribution from side reactions, such as AMM, providing polymers lacking of the intended initiator covalently bound to the polymer chains[112].

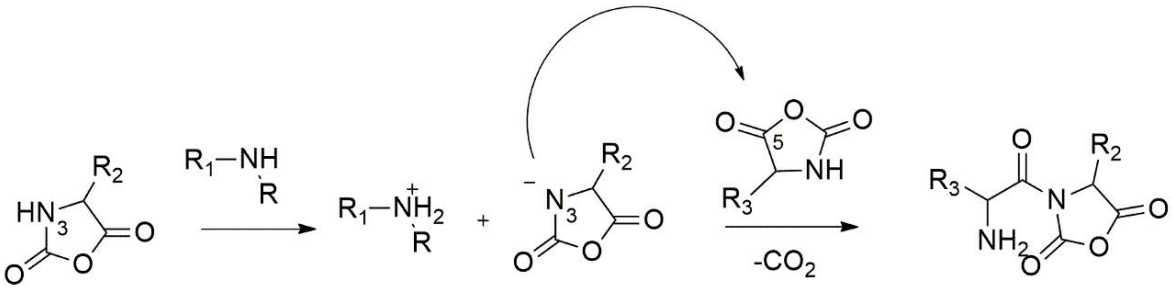

Scheme 3*. Activate Monomer Mechanism.*

Furthermore, Lu *et al.* reported that polypeptides synthesized using high vacuum techniques underwent NAM mechanism as initiation process, in contrast to the mixed mechanism, NAM and AMM, that normally occurs for polypeptides obtained at atmospheric pressure[113].

4.7. Doxorubicin

In this project we intend to develop an innovative drug delivery system that can be exploited as a therapeutic approach to treat cancer disease.

Among the different existing therapeutic strategies[42], chemotherapy is one of the most employed and it has the aim to control cancer development and progression by using low molecular weight drugs able to cause death of cancerous cells. Drugs as Doxorubicin, Cisplatin or Taxol and derivatives have been extensively used as chemotherapeutic agents[114]. Despite

this, these small molecules present the lack in selectivity for cancer cells as major drawback, resulting in severe systemic side effects[115].

Doxorubicin is an antibiotic member of the class of anthracyclines, deriving from the hydroxylation of the natural drug Daunorubicin[114,115] (Figure 8).

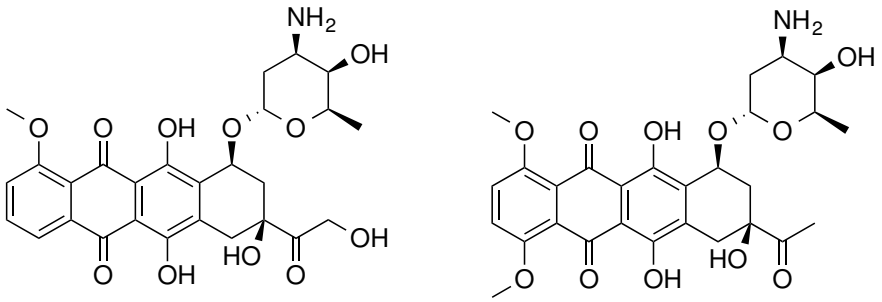

Doxorubicin Daunorubicin

Figure 8. *Chemical structures of Doxorubicin and Daunorubicin.*

Daunorubicin was firstly extracted from a *Streptomyces* peucetius bacterium in the '50 and employed as anticancer treatment against acute leukaemia[116]. Several Daunorubicin derivatives have been developed and studied among the years, nonetheless Doxorubicin displayed the broadest activity spectrum[114].

The anthracyclines structure is a four-ringed mostly-planar structure, deriving from the fusion of a cyclohexyl ring and an antraquinone moiety. In addition, the amino sugar Daunosamine is chemically linked to the cyclohexyl ring through a glycosidic bond[116]. The presence of the amino group leads to the generation of Doxorubicin hydrochloride salt, thus improving the drug solubility in water.

Doxorubicin is active toward different solid tumors, such as ovarian, breast, lung cancer, Hodgkin and non-Hodgkin lymphoma and multiple myeloma[117]. Due to its broad activity spectrum and effectiveness, Doxorubicin gained a wide clinical use, as in mono-therapy or in combination with other chemotherapeutics[116]. Unfortunately, Doxorubicin treatment could cause severe cardiac dysfunction in patients, which are generally dose-related and irreversible[115]. Furthermore, as all the anthracyclines, Doxorubicin is a substrate of the P-glycoprotein (P-gp)[116], hence it is rapidly excreted from the cytoplasm to the extracellular environment, losing its efficacy. This Multi Drug Resistance mechanism (MDR) is a further issue that affects the use of this chemotherapeutic agents as cancer treatment.

The mechanism of action through which anthracyclines act is not fully understood[116]. The anthraquinonic structure enables this family to intercalate in the double stranded DNA of cells

and interfere with Topoisomerase II, whose role is to allow the transcription relaxing DNA supercoils[116]. Doxorubicin, for instance, stabilizes the DNA-Topoisomerase II complex preventing its release[115] and, as a consequence, it blocks the replication process leading to cell death.

Doxorubicin treatments frequently induces remarkable side-effects in patients concerning cardiotoxicity, and it can be ascribed to tissue damages caused by the generation of free radical species[116]. Indeed, Doxorubicin oxidation to the unstable quinone triggers the production of oxygen reactive species (ROS). Muscle tissues are particularly sensitive to free radicals, thus major redox processes occur in muscle cell mitochondria, involving a massive oxygen quantity[116]. As a consequence, the off-target effect damages all muscular tissues, although is more pronounced in the myocardium, owing to a lack of Catalases in the cardiac tissue. This class of enzymes are involved in oxidative stress conditions and an overexpression could prevent from heat toxicity driven by the use of anthracycline[118].

In order to develop treatments with similar potency but less toxicity than Doxorubicin, other anthracyclines analogues has been studied, such as Epirubicin or Idarubicin. Despite this, the anthracycline family remain the most effective and powerful antineoplastic drugs[116]. To overcome the resistance mechanism and to limit the associated cardiotoxicity, several strategies involving the use of drug delivery systems are gaining importance. This new approach consists in the development of colloidal formulations of anthracyclines generating safer and more effective anticancer treatments.

In this project, Doxorubicin has been selected as drug model, thanks to its well-known potency and the possibility to exploit its chemical moieties for further conjugation reactions. Additionally, being fluorescent, this drug allows the use of spectroscopic techniques to investigate the features of the nanovector here proposed.

4.8. Nanomedicine in clinical phase

Medical devices are nowadays based on natural and synthetic polymers. However, the first polymer-drug therapeutics has been clinically accepted as medicine for parenteral administration only in the last decade[70]. Particularly, biocompatible and biodegradable polymeric micelles proved to be optimal for targeted and controlled delivery of anticancer drugs[119] and several polymeric micellar formulations of anticancer drugs have already reached different phases of clinical trials in USA, UK, South Korea and Japan[120].

As previously described in paragraph 4.4.1., NK911 is nowadays in clinical trial phase I at the National Cancer Centre Hospital in Tokyo[94]. NK105 has been approved for phase II in the same Hospital Institution for the treatment of recurrent gastric cancer[121]. This polymeric micellar formulation is constituted by amphiphilic di-block copolymers in which PEG and poly(aspartate) form the hydrophilic and hydrophobic block, respectively[122]. In order to increase the blocks hydrophobicity, poly(aspartate) lateral chains are functionalized with 4-phenyl-1-butanolate[122]. Paclitaxel is the drug chosen for the clinical purpose, and it is physically entrapped in the polymeric micelles core. The drug encapsulation process is driven by hydrophobic interactions which lead to the self-association of the system in polymeric micelles of 85 nm average size[122]. The nanocarrier revealed a good and uniform distribution in the tumor tissue tested, a reduction in side effects Paclitaxel-related as neurotoxicity, myelosuppression and allergic reaction[122], even though phase III will be performed to clarify the survival benefit[121].

NK012 is another promising formulation in phase I at Sarah Cannon Research Institute in Tennessee, USA[123] which has similarities with the polymeric micelles already discussed, such as PEG as component of the hydrophilic block, but poly(glutamic acid) builts the hydrophobic part of the backbone[124]. The drug selected for this study is SN38, the biologically active metabolite of Irinotecan hydrochloride (CPT-11), approved for the treatment of several solid tumors[125] although it causes relevant side-effect as severe diarrhoea and myelosuppression[123]. The active compound is covalently linked to the poly(glutamic acid) segment through a condensation reaction between the carboxylic pendant group of the polymeric backbone and the SN-38 phenol[124]. As a consequence of this condensation, the poly(glutamic acid) block gained sufficient hydrophobicity to self-assemble in aqueous environment[124]. Due to the mean micelles size of 20 nm, the system results suitable to exploit the EPR effect[124], owing to the accumulation in tumoral tissues where SN38 is gradually released by chemical hydrolysis under neutral condition[124]. Lower SN38-related side-effect with respect to the free drug were reported, highlighting the potential of the formulation as drug delivery system[123].

A further polymeric micellar formulation is Genexol-PM, a biodegradable PEG-*b*-poly(D, L lactide) (PEG-PLA) copolymer approved for the treatment of lung, breast and ovarian cancers. This is another example of Paclitaxel formulation, where the biodegradable core forming poly(D,L lactide) covers the role of drug solubilizing agent[126], increasing the water-solubility and allowing a higher dose delivery with respect to the free paclitaxel dose. The EPR

extravasation was achieved thanks to the particle size of nearly 20-50 nm in diameter[127]. Consequently, Genexol-PM reached the Korean market for the treatment of small cell lung cancer and breast cancer[128].

Notably, among these promising examples, the synthetic polymer PEG is widely employed to prolong the circulation half-time of nanocarriers and drugs through clearance inhibition and increase of the drug solubility. This polymer presents several interesting features that resulted in a widely use as nanocarriers component, such as the low cost production, the enhancement in stealth behaviour and circulation time, and the reduction of RES uptake[129]. PEGylated products possess a "conformational cloud" which prevents interactions with proteins and blood components. This characteristic leads to a reduction in opsonisation and in enzymatic degradation, lowering the immunogenicity and antigenicity[129]. Furthermore, low polydispersity index (PDI) values, obtained after the synthetic procedure, provides polymers with an acceptable uniformity to ensure reproducibility in terms of immunogenicity[129]. Despite PEG is not supposed to be affected by the opsonisation process, it is formerly reported that it can induce immune system recognition, leading to hypersensitivity reactions and anaphylactic shock[129]. Being a synthetic polymer, PEG is not biodegradable and it is excreted through glomerular filtration, hence low molecular weight chains ranging between 1 and 5 kDa are preferred[130]. Nevertheless, PEG is an FDA approved material with a widespread use in pharmaceutical formulations[130].

Another important family of biopolymers with applications in the drug delivery field is represented by polypeptides[78], thanks to their interesting features, such as water-solubility, biodegradability and safety[131]. Among polypeptides, polyaminoacids play an important role in nanocarriers design. The most relevant feature of polyaminoacids as nanocarriers is the biodegradability, indeed, due to the presence of amide bonds, they can be easily hydrolysed by lysosomal proteases releasing the aminoacid monomers[79]. Although this, polyaminoacids as poly(glutamic acid) and poly(aspartic acid) can be functionalized with active compounds at carboxylic pendant groups level, but the backbone degradation could not mean drug release[132]. Considering all these interesting features, polyaminoacids based-polymers seem to be in the forefront in nanocarrier design[133].

4.9. Aim of the Project

Self-assembling polyaminoacids based nanovectors can be developed as a promising and very versatile platform for drug delivery purpose. The aim of the present work is the generation of a family of amphiphilic di-block copolymers composed by a hydrophilic block of polyethylene glycol ($mPEG_{5kDa}$) and an amino acid-based block of γ-hydrazinamide-glutamic acid (hydGlu) and Leucine (Leu). PEGylated nanostructures are expected to remarkably increase the circulation time of the self-assembled nanocarriers bypassing the renal filtration and diminishing RES uptake. Notably, hydGlu is selected for the conjugation of Doxorubicin (Doxo) through a pH-cleavable hydrazone bond to allow for a controlled drug release once the carrier has reached the intracellular acidic compartments. Leucine is introduced in the polyaminoacidic block as a spacer between the glutamic units to minimize the steric hindrance of Doxo and as a promoter of the polymer self-assembly due to its hydrophobic feature. Doxo is expected to play a double role: first for its well-known anticancer activity, and, secondly, it participates to the self-assembly of the polymer and to the colloidal stability of the resulting nanocarrier. Indeed, after conjugation, Doxo would confer hydrophobicity to the aminoacidic portion of $mPEG_{5kDa}$-b-(γ-hyd[Doxo]-Glu_n-r-Leu_m) polymers, thus inducing the self-assembling of the amphiphilic material, leading to the formation of polymeric micelles (Figure 9.). Thus the combination of Leu and Doxo should improve the stability of the nanocarrier *in vivo*. Notably, amphiphilic polymer based micelles tend to dissociate after administration in the bloodstream as consequence of the dilution.

The goal of this project is to set up a versatile and performing platform for the passive delivery of the anticancer drug into tumour tissues, investigating their efficiency in terms of biocompatibility, controlled release and *in vivo* efficacy.

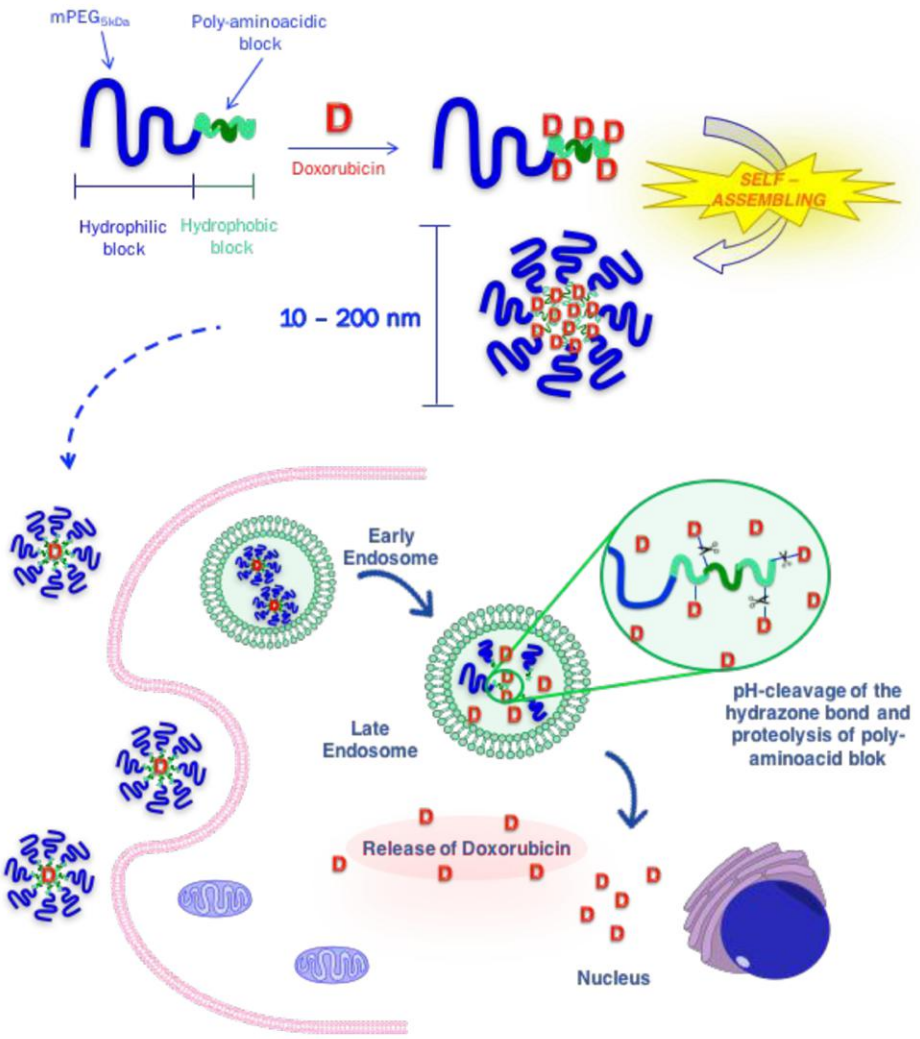

Figure 9. *Schematic representation of the self-assembling polymeric micelles composed by the amphiphilic di-block copolymers $mPEG_{5kD}$a-b-(γ-hyd[Doxo]-Glu_n-r-Leu_m), and their mechanism of action within tumoral cell.*

5. MATERIALS AND METHODS

5.1. Reagents

- Methoxypolyethylenglycol 5.0 kDa ($mPEG_{5kDa}$), allyl isocyanate, cysteamine hydrochloride, α-pinene, 2,2'-dimethoxy-2-phenylacetophenone (DPAP), γ-benzyl-glutamic acid, L-leucine, triphosgene, triethylamine (TEA), trifluoroacetic acid (TFA), glycyl-glycine, boric acid, 2,4,6-trinitrobenzensulfonic acid (TNBS), carbohydrazide, superDHB (9:1 mixture of di-hydroxy-benzoic acid and 2-hydroxy-5-methoxybenzoic acid), hydrazine monohydrate, deuterium oxide (D_2O), deuterochloroform ($CDCl_3$), hexadeuterodimethylsulfoxide (DMSO-d_6), iodine, potassium iodine, barium chloride, dimethyl sulfoxide (DMSO), dimethyl formamide (DMF), dichloromethane (CH_2Cl_2), methanol (MeOH), diethyl ether (Et_2O), isopropyl alcohol (IPA) were purchased from Sigma-Aldrich (St. Louis, USA).
- Doxorubicin Hydrochloride was provided by LC Laboratories (Woburn, USA).
- Ammonia was obtained by Scharlau (Barcelona, Spain).
- Analytical thin-layer chromatography (TLC) was carried out on aluminium sheets coated with silica gel obtained from MACHEREY-NAGEL GmbH & Co. KG (Düren, Germania).
- Buffers and salts were purchased from Fluka Analytical (Buchs SG, Switzerland) and Sigma-Aldrich (St. Louis, USA).
- Water for the production of all solutions and suspensions was "ultrapure" water (milliQ-grade, 0.06 μSiemens cm^{-1}) generated with the Millipore Milli-Q® purification system (Merk, MA, USA).
- All the materials used for cell culture were obtained from Gibco (Life Technologies, USA), including phosphate buffered saline (PBS), RPMI 1640 Medium, Foetal Bovine Serum (FBS), Penicillin G sodium, Streptomycin sulfate. 3-(4,5-Dimethylthiazol-2-yl)-2,5-diphenyltetrazolium bromide (MTT), Rat Serum, Tryton® X-100 and Corning® T-75 flaks were purchased from from Sigma-Aldrich (St. Louis, USA).
- CT26 colorectal carcinoma cell line and 4T1 breast carcinoma cell line were acquired from ATCC cell bank (Manassas, VA, USA).
- Anti-Mouse CD 107a (LAMP-1), Goat anti-Rat IgG Antibody DyLight® 488 conjugate and HIGHDEF® IHC fluoromont were obtained by Invitrogen, ThermoFisher Scientific

(Waltham, USA).

- 6 weeks old BALB/c female mice were acquired from Janvier, Genest-St-Isle, France.

5.2. Scientific equipments

- Spectrophotometric measurements were carried out with an UV-Vis Evolution 210 specrtophotometer and Nanodrop 2000 (ThermoFisher Scientific, USA). Data were analyzed with ThermoInsight 2 software.
- Mass spectrometry was carried out on Mariner ESI-TOF (Monza, MI; Italy) and on 400 Plus MALDI TOF/TOF Analyzer (AB Sciex, MA, USA).
- Multiwell plate detections were carried out with MultiSkan EX plate reader (Thermo Fisher Scientific, USA).
- Samples were stirred with Rotating stirrer, MOD 708 and VDRL Stirrer, MOD 711 (ASAL S.r.l., Italy).
- Lyophilization was performed with freeze-dryer Hetossic HETO Lab Equipment (Birkerod, Denmark).
- Solvents were removed by a BÜCHI® Rotavapor, model R-114 (BÜCHI Labortechnik AG, Postfach, Switzerland).
- pH measurements were carried out with a pH-meter Seven Easy 20-K Mettler Toledo equipped with a Mettler Toledo Inlab 413 electrode (Schwerzenbach, Switzerland).
- Samples were centrifugated with a Centrikon T-42K, Kontron Instruments, Eching, Germany and on a Sigma 1-14 Microfuge (Celbio Spa).
- Dynamic Light Scattering measurements were carried out with a Zetasizer NanoZS (Malvern instruments Ltd, UK).
- TEM images were obtained with a Tecnai G2 electron microscope (FEI, Oregon, USA).
- ^{1}H and ^{13}C NMR spectra were recorded on a Bruker Spectrospin AMX 300 MHz spectrometer and Bruker DPX400 Ultrashield (Fallanden, Switzerland). All NMR data were processed using MestreNova 6.2.1 Software.
- FT-IR spectra were obtained with Agilent Cary 630 FTIR
- Gel permeation chromatography (GPC) was carried out using a PL50 apparatus (Polymer Laboratories, Shropshire, UK) equipped with two columns (Agilent PLgel 5 μm Mixed D, 7,5 x 300 mm) connected in series and an RI detector, eluting with DMF added of 0.1 % w/w Lithium Bromide (LiBr) as the mobile phase, at flow rate of 1 mL/min, at 50°C. Narrow-

PPMA standards (162-371,000 g/mol) were used to calibrate the GPC. Data processing was carried out using Cirrus GPC/SEC 3.0 software.

- Fluorimetric analyses were carried out using a LS 50 B Perkin-Elmer fluorimeter (Wellesley, MA, USA).
- Confocal microscopy images were recorded using a Zeiss™ confocal laser-scanning microscope (LSM 800, Jena, Germany), using an immersion lens with 63x of magnification. Image elaboration were performed using ZEN 2 (blue edition) from Zeiss™ Softwares.
- Membranes with 3.5-5 kDa of molecular weight cut off (MWCO) from Delchimica scientific glassware (Napoli, Italia) and Spectra/Por® Float-a-Lyzer with the same cut off from Prodotti Gianni (Milan, Italy) were used for dialyses.

5.3. Analytical Methods

5.3.1. Iodine Assay for quantitative evaluation of polyethylene glycol and its derivatives

The colorimetric "Iodine assay" was originally described by Sims and Snape[134]. This test assesses the polyethylene glycol (PEG) concentration in aqueous solutions by using two reagent solutions: Barium chloride (5% w/v in 1M HCl) and Iodine (1.27 g I_2 in 100 mL of a 2% w/v KI solution) solutions. PEG forms a complex with Barium Iodide that absorbs light at 535 nm. Briefly, 1 mL of PEG solutions of unknown concentration in milliQ water were added of 250 µL of Iodine solution and 250 µL of Barium chloride solution. A blank sample was prepared as described above by replacing the PEG solution with an equal volume of milliQ water. Samples were incubated at room temperature for 15 minutes, and then analyzed spectrophotometrically at 535 nm.

The PEG concentration was calculated referring to the calibration curves previously obtained from a serial dilution of a 10 mg/mL stock solution of $mPEG_{5kDa}$-cysteamine ($mPEG_{5kDa}$-NH_2) in milliQ water (Figure 10.), and a 10 mg/mL stock solution of $mPEG_{5kDa}$-*b*-(γ-hyd-Glu_6-*r*-Leu_{10}) in milliQ water (Figure 11.). Calibration curves were found to be linear in a 0-10 µg/mL PEG concentration range. Sample were prepared in triplicate.

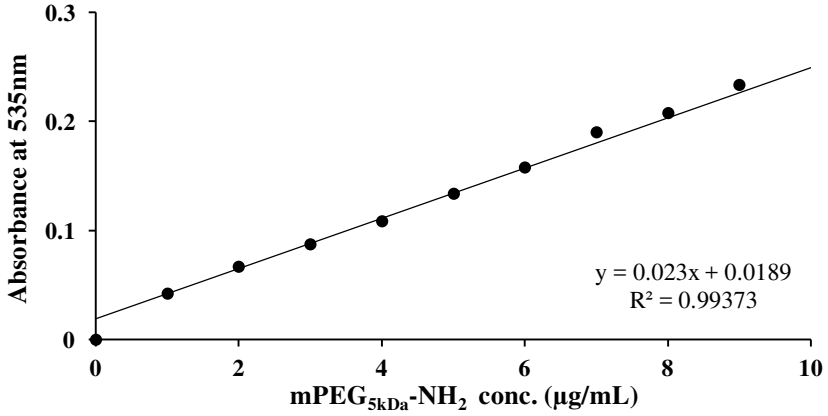

Figure 10. *Calibration curve of $mPEG_{5kDa}$-NH_2 obtained by Iodine assay. Spectrophotometric absorbance was measured at 535 nm.*

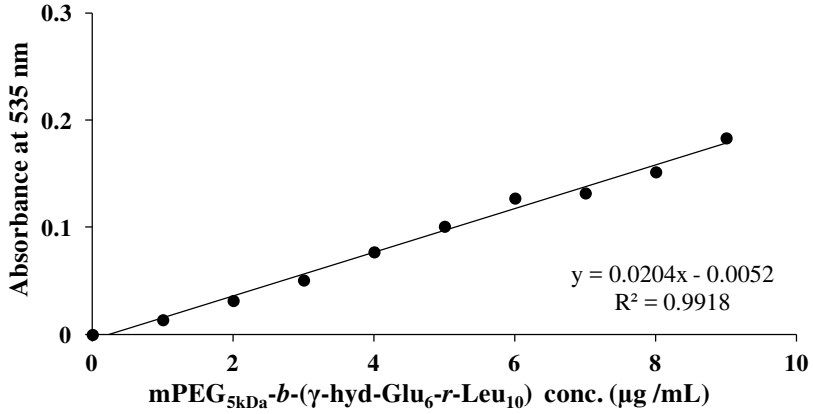

Figure 11. *Calibration curve of $mPEG_{5kDa}$-b-(γ-hyd-Glu_6-r-Leu_{10}) obtained by Iodine assay. Spectrophotometric absorbance was measured at 535 nm.*

5.3.2. Snyder assay for the quantification of hydrazide groups

2,4,6-trinitrobenzene sulfonic acid (TNBS) reacts with primary amines generating a highly chromogenic product that can be readily measured at 420 nm. A modified protocol of the Snyder assay[135] was used to quantify the content of hydrazide groups in solution which show a maximum of absorption at 500 nm.

A 0.2 mM carbohydrazide stock solution in borate buffer (0.1 M pH 9.3) was prepared. Hydrazide solutions in the concentration range of 0.006-0.1 mM were obtained by serial

dilution of the stock solution. To 970 µL of these solutions, 30 µL of a 0.033 M TNBS solution in milliQ water were added and samples were incubated for 30 minutes at room temperature in the dark. Afterwards, the absorption of each sample was measured at 500 nm, and the values plotted against the concentration to obtain a calibration curve (Figure 12.). Control samples were obtained by replacing hydrazide solutions with an equal volume of borate buffer. The test was performed in triplicate.

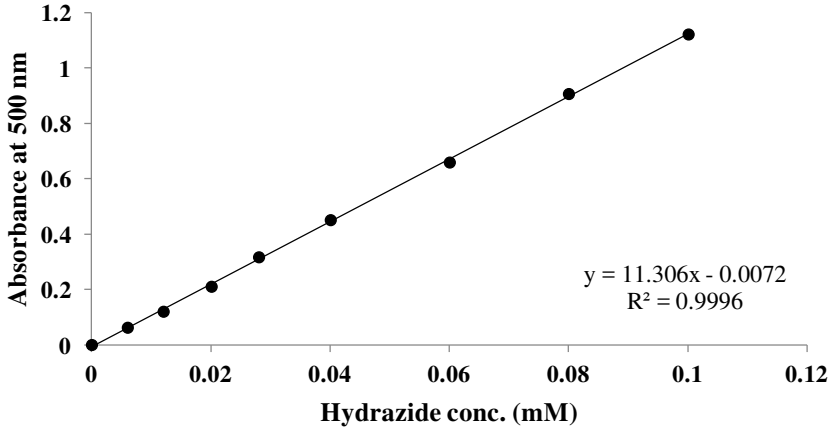

Figure 12. *Calibration curve of carbohydrazide obtained by modified Snyder's assay. Absorbance was measured at 500 nm.*

5.3.3. UV-Vis spectroscopic quantification of Doxorubicin

Doxorubicin (Doxo) is an anthracycline that absorbs light in the wavelength range between 400 to 550 nm. To set up a calibration curve (Figure 13.), a 7.1 mM Doxorubicin hydrochloride (Doxo HCl) stock solution was prepared by dissolving 4.1 mg of drug in 1 mL of dimethylsulfoxide (DMSO). Solutions in the concentration range 0.003-0.08 mM were obtained by serial dilution of the stock solution in milliQ water. All samples were prepared in triplicate and the absorbance values were read at 488 nm. Control samples were prepared by using milliQ water only.

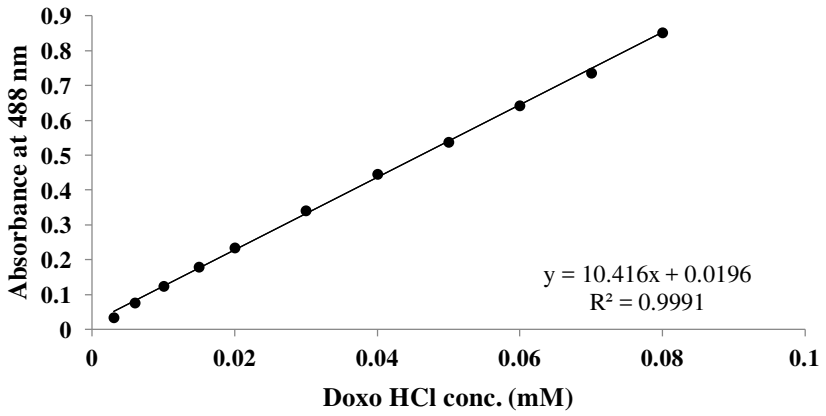

Figure 13. *Doxorubicin hydrochloride calibration curve in milliQ water. Absorbance was measured at 488 nm.*

5.4. Synthesis of $mPEG_{5kDa}$-cysteamine macroinitiator

$mPEG_{5kDa}$-cysteamine ($mPEG_{5kDa}$-NH_2) macroinitiator was synthetized from methoxy-PEG_{5kDa}-OH in order to obtain a primary amino group at the end of the polymer chain, that can act as a nucleophilic reactive group towards the *N*-carboxy anhydride (NCA) monomers to generate a library of di-block copolymers.

5.4.1. Synthesis of $mPEG_{5kDa}$-allyl carbamate

$mPEG_{5kDa}$-OH (20.0 g, 4.02 mmol) was dissolved in 15 mL of chloroform ($CHCl_3$) and allyl isocyanate (1.30 g, 15.6 mmol) and triethylamine (2.02 g, 0.0200 mol) were added. The resulting mixture was left under stirring for 18 hours at room temperature. The solution was precipitated in diethyl ether (Et_2O) under stirring, centrifuged at 5000 rpm for 5 minutes, rinsed three times with Et_2O (40 mL) and finally dried under reduced pressure. The $mPEG_{5kDa}$-allyl carbamate product (19.54 g, 3.82 mmol) was obtained as a white solid with 98% recovery yield (% mol/mol). The product was analysed using ^{1}H-NMR and MALDI-TOF. MALDI-TOF mass spectroscopy of $mPEG_{5kDa}$-allyl carbamate was performed using SuperDHB as matrix, and samples were prepared dissolving the polymer in dichloromethane (CH_2Cl_2) at 10 mg/mL concentration. Then 10 µL of SuperDHB matrix were added to 20 µL of the sample solution. 2 µL of the resulting mixture were spotted on the MALDI plate and analysed after drying.

^{1}H NMR (400 MHz, $CDCl_3$) δ 5.82 (ddd, J =26.0, 10.3, 5.5 Hz, 1H, CH=CH_2), 5.20 (dddd, J = 26.0, 10.3, 2.9, 1.5 Hz, 2H, CH=CH_2), 4.97 (bs, 1H, (C=O)N*H*), 4.22 (m, 2H, -CH_2O), 3.63 (s, 476H, -(OCH_2CH_2)$_n$), 3.36 (s, 3H, CH_3O-).

5.4.2. Synthesis of mPEG$_{5kDa}$-NH$_2$ through radical addiction of cysteamine

mPEG$_{5kDa}$-allyl carbamate (10.1 g, 1.99 mmol) was dissolved in 10 mL of methanol (MeOH). Cysteamine hydrochloride (1.13 g, 9.95 mmol) and 2,2'- dimethoxy-2-phenylacetophenone (DPAP) (0.102 g, 0.400 mmol) were both solubilized separately in 2 mL and 1 mL of MeOH, respectively, and then sequentially added to the mPEG$_{5kDa}$-allyl carbamate solution. The final mixture was aliquoted in vials and irradiated with UV light (λ=350 nm, 36W) for 3 hours. When allyl signals could no longer be detected by ^{1}H NMR, the aliquots were pulled together and methanol was removed under vacuum. The obtained residue was solubilized in water (100 mL) and extracted with 3x100mL of ethyl acetate (EtOAc) to remove organic species deriving from the decomposition of DPAP. Then, the aqueous phase was extracted 2x100mL with a 3:1 dichloromethane:isopropanol (CH_2Cl_2:IPA) mixture and the organic phase was dried under reduced pressure to obtain the mPEG$_{5kDa}$-cysteamine (mPEG$_{5kDa}$-NH$_2$) as a white powder (9.95 g, 1.92 mmol), with a 98% (mol/mol) recovery yield. MALDI-TOF analysis of mPEG$_{5kDa}$-NH$_2$ was performed using SuperDHB as matrix.

GPC analysis (DMF + 0.1% LiBr): $M_{n,GPC}$= 7.3 kDa; Đ=1.09.

^{1}H NMR (400 MHz, $CDCl_3$) δ 4.22 (s, 2H, -CH_2O), 3.63 (d, J = 14.2 Hz, 476H, -(OCH_2CH_2)$_n$), 3.37 (s, 3H, CH_3O-), 3.29 (dd, J = 11.3, 5.3 Hz, 2H, NHCH_2), 3.17 (s, 2H, CH_2NH$_2$), 2.94 (t, J = 7.3 Hz, 2H, CH_2CH$_2$NH$_2$), 2.63 (t, J = 7.1 Hz, 2H,CH_2S), 1.90 (m, 2H,CH_2CH$_2$S).

5.5. Synthesis of *N*-Carboxy Anhydride (NCA) monomers

5.5.1. Synthesis of γ-benzyl-glutamic acid *N*-carboxy anhydride (Glu-NCA)

The synthetic protocol for γ-benzyl-glutamic acid NCA was adapted from Markland *et al.*[136] and Williams *et al.*[137] works.

γ benzyl-glutamic acid (19.9 g, 83.8 mmol) was suspended in tetrahydrofuran (THF, 200 mL). α-pinene (33.0 mL, 20.9 mmol) and solid triphosgene (9.14 g, 30.8 mmol) were sequentially added to the suspension under nitrogen. The resulting mixture was heated under reflux at 56 °C until the suspension turned yellow and clear (90 minutes). The solution was then cooled down

to room temperature, and bubbled with nitrogen for 4 hours to remove gaseous co-products and potential traces of unreacted phosgene. An aqueous NaOH trap was connected to the system during this procedure, to neutralise the gaseous species removed from the reaction solution. The volume was then reduced to 70 mL and petroleum ether was added (50 mL). The resulting solution was transferred into a conical flask and left to crystallize at -18°C overnight. γ benzyl-glutamic acid NCA (16.35 g, 61.7 mmol) was isolated by filtration with a recovery yield of 82% (mol/mol).

^{1}H NMR δ 7.35 (m, 5H, C*H* aromatic), 6.64 (s, 1H, N*H*CH), 5.14 (s, 2H, CH_2-Ar), 4.38 (t, J = 6.1 Hz, 1H, NHC*H*), 2.59 (t, J = 6.9 Hz, 2H, CH_2C=O), 2.26 (m, 1H, CHC*H*H), 2.13 (m, 1H, CHCH*H*)

^{13}C NMR δ 172.52 (1C, (*C*=O)CH), 169.48 (1C, (*C*=O)O-), 151.97 (1C, (*C*=O)NH), 135.35 (1C, C aromatic), 128.85 (2C, C aromatic), 128.73 (2C, C aromatic), 128.50 (1C, C aromatic), 67.25 (1C, *C*H_2-Ar), 57.07 (1C, *C*HCH$_2$), 29.98 (1C, CH$_2$*C*H$_2$), 27.05 (1C, *C*H$_2$CH$_2$).

FT-IR: υ 3247, 2320, 1862, 1772, 1718, 1493, 1396, 1251, 1183, 1110, 796, 961 cm^{-1}.

5.5.2. Synthesis of leucine *N*-carboxy anhydride (Leu-NCA)

According to the method of Smeets *et al.*[138], leucine (8.02 g, 61.0 mmol) was suspended in anhydrous THF (100 mL). α-pinene (25.0 mL, 157 mmol) and solid triphosgene (6.70 g, 22.2 mmol) were sequentially added under nitrogen. The suspension was heated under reflux at 64°C until the suspension turned yellow and clear (30 min). The solution was then cooled down to room temperature, and bubbled with nitrogen following the same procedure described for γ-benzyl-glutamic acid NCA. The solvent was then removed under vacuum to yield a yellow oil. Petroleum ether (300 mL) was isolate pure leucine NCA as a white solid by precipitation. This precipitate was filtered, washed several times with cold petroleum ether (3x25 mL), and dried under reduced pressure, with a recovery yield of 95% (mol/mol) (7.65 g, 48.6 mmol).

^{1}H NMR (400 MHz, $CDCl_3$) δ 6.43 (bs, 1H, N*H*CH) 4.33 (dd, J = 8.9, 4.0 Hz, 1H, NHC*H*), 1.82 (m, 2H, CH_2CH), 1.68 (m, 1H, CH$_2$C*H*), 0.99 (dd, J = 9.3, 6.4 Hz, 6H, CH(CH_3)$_2$)

^{13}C NMR (101 MHz, $CDCl_3$) δ 170.25 (1C, (*C*=O)CH), 153.38 (1C, (*C*=O)NH), 56.33 (1C, *C*HCH$_2$), 40.88 (1C, *C*H$_2$CH), 25.06 (1C, *C*H(CH$_3$)$_2$), 22.79 - 21.59 (2C, CH(*CH*$_3$)$_2$).

FT-IR: υ 2960, 1798, 1750, 1468, 1117, 1079 cm^{-1}.

5.6. Synthesis of $mPEG_{5kDa}$-*b*-(γ-benzyl-Glu_n-*r*-Leu_m) random copolymers

This procedure was adapted from the protocol reported by Zhao *et al.*[78].

The $mPEG_{5kDa}$-*b*-(γ-benzyl-Glu_n-*r*-Leu_m) copolymer library was synthetized by Ring Opening Polymerization (ROP) using $mPEG_{5kDa}$-NH_2 as initiator and γ-benzyl-glutamic N-carboxyanhydride (Glu-NCA) and leucine N-carboxyanhydride (Leu-NCA) as monomeric units with different monomer molar ratio. For the synthesis of all polymers, the amount of monomers to be used was calculated considering the monomer conversion of 90% and 70% for γ-benzyl-glutamic acid NCA and leucine NCA, respectively, based on preliminary polymerization studies (data not shown).

$mPEG_{5kDa}$-NH_2 (0.500 g, 0.0970 mmol) was dissolved in toluene (10 mL), and then dried under reduced pressure to azeotropically remove moisture. This procedure was repeated for further four times. In the case of $mPEG_{5kDa}$-*b*-(γ-benzyl-Glu_8-*r*-Leu_8), Glu-NCA (0.255 g, 0.871 mmol) and Leu-NCA (0.183 g, 1.16 mmol) were added to a second flask under Argon atmosphere to obtain a $mPEG_{5kDa}$-NH_2:γ-benzyl-Glu:Leu feed ratio of 1:9:12. Anhydrous DMF (12 mL) was added to the $mPEG_{5kDa}$-NH_2 under Argon atmosphere, the flask was sonicated for five minutes to completely solubilize the macroinitiator, then the solution was degassed by bubbling Argon for 30 minutes. Afterwards, the initiator solution was cannulated into the flask containing the NCA monomers, and the resulting solution was stirred at room temperature. The solution was degassed twice a day for 30 minutes and the reaction was carried out for 7 days. The mixture was then precipitated dropwise under stirring in Et_2O, and the resulting suspension centrifuged for five minutes at 5000 rpm. The precipitate was solubilized in CH_2Cl_2 and then precipitated in MeOH to remove the side products, consisting in poly(γ-Glu_n-r-Leu_m) oligomers. After centrifugation for 5 minutes at 5000 rpm, the supernatant was recovered and precipitated dropwise in Et_2O to isolate $mPEG_{5kDa}$-*b*-(γ-benzyl-Glu_8-*r*-Leu_8) as a white solid. The precipitate was desiccated for 24 hours under reduced pressure to remove traces of solvents, then characterized by ^{1}H NMR and GPC (yield of purification process 69% mol/mol).

^{1}H NMR (400 MHz, $CDCl_3$) δ 7.28 (m, 40H, Hh), 5.02 (s, 16H, Hg), 4.01 (m, 16H, Hd, Hi), 3.64 (s, 476H, Hb), 3.38 (s, 3H, Ha), 2.70 – 2.17 (m, 58H, Hc, He, Hf, Hj), 0.86 (m, 48H, Hk).

GPC analysis (DMF + 0.1% LiBr): M_n= 10.6 kDa; Đ=1.11

$mPEG_{5kDa}$-b-(γ-benzyl-Glu_{16})

^{1}H NMR (400 MHz, $CDCl_3$) δ 7.43 – 7.14 (m, 80H, Hh), 5.02 (s, 32H, Hg), 4.19- 3.92 (m, 16H, Hd), 3.64 (s, 476H, Hb), 3.38 (s, 3H, Ha), 2.62 – 2.26 (m, 74H, Hc, He, Hf).

GPC analysis (DMF + 0.1% LiBr): M_n= 12.2 kDa; Đ=1.07.

Yield of purification process 75% (mol/mol)

$mPEG_{5kDa}$-b-(γ-benzyl-Glu_6-r-Leu_{10})

^{1}H NMR (400 MHz, $CDCl_3$) δ 7.32 (m, 30H, Hh), 5.03 (s, 18H, Hg), 4.02 (m, 16H, Hd, Hi), 3.64 (s, 476H, Hb), 3.38 (s, 3H, Ha), 2.71- 2.17 (m, 54H, Hc, He, Hf, Hj), 0.88 (m, 60H, Hk).

GPC analysis (DMF + 0.1% LiBr): M_n= 10.4 kDa; Đ=1.10

Yield of purification process 72% (mol/mol)

$mPEG_{5kDa}$-b-(γ-benzyl-Glu_4-r-Leu_{12})

^{1}H NMR (400 MHz, $CDCl_3$) δ 7.32 (m, 20H, Hh), 5.03 (s, 8H, Hg), 4.02 (m, 16H, Hd, Hi), 3.64 (s, 476H, Hb), 3.38 (s, 3H, Ha), 2.72 – 2.17 (m, 50H, Hc, He, Hg, Hj), 0.89 (m, 72H, Hk).

GPC analysis (DMF + 0.1% LiBr): M_n= 9.9 kDa; Đ=1.12

Yield of purification process 77% (mol/mol)

5.7. Deprotection of γ-benzyl-glutamic acid residues with hydrazine hydrate: synthesis of $mPEG_{5kDa}$-*b*-(γ-hyd-Glu_n-*r*-Leu_m)

The protocol was adapted from Bae *et al.*[99].

$mPEG_{5kDa}$-*b*-(γ-benzyl-Glu_8-*r*-Leu_8) (0.500 g, 0.0639 mmol) was dissolved was dissolved in toluene and the solvent was removed under reduced pressure to azeotropically remove moisture. Anhydrous DMF (3.50 mL) was then added to the solution under Argon atmosphere, followed by dropwise addition of hydrazine hydrate (0.631 g, 19.7 mmol). The reaction was carried out at 40°C under stirring for 48 hours. The resulting gel-like solution was diluted with additional DMF to decrease viscosity. The resulting solution was precipitated in Et_2O and the white solid was isolated by centrifugation. Then, the product was re-dissolved in water and purified by

dialysis (MWCO 3.5 kDa) for two days using deionized water as releasing medium. The polymer containing solution was freeze-dried to obtain $mPEG_{5kDa}$-*b*-(γ-hyd-Glu_8-*r*-Leu_8) as a white solid (0.389 g, 0.0470 mmol, 74% mol/mol yield). The γ-hydrazide Glutamate:Leucine monomer ratio of was estimated by ^{1}H-NMR. The number of hydrazide groups per polymer chain was calculated according to the modified Snyder's assay[135] for the evaluation of hydrazide content (λ=500 nm, calibration curve: y=11.997x – 0.0318. R^2=0.9982), and the iodine assay[134] for PEG detection (λ=535 nm, calibration curve: y = 0.0229x + 0.0207. R^2 = 0.9933). The same synthetic procedure has been applied to generate $mPEG_{5kDa}$-b-(γ-benzyl-Glu_6-r-Leu_{10}), $mPEG_{5kDa}$-b-(γ-benzyl-Glu_4-r-Leu_{12}), $mPEG_{5kDa}$-b-(γ-benzyl-Glu_{16}).

^{1}H NMR (400 MHz, DMSO) δ 4.16 (m, 16H, (C=O)C*H*, (C=O)C*H*NH_2), 3.51 (s, 476H, -(OCH_2CH_2)$_n$), 3.24 (s, 3H, CH_3O-), 2.05 – 1.45 (m, 58H, NH(CH_2)$_3$S(CH_2)$_2$, CH_2CH_2C=O, CH_2CH(CH_3)$_2$), 0.86 (m, 48H, CH(CH_3)$_2$).

GPC analysis (DMF + 0.1% LiBr): M_n= 8.5 kDa; Đ=1.31.

Number of hydrazide per polymer chain: 8.7

$mPEG_{5kDa}$-b-(γ-hyd-Glu_{16})

^{1}H NMR (400 MHz, D_2O) δ 4.34 (m, 16H, (C=O)C*H*), 3.74 (s, 476H, -(OCH_2CH_2)$_n$), 3.42 (s, 3H, CH_3O-), 2.75 – 1.81 (m, 74H, NH(CH_2)$_3$S(CH_2)$_2$, CH_2CH_2C=O).

GPC analysis (DMF + 0.1% LiBr): M_n= 12.3 kDa; Đ=1.03

Number of hydrazide per polymer chain: 16.1

Yield of purification process 68% (mol/mol) (0.326 g, 0.0424 mmol).

$mPEG_{5kDa}$-b-(γ-hyd-Glu_6-r-Leu_{10})

^{1}H NMR (400 MHz, DMSO) δ 4.16 (m, 16H, (C=O)C*H*, (C=O)C*H*NH_2), 3.51 (s, 476H, -(OCH_2CH_2)$_n$), 3.24 (s, 3H, CH_3O-), 2.05 – 1.45 (m, 54H, NH(CH_2)$_3$S(CH_2)$_2$, CH_2CH_2C=O, CH_2CH(CH_3)$_2$), 0.87 (m, 60H, CH(CH_3)$_2$).

GPC analysis (DMF + 0.1% LiBr): M_n= 10.1 kDa; Đ=1.20.

Number of hydrazide per polymer chain: 6.7

Yield of purification process 75% (mol/mol) (0.354 g, 0.0495 mmol).

$mPEG_{5kDa}$-b-(γ-hyd-Glu_4-r-Leu_{12})

^{1}H NMR (400 MHz, DMSO) δ 4.07 (m, 16H, (C=O)C*H*, (C=O)C*H*NH_2), 3.51 (s, 476H, -(OCH_2CH_2)$_n$), 3.24 (s, 3H, CH_3O-), 2.02 – 1.43 (m, 50H, $NH(CH_2)_3S(CH_2)_2$, CH_2CH_2C=O, $CH_2CH(CH_3)_2$), 0.87 (m, 72H, $CH(CH_3)_2$).

GPC analysis (DMF + 0.1% LiBr): M_n= 10.4 kDa; Đ=1.21

Number of hydrazide per polymer chain: 4.7

Yield of purification process 70% (mol/mol) (0.336 g, 0.0474 mmol).

5.8. Conjugation of Doxorubicin HCl to $mPEG_{5kDa}$-*b*-(γ-hyd-Glu_n-*r*-Leu_m) and micelle self-assembling

Doxorubicin conjugation to $mPEG_{5kDa}$-b-(γ-hyd-Glu_n-r-Leu_m) was performed using an adapted protocol from Bae *et al.* protocol[99].

$mPEG_{5kDa}$-*b*-(γ-hyd-Glu_8-*r*-Leu_8) (0.300 g, 0.0416 mmol) was dissolved in 4.5 mL of an anhydrous MeOH:DMSO 1:2 mixture. Doxorubicin hydrochloride (Doxo HCl) (0.386 g, 0.666 mmol) was solubilized in 1.5 mL of anhydrous DMSO. The two solutions were mixed and trifluoroacetic acid (TFA) (0.076 mg, 0.666 mmol) was added as a catalyst. The reaction mixture was left under stirring in the dark at room temperature for three days. The solution was then precipitated in Et_2O (5x40 mL), and the red precipitate was collected by centrifugation (5000 rpm, 5 minutes), and then desiccated under reduced pressure. To remove the unreacted Doxo, the obtained red powder was dissolved in 1:1 DMSO:Phosphate Buffer (PB) (10 mM, pH 7.8) mixture, transferred into a 3.5-5 kDa MWCO dialysis bag and dialyzed against the same solvent mixture for 24 hours, replacing the solvent four times. The presence of the unreacted drug was monitored by thin layer chromatography (TLC) in MeOH preconditioned with 5% v/v triethylamine (TEA) in MeOH. Dialysis was carried out until complete disappearance of free Doxo spot in the dialysis bag solution. Afterwards, the composition of the releasing mixture was gradually varied from a 1:1 to 0:1 DMSO:PB ratio in six hours to eliminate the organic solvent and, to induce spontaneous self-assembling of the conjugates.

Finally, the external solvent was changed to deionized water (DI water) adjusted to pH 7.8 with ammonia and dialysed for further three hours to remove salts. The polymeric self-assembled micelle suspensions was then freeze-dried and stored at –20 °C until reconstitution, performed by dissolving micelle powders in the required solvent and stirred overnight on an orbital shaker. The conjugation yield was assessed by calculating the number of Doxo molecules per polymer chain. The molar ratio was estimated according to the spectrophotometric absorbance of the drug at λ 488 nm in PB (calibration curve: y= 10.416x + 0.0196, R^2 = 0.9991), and the iodine assay[134] for PEG detection (λ=535 nm, calibration curve: y= 0.0204x – 0.0052, R^2 = 0.9918). The same protocol was adopted to $mPEG_{5kDa}$-*b*-(γ-hyd-Glu_6-*r*-Leu_{10}), $mPEG5_{kDa}$-*b*-(γ-hyd-Glu_4-*r*-Leu_{12}), $mPEG_{5kDa}$-*b*-(γ-hyd-Glu_{16}). As a control, the same dialysis procedure was performed also on drug free conjugated polymers, in order to evaluate the formation of micelles in absence of the linked drug.

$mPEG_{5kDa}$-b-(γ-hyd[Doxo]-Glu_{16})

Conjugation yield 43.75% (mol/mol), 7.0 Doxorubicin molecules/polymer chain.

Doxorubicin content: 34% (w/w).

$mPEG_{5kDa}$-b-(γ-hyd[Doxo]-Glu_8-r-Leu_8)

Conjugation yield 70% (mol/mol), 5.5 Doxorubicin molecules/polymer chain.

Doxorubicin content: 30% (w/w).

$mPEG_{5kDa}$-b-(γ-hyd[Doxo]-Glu_6-r-Leu_{10})

Conjugation yield 88% (mol/mol), 5.2 Doxorubicin molecules/polymer chain.

Doxorubicin content: 29% (w/w).

$mPEG_{5kDa}$-b-(γ-hyd[Doxo] -Glu_4-r-Leu_{12})

Conjugation yield 100% (mol/mol), 4.1 Doxorubicin molecules/polymer chain.

Doxorubicin content: 24% (w/w).

5.9. Characterization of the self-assembling colloidal systems

5.9.1. Dynamic light scattering and zeta potential analysis

The particle size and size distribution and zeta potential of 20 μM $mPEG_{5kDa}$-*b*-(γ-hyd-Glu_n-*r*-Leu_m) and $mPEG_{5kDa}$-*b*-(γ-hyd[Doxo]–Glu_n-*r*-Leu_m) colloidal suspensions in PBS were determined by dynamic light scattering (DLS) analysis at 25°C, using a Dynamic Light Scattering Zetasizer Nano equipped with a red laser (λ=633 nm) at a fixed angle of 173°. DTS applications 6.12 software was used to analyse the data. All size values were reported as volume. For each sample, three DLS measurements were performed with 10 runs per 10 second measurement.

5.9.2. Transmission electron microscopy

A drop of a 20 μM colloidal suspension in MilliQ water were placed on a homemade carbon coated copper grid, and the solvent was allowed to dry at room temperature. Then, the samples were treated with 1% uranyl acetate dissolved in distilled water for 5 minutes at room temperature to provide for a negative staining. Transmission electron microscopy analyses were carried out using a Tecnai G2 microscope (FEI). Particle size analysis was performed with ImageJ Software (developed at the National Institute of Health, USA).
The average diameter of the particulate system was calculated by measuring 50 individual particles with ImageJ software.

5.9.3. Determination of the critical micelle concentration (CMC)

Pyrene assay. In order to characterize the capacity of the polymer to self-assemble in colloidal system, a Critical Micelle Concentration assay was performed. The CMC for $mPEG_{5kDa}$-*b*-(γ-hyd-Glu_n-*r*-Leu_m) formulations was estimated according to the protocol described by Ambrosio *et al.*[139].
20 μL aliquots of a 5mg/mL pyrene solution in acetone were desiccated under vacuum. Then, 1 mL of an aqueous formulations of $mPEG_{5kDa}$-b-(γ-hyd-Glu_n-r-Leu_m) in the range 5-300 μM was added to each aliquots and stirred overnight on an orbital shaker in the dark at room temperature. Afterwards, the samples were centrifuged three times at 13000 rpm for 3 minutes, and the supernatants were analysed by fluorescence spectroscopy with an excitation wavelength of 335 nm and recording the emission spectra from 350 to 450 nm. The ratio between the

emission intensities at 384 nm (I_3) and 373 nm (I_1), I_3/I_1, was plotted versus the polymer logarithmic concentration. The CMC value was assessed at the intersection of the two lines obtained by linear regression[140,141]. Each experimental point was repeated three times.

Fluorimetric analysis. The CMC of $mPEG_{5kDa}$-*b*-(γ-hyd[Doxo]-Glu_n-*r*-Leu_m) was estimated by spectrofluorimetric measurements.
1 mL of a 0.25-50 μM $mPEG_{5kDa}$-*b*-(γ-hyd[Doxo]-Glu_n-r-Leu_m) colloidal suspension in PB (10 mM, pH 7.8) was prepared and stirred overnight on an orbital shaker in the dark at room temperature. Then, the samples were analysed by fluorescence spectroscopy with an excitation wavelength of 490 nm, recording the emission spectra in the range 510-600 nm. The ratio between the emission intensities at 585 nm and 555 nm, corresponding to the second and first maximum emission peaks, respectively, was plotted versus the logarithmic polymer concentration. The CMC value was determined at the intersection of the two lines obtained by linear regression. Each experimental point was repeated three times.

5.10. Release Studies

Solutions of free Doxo and self-assembled micelles in PBS were diluted at a Doxo equivalent concentration of 400 μM in PBS, pH 7.4, or 100 mM sodium acetate, pH 5.5. A volume of 1.5 mL of these solutions were transferred into a Float-A-Lyzer® G2 system, 3.5–5 kDa MWCO and dialyzed against 500 mL of the same buffer. At fixed time points, the concentration of doxorubicin inside the dialysis bag was determined by sampling 20 μL of the solution and analysing them by spectrophotometric analysis (λ_{max} 488 nm). The experiment was performed in triplicate.

5.11. *In vitro* cellular studies

5.11.1. Cell cultures

CT26 murine colorectal carcinoma cell line and 4T1 murine mammary carcinoma cell line were cultured using RPMI 1640 Medium supplemented with 10% Foetal Bovine Serum (FBS), 100U/mL penicillin G sodium and 100 μg/mL streptomycin sulphate (complete medium). Cells were subcultured in 75 cm^2 culture flasks and incubated at 37 °C and 5% CO_2 atmosphere.

5.11.2. Cell viability studies

CT26 and 4T1 cell viability was quantified by the MTT (Thiazolyl Blue Tetrazolium Bromide) assay[142] that assesses the living cells metabolic activity after treatment with the free drug and the micellar formulations. Cells were seeded in a 96-well plate at a density of $6x10^3$ cells/well (200 µL/well) and incubated at 37°C and 5% CO_2 for 24 hours. Then, the medium was replaced with 100 µL of free drug or micellar solutions, in the Doxo equivalent concentration range of 0.01 nM-100 µM, in complete medium. Cells were incubated with complete medium only were used as control.

After 48 or 72 hours of incubation, the medium was discharged and cells were gently rinsed with PBS (200 µL) and incubated with 200 µL of MTT solution (0.5 mg/mL in complete medium) for 3 hours at 37 °C. Then, the medium was removed and DMSO (200 µL) was added to each well to dissolve the formazane crystals. The absorbance at 560 nm was measured using the MultiSkan EX plate reader. The cell viability was expressed as relative percentage of living cells compared to the untreated ones, considered as negative control (N=3, n=17).

5.11.3. Confocal Microscopy imaging

CT26 cells were seeded in 12-well plates containing glass dishes at a density of $10x10^4$ cells/well (1 mL/well) in complete medium and allowed to grow for 24 hours under culture conditions. Afterwards, the medium was discharged and replaced with 1 mL of Doxo or $mPEG_{5kDa}$-*b*-(γ-hyd[Doxo]-Glu_6-*r*-Leu_{10}) micelles, namely DoxoMC-E_6L_{10}, (5 µM Doxorubicin equivalent concentration) in complete medium. Cell were incubated at 37°C for 2 or 24 hours. After the incubation time, cells were gently rinsed once with PBS (400 µL), fixed for 20 minutes at RT in the dark with 4% w/v paraformaldehyde (PFA) solution in PBS and rinsed with PBS (3x400 µL). Then, cells were incubated for 45 minutes at RT with a 5% v/v Rat Serum, 0.25% v/v Triton® X-100 solution in PBS (400 µL) to permeabilize the cell membrane. Afterwards, the solution was discharged and the cells were incubated with 200 µL of a rat anti-mouse anti-lysosomal-associated membrane protein 1 (anti-LAMP-1) antibody solution (1:100 dilution in 5% rat serum solution in PBS). After 1 hour, cells were rinsed three times with PBS and incubated for 1 hour with a 2 µg/mL 4′,6-diamidino-2-phenylindole (DAPI) and goat anti-rat secondary antibody DyLight® 488 conjugate (1:500 dilution) solution in PBS added of 5% rat serum (200 µL), for nuclei and lysosome staining, respectively. Finally, the dishes were gently rinsed three times with PBS and once with MilliQ water before being mounted on microscope slides using HIGHDEF® IHC fluoromont as mounting media. Cells

were imaged with a Zeiss™ confocal laser-scanning microscope (LSM 800, Zeiss, Jena, Germany) using an immersion lens with 63x magnification, with emission wavelengths at 506 nm (blue, DAPI) for nuclei detection, 531 nm for lysosome imaging (green, anti-LAMP-antibody) and 700 nm for Doxorubicin detection (red). The images were then processed with ZEN 2 (blue edition) from Zeiss™ Softwares.

5.12. *In vivo* studies

The experiments were performed following the Belgian national regulations guidelines and in accordance with EU Directive 1010/63/EU concerning the use of animals for experimental purposes. The experiments were approved by the ethical committee for animal care of the faculty of medicine of the Université catholique de Louvain (2017/UCL/MD/34). Animals had free access to water and food and the animal body weight was constantly monitored.

5.12.1. Anticancer activity on subcutaneous colorectal tumor model

CT26 cells ($5x10^5$ cells/mouse) were subcutaneously injected into the right flank of 6 weeks old BALB/c female mice to allow reproducible tumor volume measurements using an electronic caliper. Tumor volume was calculated according to the following equation (Eq.1):

$$\text{Volume} = \pi/6 \times \text{length} \times \text{width}^2 \quad \text{(Eq.1)}^{143}$$

Mice were randomly assigned to treatment groups when the tumor reached the volume of 25 ± 2 mm^3. Treatments were injected through local intratumoral injection or through the tail vein for intravenous administration. Five groups were defined: Group 1: control group (untreated, n=9); Group 2: intratumoral injection of Doxo HCl, (30 µL, n=7); Group 3: intratumoral injection of DoxoMC-E_6L_{10} (30 µL, n=6); Group 4: intravenous injection of Doxo HCl (150 µL, n= 7); Group 5: intravenous injection of DoxoMC-E_6L_{10} (150 µL, n=8). The injected drug doses were 2.4 mg/kg and 12 mg/kg, for the intratumoral and intravenous administration, respectively. The treatment effect on tumor growth was evaluated by measuring the tumor volume every other day. Body weights were assessed prior to tumor volume measurements. The experiment end point was determined when the tumor volume reached 800 mm^3 or at 20% body weight loss. At this point mice were sacrificed.

5.12.2. Anticancer activity on subcutaneous breast tumor model

4T1 cells ($1x10^6$ cells/mouse) were subcutaneously injected into the right flank of 6 weeks old BALB/c mice, and the tumour growth was monitored with the procedure previously described. Mice were randomly assigned to treatment group when the tumor volume reached 26 ± 1 mm^3. Treatments were injected through local intratumoral injection or through the tail vein for intravenous administration. Eight groups were defined: Group 1: control group (untreated, n=9); Group 2: intratumoral injection of Doxo HCl (30 µL, n=11); Group 3: intratumoral injection of DoxoMC-E_6L_{10} (30 µL, n=10); Group 4: intravenous injection of Doxo HCl (150 µL, n= 8); Group 5: single intravenous injection of DoxoMC-E_6L_{10} (150 µL, n=8); Group 6: single intravenous injection of Caelyx® (150 µL, n=8); Group 7: multiple intravenous injection on days 0, 7, 14 of DoxoMC-E_6L_{10} (150 µL, n=8); Group 8: multiple intravenous injection on days 0, 7, 14 of Caelyx® (150 µL, n=7). The dose of drug intratumorally injected was 3 mg/kg, while it was 15 mg/kg for each intravenous injection. Tumor progression was monitored by caliper measurement, and body weight and tumor volume were assessed every three days. The experimental end points were tumor volume of 800 mm^3, 20% body weight loss or metastasis-related side effects.

5.13. Statistical Analyses

Statistical analysis was performed using GraphPad Prism, version 7.0a (GraphPad Software, USA). All results are expressed as mean ± standard deviation (SD), except for results arising from *in vitro* and *in vivo* studies which are expressed as mean ± standard error of the mean (SEM). The half maximal inhibitory concentration (IC_{50}) values were calculated using a nonlinear regression log(inhibitor) versus response variable slope. Statistical significance was attained for values of $p < 0.05$ and assessed using two-way ANOVA for the *in vitro* and *in vivo* studies. Survival curves were compared using a Mantel-Cox (log-rank) test and mouse body weight *vs* time were compared using Student's *t*-test. Outliers were calculated using GraphPad software (significance level 0.01, two-sided) and removed from the study.

6. RESULTS AND DISCUSSION

The purpose of the project was to design and develop a library of amphiphilic di-block copolymers able to self-assemble in micellar systems and composed by a hydrophilic block of polyethylene glycol and an amino acid-based block of γ-hydrazinamide-glutamic acid (hydGlu) and Leucine. In particular, hydGlu was selected for the conjugation of Doxorubicin through a pH-cleavable hydrazone bond to allow for a controlled drug release once reached the intracellular acidic compartments, namely endosomes and lysosomes, through cell uptake. Doxorubicin was selected for two specific reasons: firstly, for its well-known anticancer activity and, secondly, to play an active role in the polymer self-assembling step. Leucine was used as a spacer between the glutamic units to minimize the steric hindrance of the drug and to allow its accommodation along the polyaminoacidic chain. Furthermore, Leucine aminoacid, which is a hundred times more hydrophobic with respect to glutamic acid, was selected as functional monomer to modulate the final hydrophobicity of the polyaminoacid block and, thus, the self-assembling features of the resulting di-block copolymer. In virtue of the self-assembling feature of the materials, they are programmed to generate nanoparticulate systems with a flexible and hydrophilic surface (PEG) that allows for its circulation in the bloodstream upon parenteral administration and passive accumulation in the tumor tissue according to the EPR effect.

Molecular structure, physicochemical properties, self-assembling behaviour and the *in vitro* drug release profile of the smart system were assessed. Then, *in vitro* cytotoxicity and internalization of the formulations by CT26 murine colorectal cell line and 4T1 murine mammary carcinoma, selected as models for solid tumors, were evaluated and, finally, the antitumor efficacy of a selected colloidal system was estimated in two different solid tumor models, evaluating two alternative administration routes.

6.1. Synthesis of $mPEG_{5kDa}$-NH_2 macroinitiator

The synthesis of the macroinitiator $mPEG_{5kDa}$-NH_2 was performed following the procedure reported in Scheme 1.

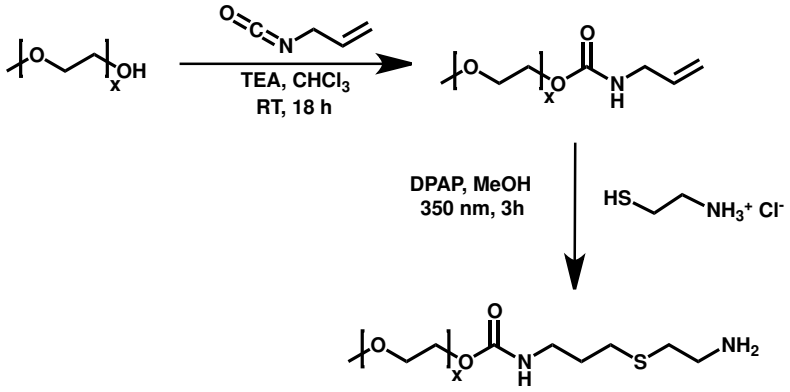

Scheme 4 *Synthesis of $mPEG_{5kDa}$-NH_2.*

$mPEG_{5kDa}$-NH_2 was obtained from $mPEG_{5kDa}$-OH through a two steps synthesis involving the radical addition reaction of cysteamine. In the first step, using TEA as a catalyst, the condensation reaction was performed to convert the reactant into the $mPEG_{5kDa}$-allyl carbamate intermediate. The reaction was monitored through ^{1}H-NMR analysis, evaluating the appearance of the triplet signal (Hb) at 4.22 ppm, indicating the formation of the desired carbamate moiety (Figure 10.).

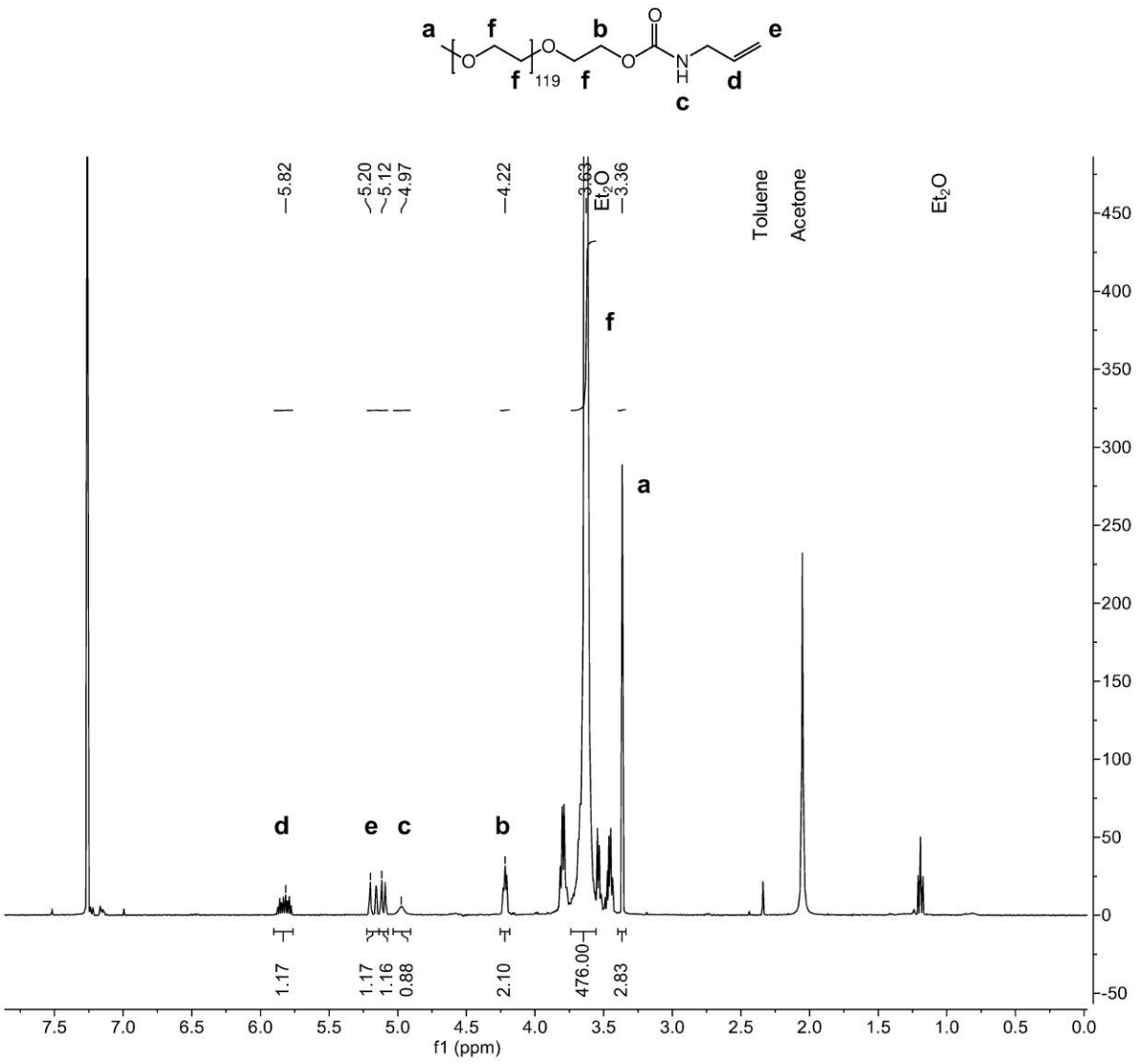

Figure 10. *^{1}H-NMR spectrum of purified mPEG$_{5kDa}$-allyl carbamate in CDCl$_3$.*

The conversion yield of the mPEG$_{5kDa}$-OH to mPEG$_{5kDa}$-allyl carbamate was assessed after purification by comparing the ^{1}H-NMR integrals of the allyl-ending signals (H_c) to the mPEG$_{5kDa}$ ethoxyl protons (H_f), and it was found to be quantitative, as shown also by the proton signal of carbamate group (H_b) integrating for two protons.

The second step of the synthesis involved a click thiol-ene coupling reaction between the intermediate mPEG$_{5kDa}$-allyl carbamate and cysteamine[144], which afforded an anti-Markovnikov thioether adduct where cysteamine was covalently linked to mPEG$_{5kDa}$-allyl carbamate. The photochemical cleavage of the photoinitiator 2,2'-dimethoxy-2-phenylacetophenone (DPAP) was performed by UV light irradiation at 350 nm leading to the formation of radical species[145] that activated cysteamine to react with the allyl moiety .

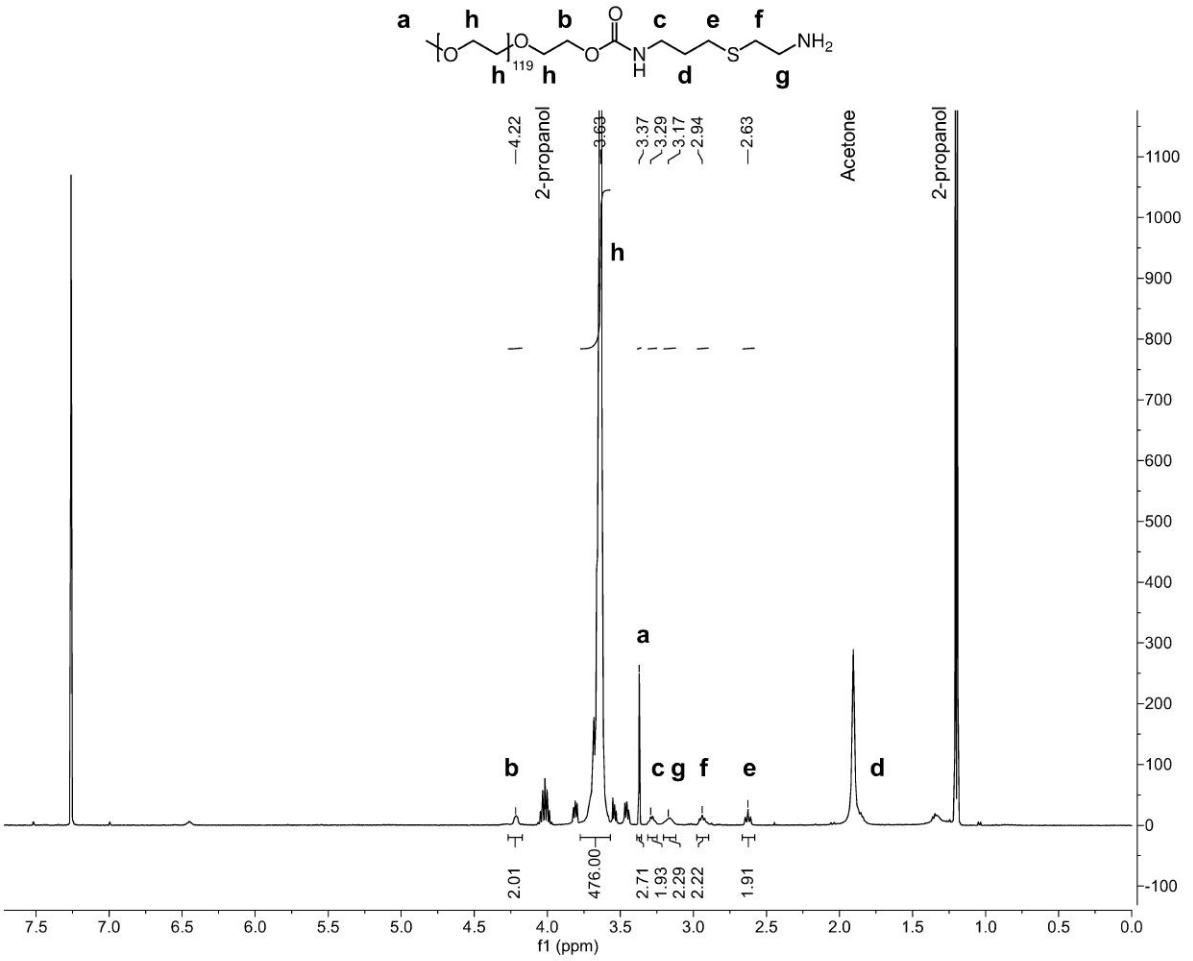

Figure 11. *^{1}H-NMR spectrum of purified mPEG$_{5kDa}$-NH$_2$ in CDCl$_3$.*

Comparing the ^{1}H-NMR integrals (Figure 11.) of the proton signals of the conjugated cysteamine moiety (H_f, H_g) with those of mPEG$_{5kDa}$ (H_h), the conversion yield was found to be quantitative. Furthermore, the disappearance of the vinyl signals of mPEG$_{5kDa}$-allyl carbamate and no traces of cysteamine-derived by-products were detected.

Gel Permeation Chromatography (GPC) analysis was carried out on mPEG$_{5kDa}$-NH$_2$, revealing a well-defined and monodisperse profile, with a low polydispersity index of 1.09. The estimated average molecular weight of 7.3 kDa was found to be slightly higher than expected, due to the fact that the analytical system was calibrated with a different standard, polymethylmetacrylate (PMMA). Finally, the molecular weight of mPEG$_{5kDa}$-NH$_2$ was confirmed by MALDI-TOF analysis showing a bell shape m/z profile centred at 5369, which is in good agreement with the expected molecular weight.

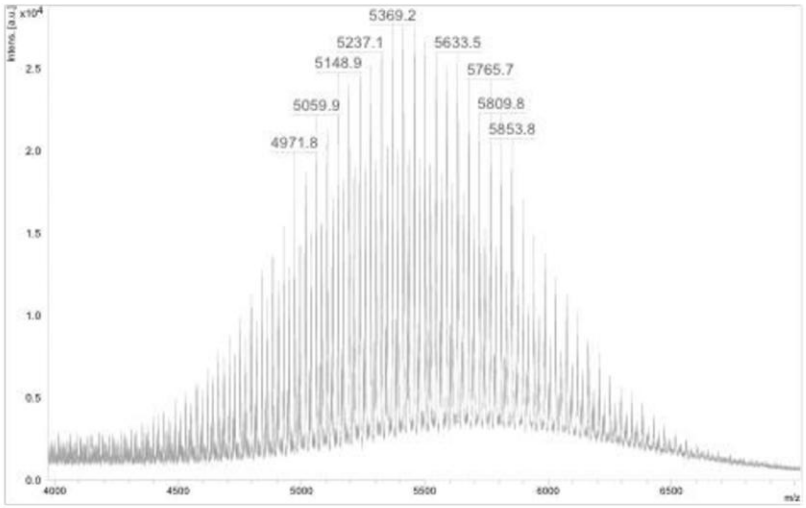

Figure 12. *MALDI-TOF analysis of $mPEG_{5kDa}$-NH_2*

6.2. Synthesis of NCA monomers

To obtain reactive monomers for the polymerization of amphiphilic random di-block co-polymers, N-carboxyanhydride derivatives were synthetized from aminoacid-based commercially available precursors.

Triphosgene was selected as a reactant to generate the required NCA functionality starting from γ-benzyl glutamate and leucine, while α-pinene was added as HCl scavenger to avoid the protonation of the carboxylic group, which would prevent the cyclic anhydride formation[138].

The γ-benzyl ester of glutamic acid was selected to avoid possible side-reactions of the γ-carboxyl group during both the NCA synthesis, where it could react with triphosgene, and the following polymerization reactions. Furthermore, as shown previously by our group, γ-benzyl ester of glutamic acid can be easily converted by post-polymerization deprotection into the corresponding γ-hydrazide moiety by treatment with an excess of hydrazine hydrate, allowing drug conjugation upon formation of the pH cleavable hydrazone bond.

6.2.1. Synthesis of γ-benzyl glutamate NCA monomer

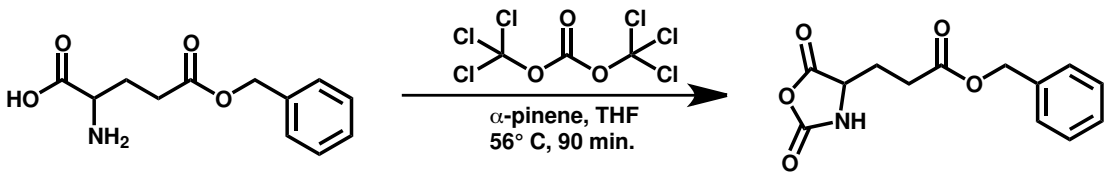

***Scheme 5**. Synthesis of γ-benzyl glutamate NCA monomer.*

The synthesis of Glu-NCA was carried out in THF at 56°C until the reaction suspension became a clear and yellowish solution, indicating that γ-benzyl glutamate, which is not completely soluble in THF, was converted into the completely soluble desired product (Scheme 5). The identity of the NCA derivate was confirmed by the shift of the α-proton to 4.46 ppm in the ^{1}H-NMR spectrum (Figure 13.) and the presence of the anhydride carbonyl groups signals at 172.51 ppm and 152.06 ppm in ^{13}C-NMR spectrum (Figure 14.).

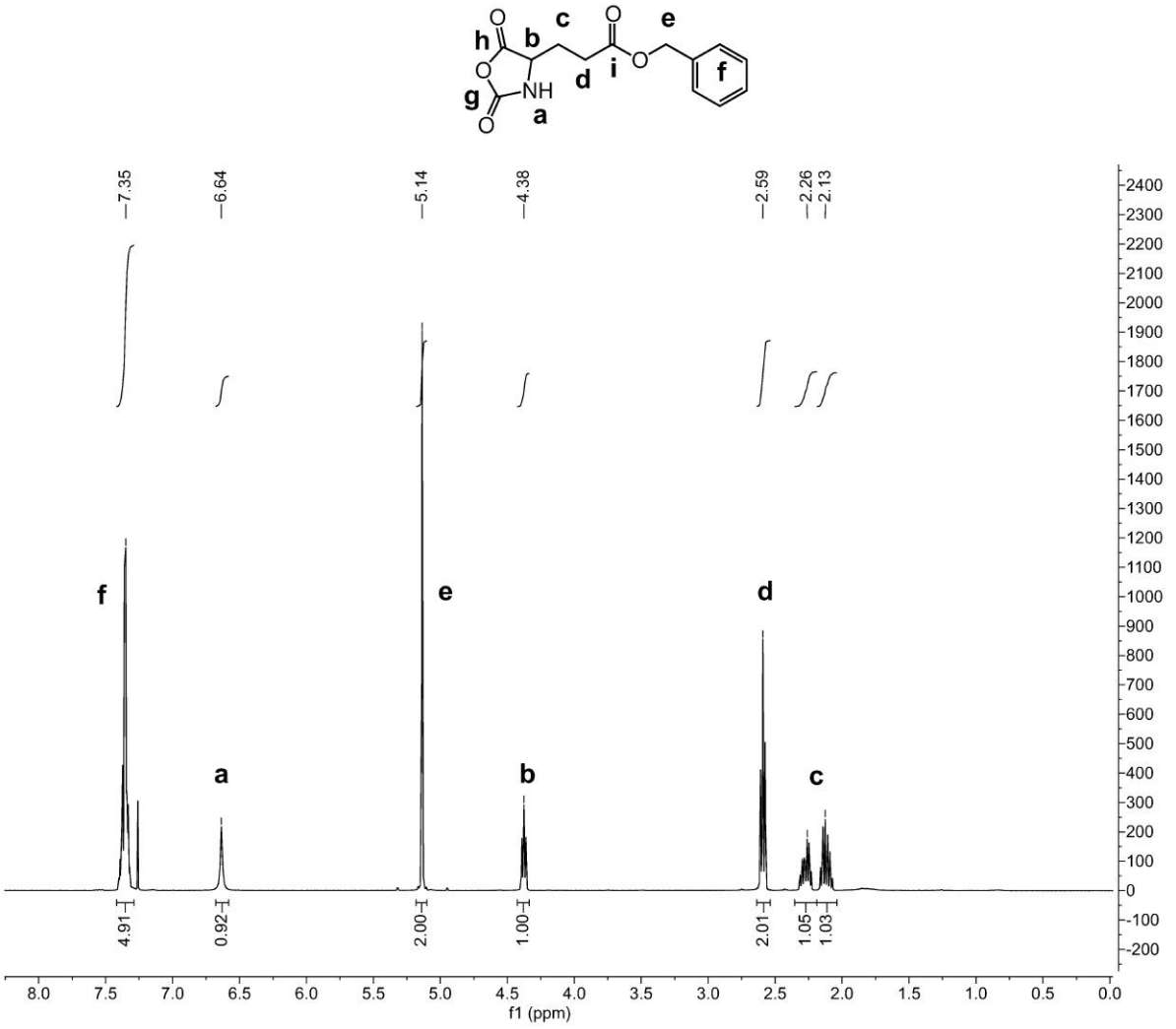

Figure 13. *^{1}H-NMR spectrum of γ- benzyl glutamate NCA in $CDCl_3$.*

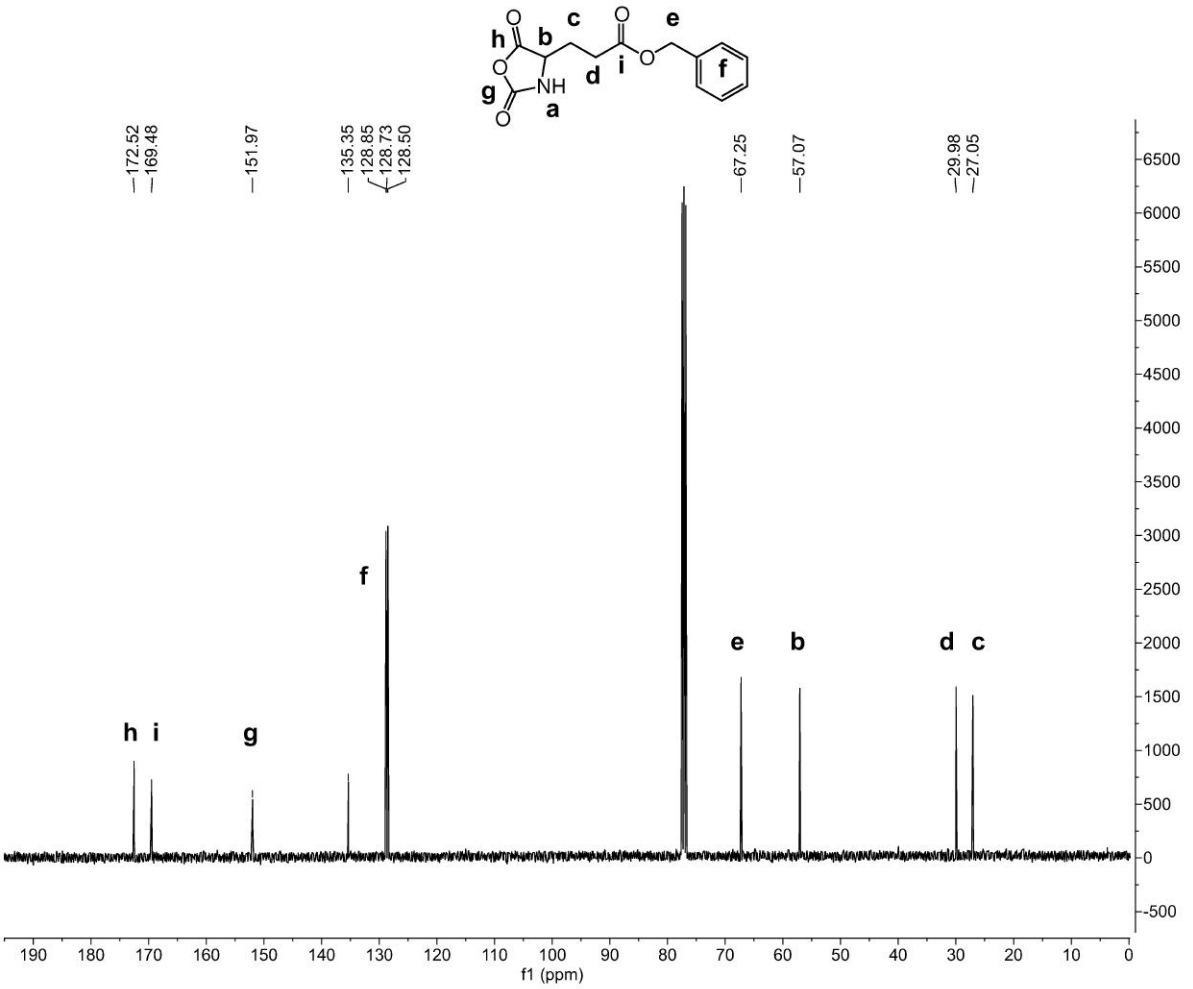

Figure 14. *^{13}C-NMR spectrum of γ- benzyl glutamate NCA in $CDCl_3$.*

Notably, no signals of the open form of γ- benzyl glutamate were detected, which support for the purity of the crystallized product. Moreover, Figure 15., showing the FT-IR spectra of γ-benzyl glutamate (A) and γ- benzyl glutamate NCA (B), revealed two bands at 1772 and 1718 cm^{-1} corresponding to the anhydride carbonyl groups, and the reduction of the large peak at 3100 $cm^{-1,}$ corresponding to the NH and OH stretching bands of the γ-benzyl glutamate, confirmed the anhydride formation and the cyclization of the monomer.

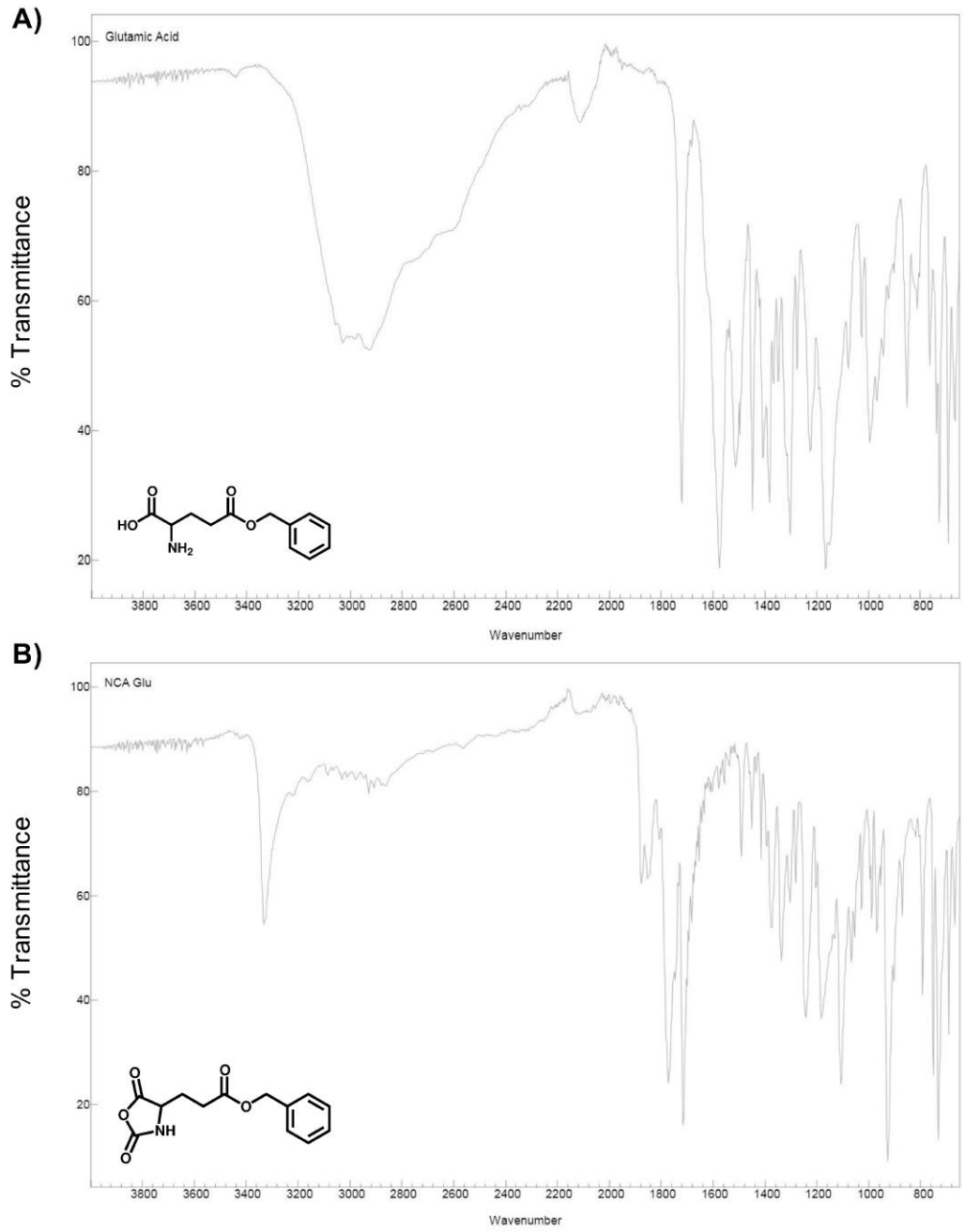

Figure 15. *FT-IR spectrum of γ-benzyl glutamate (A) and γ-benzyl glutamate NCA (B).*

6.2.2. Synthesis of Leucine NCA monomer

Leu-NCA synthesis was performed using the same synthetic procedure employed for Glu-NCA. (Scheme 6).

Leucine was found to be insoluble in most of organic solvents. Despite this, tetrahydrofuran (THF) was found to dissolve the aminoacid to a portion that still allowed the reaction to proceed.

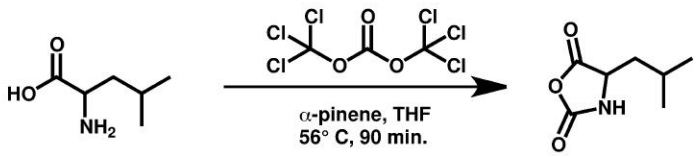

Scheme 6. *Synthesis of Leucine NCA monomer.*

The pure NCA derivative was recovered after precipitation in petroleum ether, and its purity was established by ^{1}H-NMR analysis (Figure 16.), which revealed the shift of the α-proton signal corresponding to the open form of the aminoacid in the 3.5-4 ppm range, to 4.33 ppm corresponding to the α-proton in the cyclic form (H_b).

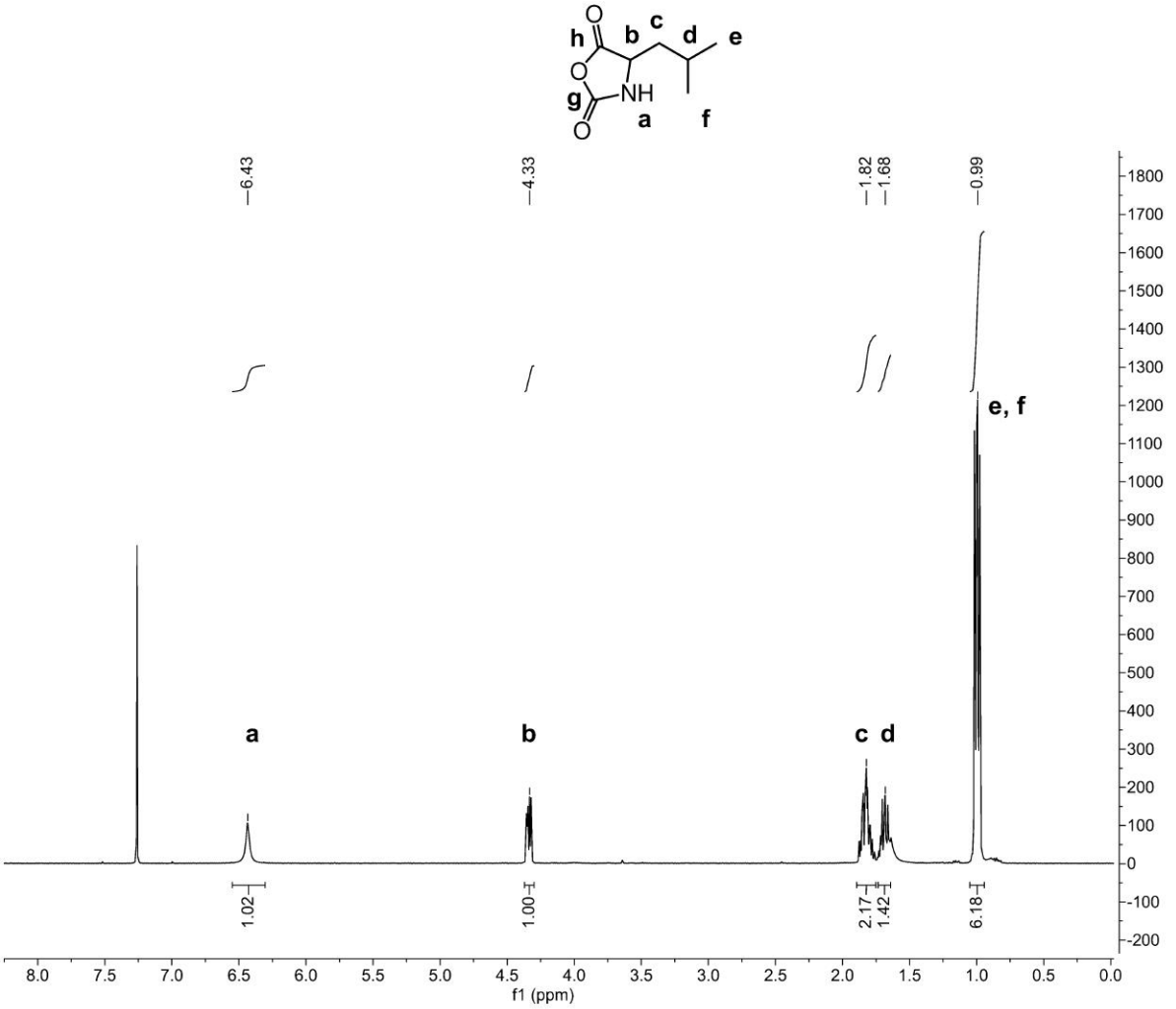

Figure 16. *^{1}H-NMR spectrum of Leucine NCAin $CDCl_3$.*

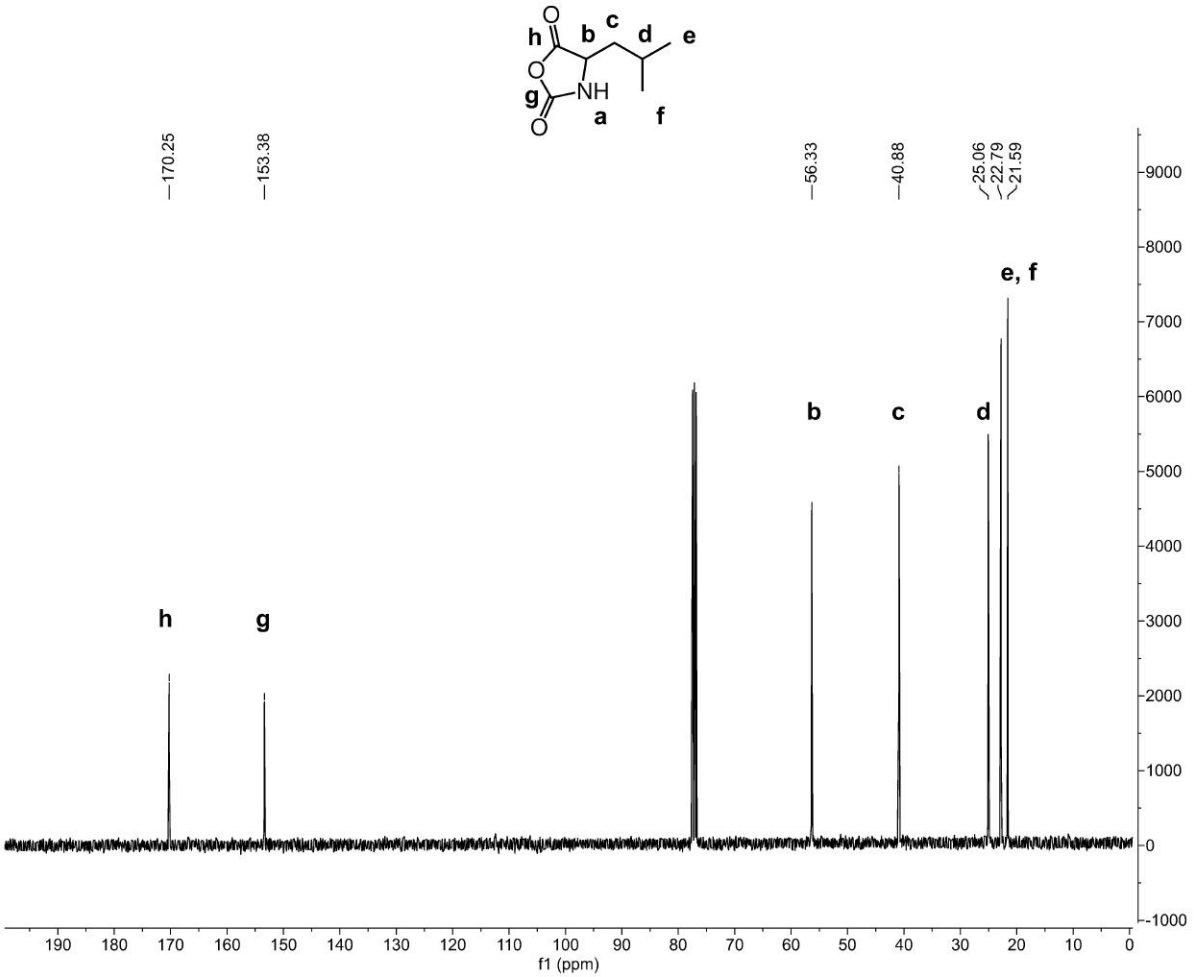

Figure 17. *^{13}C-NMR spectrum of Leucine NCAin $CDCl_3$.*

Furthermore, the carbon signals at 170.25 ppm (Ch) and 153.38 ppm (Cg) in the ^{13}C-NMR (Figure 17.) and the two stretching bands at 1798 and 1750 cm^{-1} corresponding to the anhydride carbonyl groups in the FT-IR spectrum (Figure 18.) endorsed the conversion into the anhydride form.

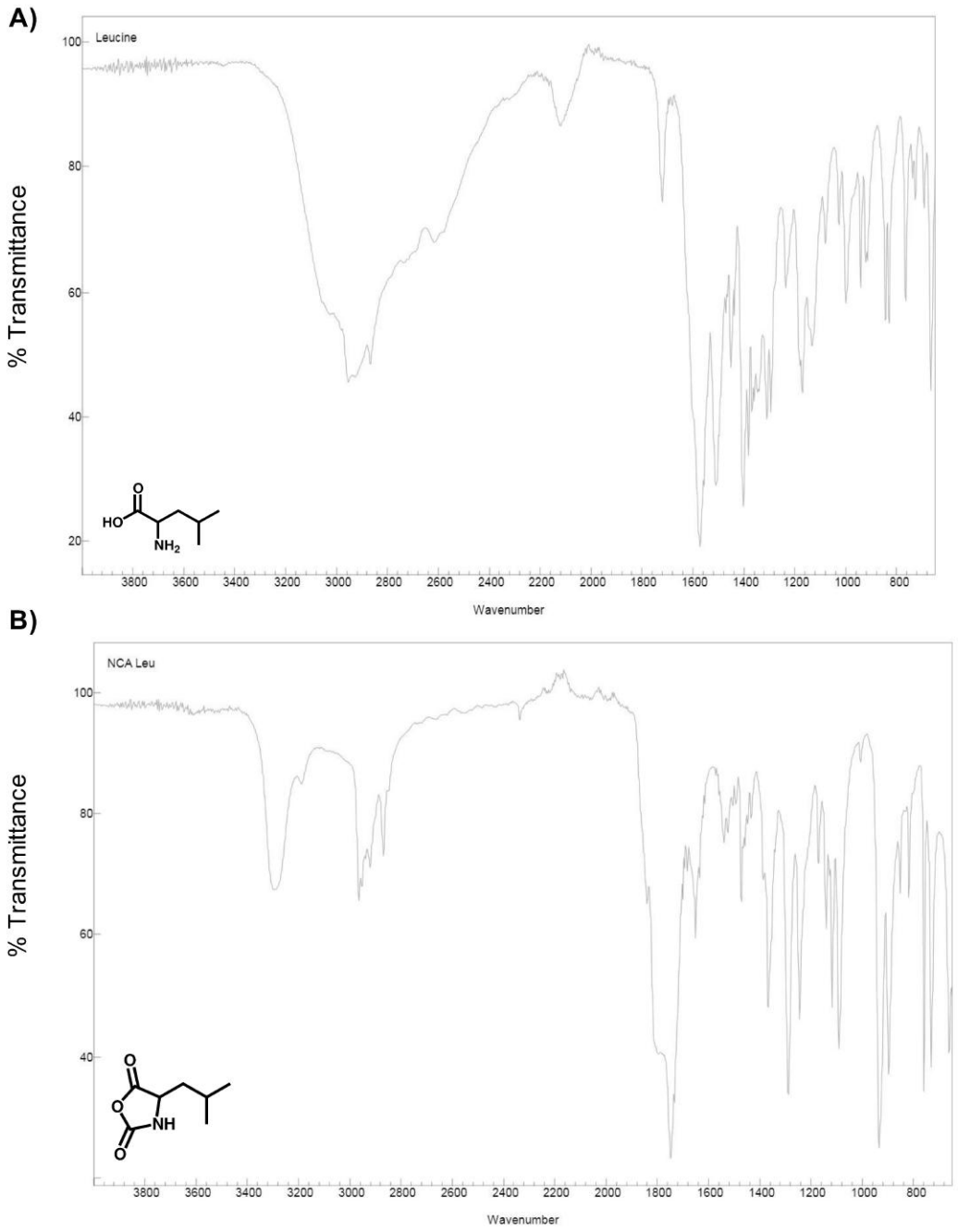

Figure 18. *FT-IR spectrum of Leucine (A) and Leucine NCA (B).*

Leu-NCA was chosen as a constituent of the polyaminoacidic block of the di-block copolymer to act as a spacer between the drug conjugated glutamic monomers, thus reducing the steric hindrance of sequential drug molecules, and to increase the hydrophobic character of the polyaminoacidic block of polymer chains. As reported in literature[146], a low Doxo conjugation to the glutamic moieties could be due to steric hindrance, limiting the conjugation efficiency. Thus, the inclusion of Leucine monomers in the polymeric backbone ensures the

polyaminoacidic block hydrophobic feature and the consequent self-assembling into colloidal structures and, in addition, it could increase drug conjugation efficiency.

6.3. Synthesis of mPEG$_{5kDa}$-b-(γ-hyd-Glu$_n$-r-Leu$_m$) random copolymers

A library of four di-block random copolymers with a mPEG$_{5kDa}$-b-(γ-benzyl-Glu$_n$-r-Leu$_m$) generic structure was synthetized through Ring Opening Polymerization[109], as reported in Scheme 7, taking into account that the 55-70 % w/w total weight of the polymer should be constituted by the hydrophilic block to obtain self-assembling colloidal systems[147].

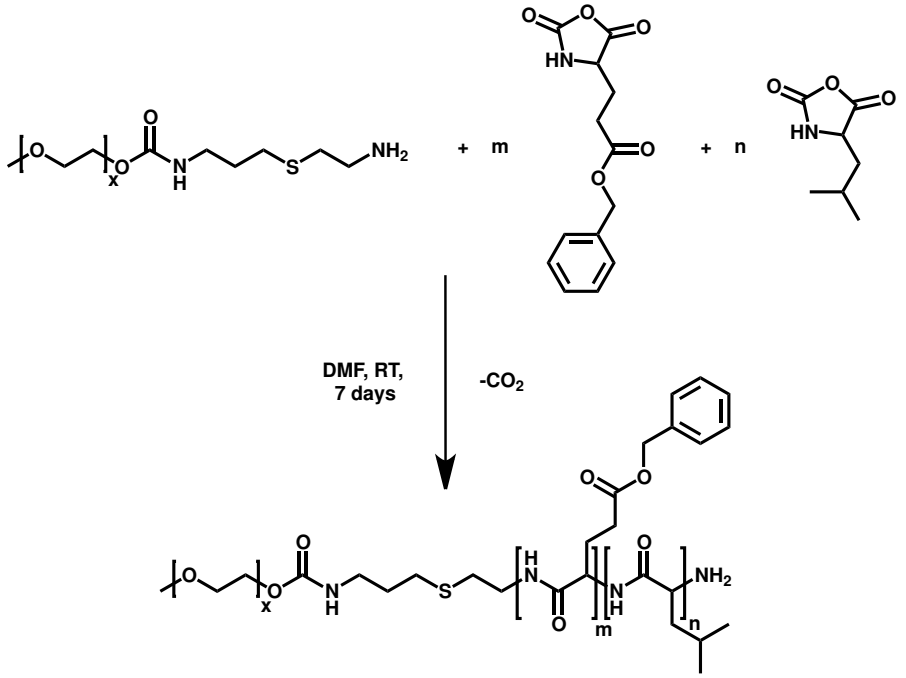

***Scheme 7**. Synthesis of mPEG$_{5kDa}$-b-(γ-benzyl-Glu$_n$-r-Leu$_m$)polymer set through Ring Opening Polymerization.*

As a consequence, the copolymer has been designed starting from mPEG$_{5kDa}$-NH$_2$ as hydrophilic block conjugated to a polyaminoacidic block made of nearly 16 aminoacidic units at a different hydGlu:Leu ratios, namely 16:0, 8:8, 6:10, 4:12, in order to generate a set of materials with different feature, namely different spacer length between sequential glutamic monomers, and select the best performing in terms of drug conjugation yield, self-assembling behaviour, and suitable biopharmaceutical properties, including stability, pH sensible drug release, and *in vitro* and *in vivo* activity.

The Ring Opening Polymerization reaction proceeds through the "Normal Amine Mechanism", in which the primary amine of the mPEG$_{5kDa}$-NH$_2$ macroinitiator acts as a nucleophile towards

the carbonyl group of the NCA monomer, leading to the opening of the NCA ring and the elimination of carbon dioxide (CO_2)[107,109]. This mechanism generates a NH_2 terminal group that can further react with other NCA monomers, allowing the propagation of the reaction.

To assess the monomer conversion, a preliminary reaction was carried out using 20 equivalents of both Glu-NCA and Leu-NCA monomers leading to the formation of $mPEG_{5kDa}$-b-(γ-benzyl-Glu_{18}-r-Leu_{14}). The resulting monomer conversion of 90% and 70% for Glu-NCA and Leu-NCA, respectively, was taken into account to perform the synthesis of the desired di-block copolymers and the monomer feed ratios were adjusted accordingly.

The copolymers were successfully synthetized and ^{1}H-NMR analysis was performed to quantify the aminoacidic monomer units per polymer chain using the ethoxyl proton singlet of mPEG (H_b) as an internal reference (476 protons). Leu integrals, H_k and H_i, and γ-benzyl-Glu integrals, H_g and H_d, referring to the proton signals of Leu and γ-benzyl-Glu lateral chains, were compared to H_b PEG integral providing the number of each aminoacidic monomer in the polyaminoacidic block. The ^{1}H-NMR spectra (Figures 19., 20., 21. and 22.) of the purified products confirmed the identity of the desired polymers since the number of the monomers corresponded to the aimed ratio.

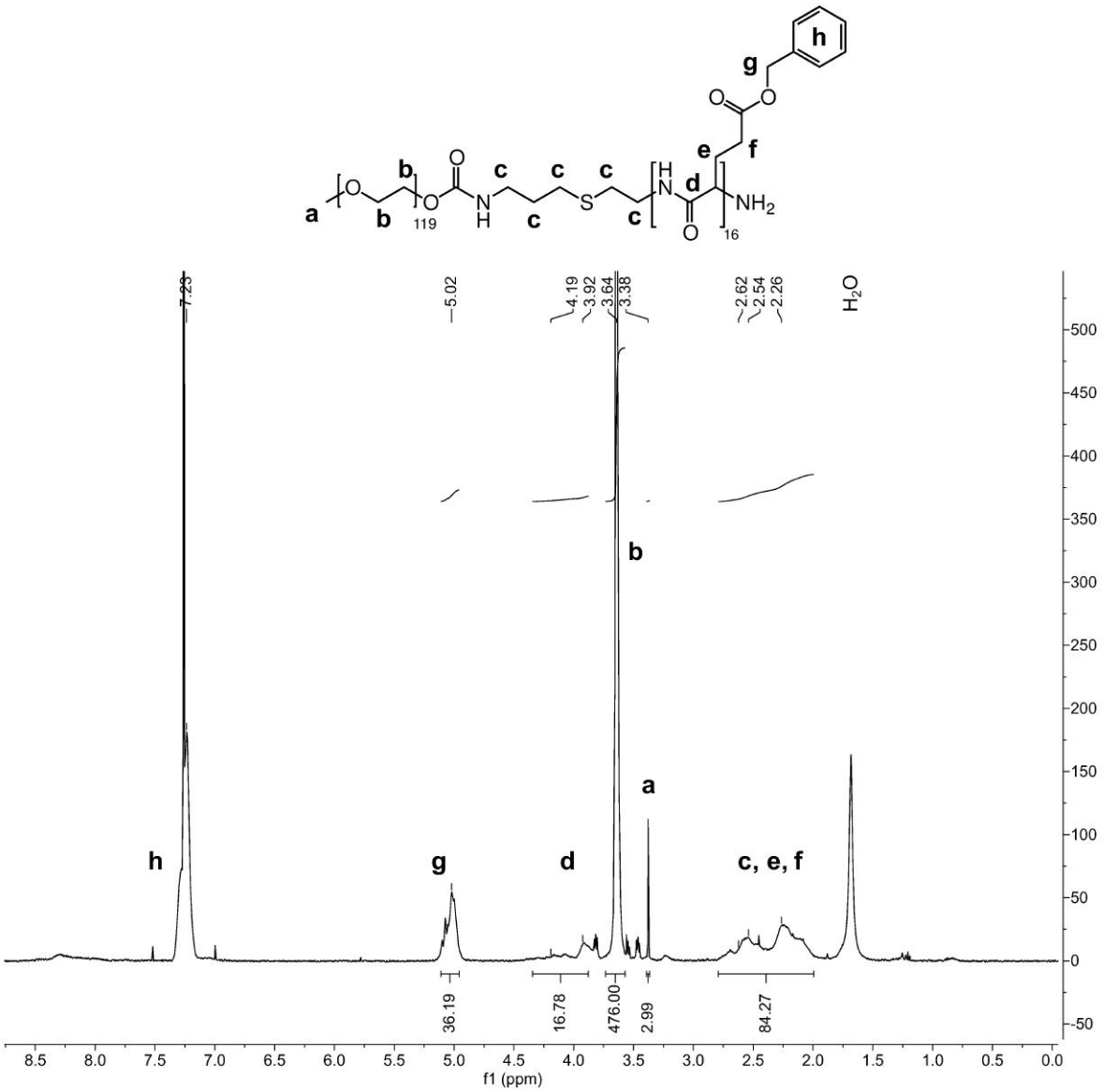

Figure 19. *^{1}H-NMR spectrum of purified $mPEG_{5kDa}$-b-(γ-benzyl-Glu_{16}) in $CDCl_3$.*

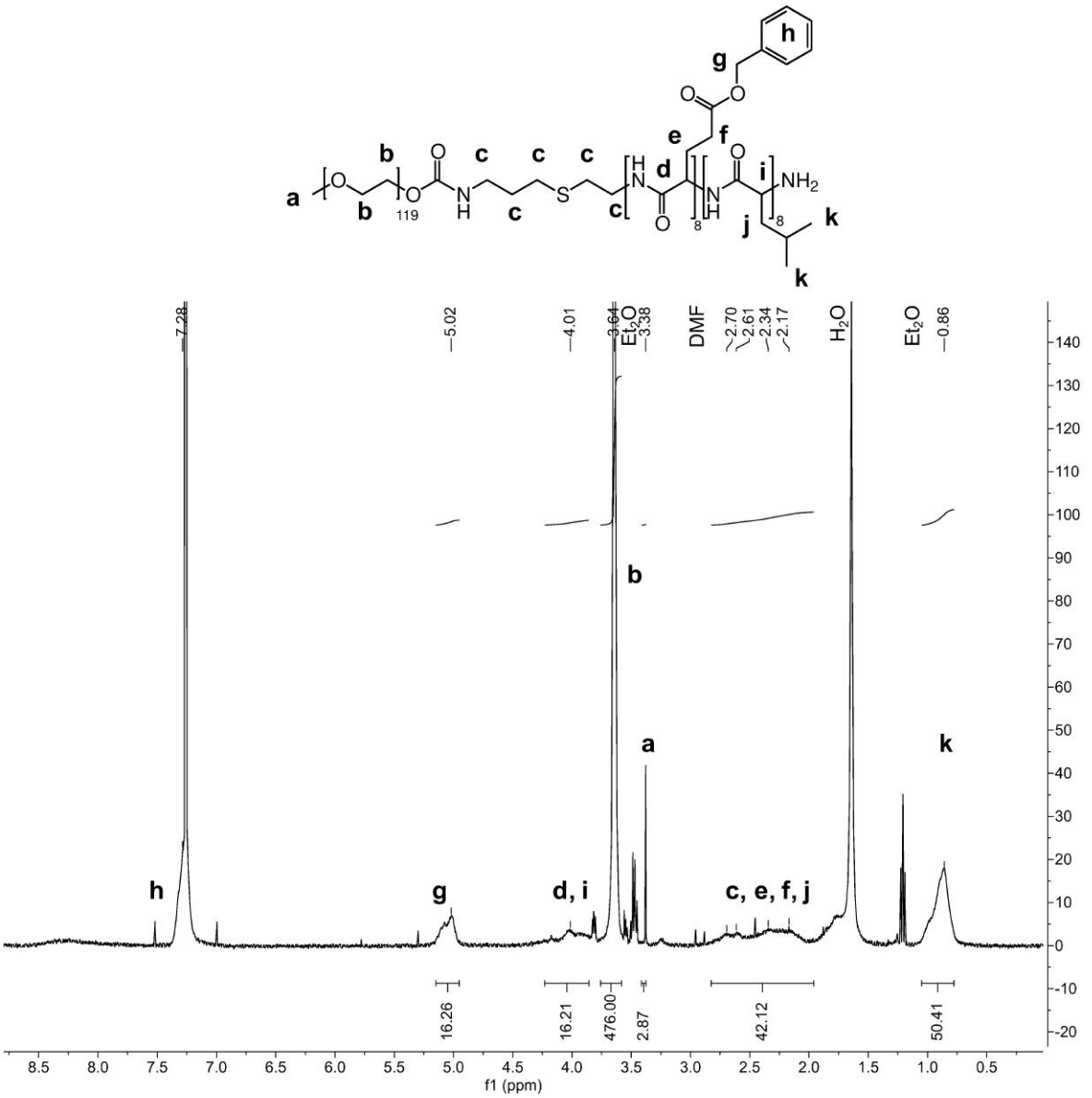

Figure 20. *^{1}H-NMR spectrum of purified $mPEG_{5kDa}$-b-(γ-benzyl-Glu_8-r-Leu_8) in $CDCl_3$*

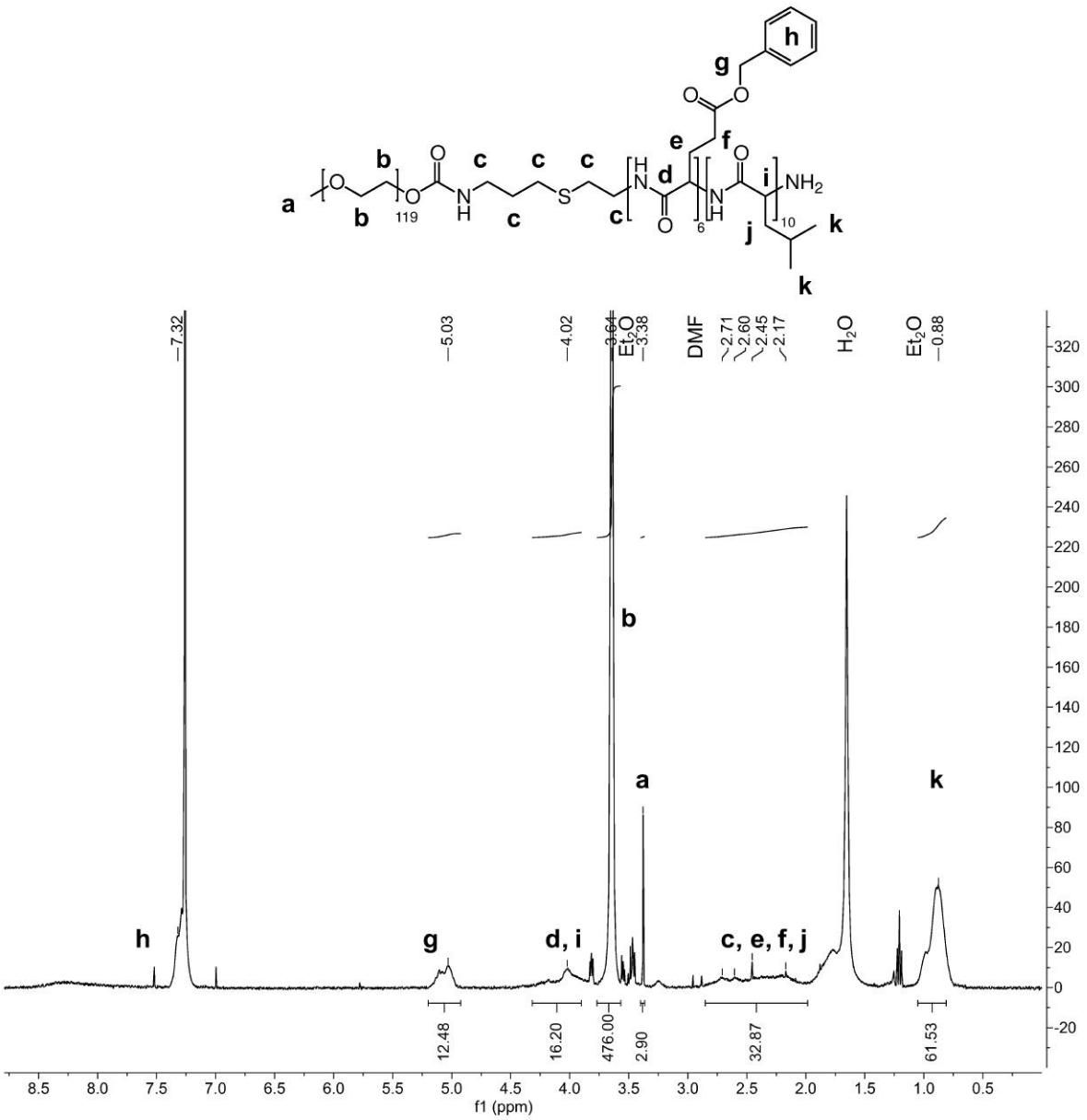

Figure 21. *^{1}H-NMR spectrum of purified $mPEG_{5kDa}$-b-(γ-benzyl-Glu_6-r-Leu_{10}) in $CDCl_3$.*

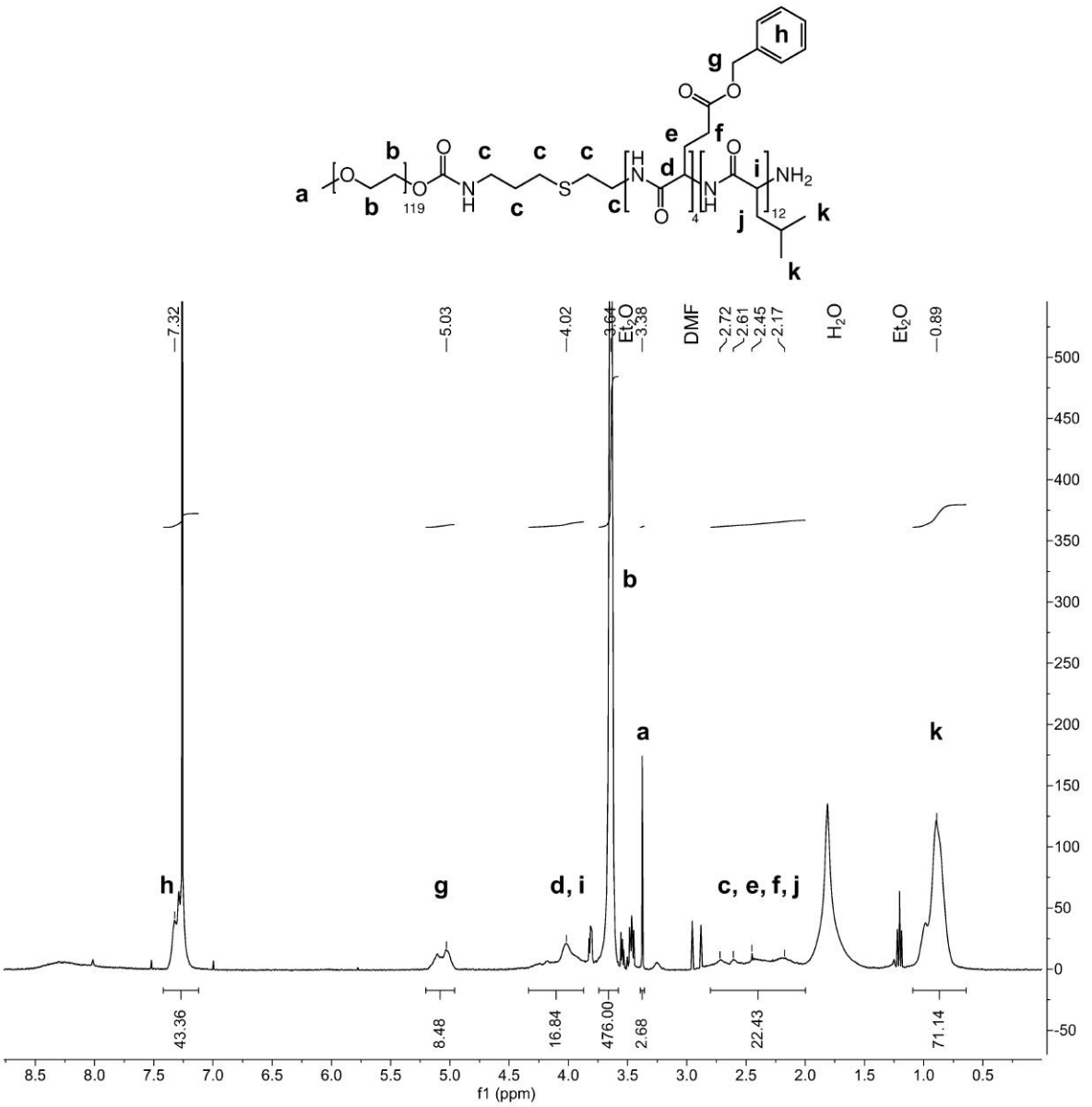

Figure 22. *^{1}H-NMR spectrum of purified mPEG$_{5kDa}$-b-(γ-benzyl-Glu$_4$-r-Leu$_{12}$) in CDCl$_3$.*

Furthermore, GPC analyses in DMF added of 0.1% LiBr were carried out to confirm the purity of the synthetized copolymers and to evaluate the polydispersity index. The analyses showed that the obtained molecular weight for PEG$_{5kDa}$-b-(γ-benzyl-Glu$_{16}$), mPEG$_{5kDa}$-b-(γ-benzyl-Glu$_8$-r-Leu$_8$), mPEG$_{5kDa}$-b-(γ-benzyl-Glu$_6$-r-Leu$_{10}$), mPEG$_{5kDa}$-b-(γ-benzyl-Glu$_4$-r-Leu$_{12}$) were 12.2 kDa (Đ 1.07), 10.5 kDa (Đ 1.11), 10.4 kDa (Đ 1.09) and 9.9 kDa (Đ 1.08) respectively, in good agreement with the calculated ones and showing a narrow molecular weight distribution.

In order to conjugate Doxo to the di-block copolymers, the γ-benzyl protecting group of the glutamic monomers was substituted with hydrazine hydrate through an ester-amide exchange aminolysis reaction[99] (Scheme 8).

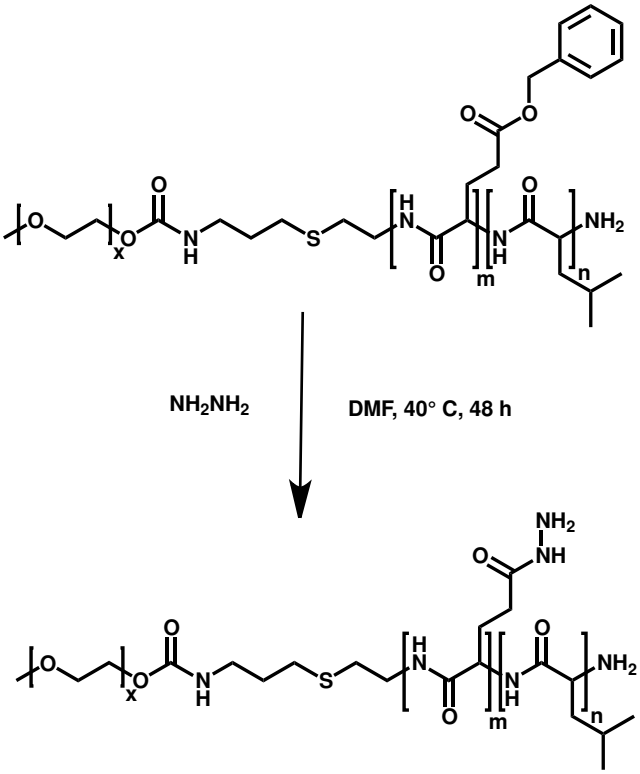

Scheme 8. *Synthesis of $mPEG_{5kDa}$-b-(γ-hyd-Glu_n-r-Leu_m).*

All polymers were characterized by ^{1}H-NMR spectroscopy (Figure 23., 24., 25., 26.), that displayed the absence of proton signals at 7 ppm and 5 ppm of the γ-benzyl group, confirming the complete conversion in γ-hydrazide group, and by GPC analysis, showing a slight increase in the polymer polydispersity as compared to the γ-benzyl-Glu protected analogues.

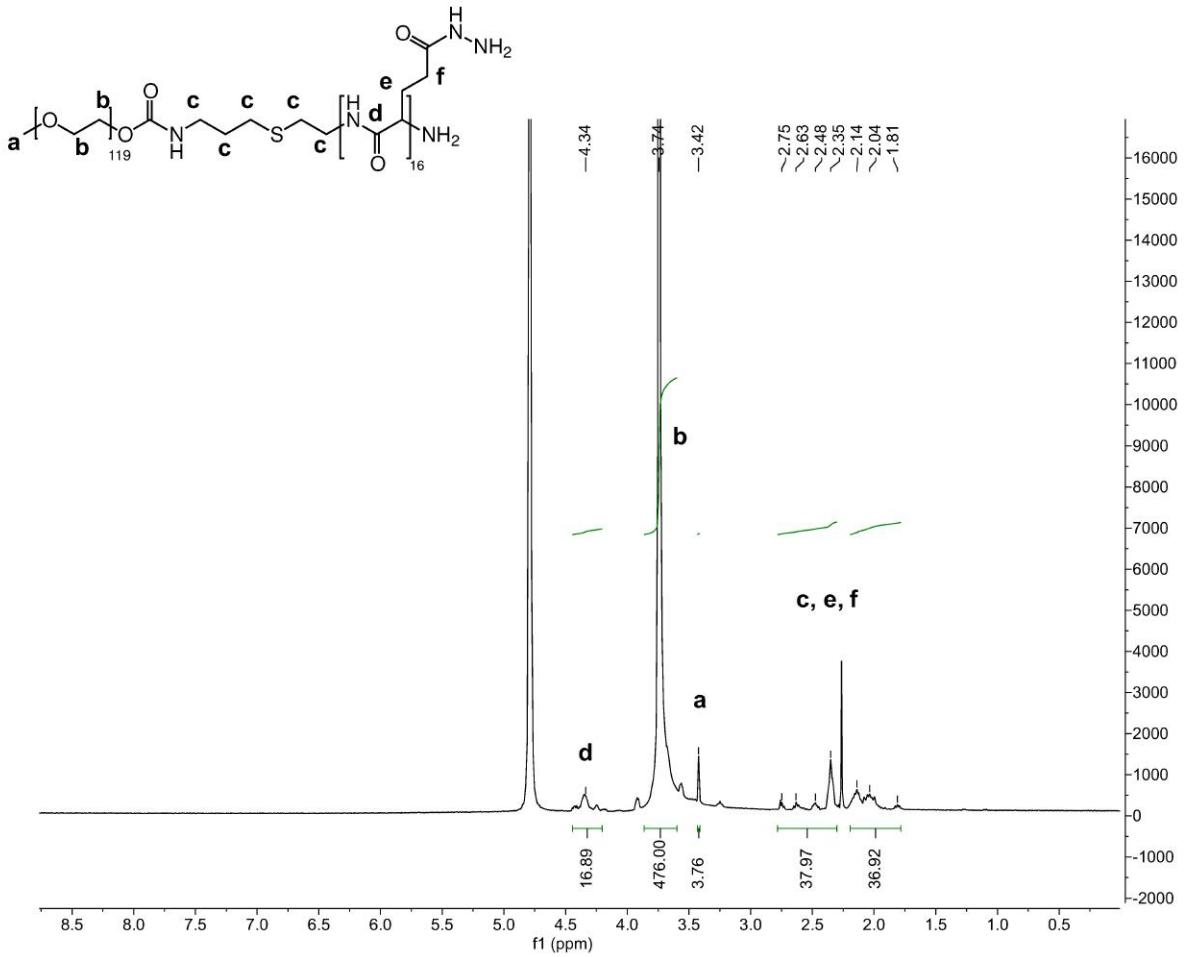

Figure 23. *^{1}H-NMR spectrum of $mPEG_{5kDa}$-b-(γ-hyd-Glu_4-r-Leu_{12}) in D_2O.*

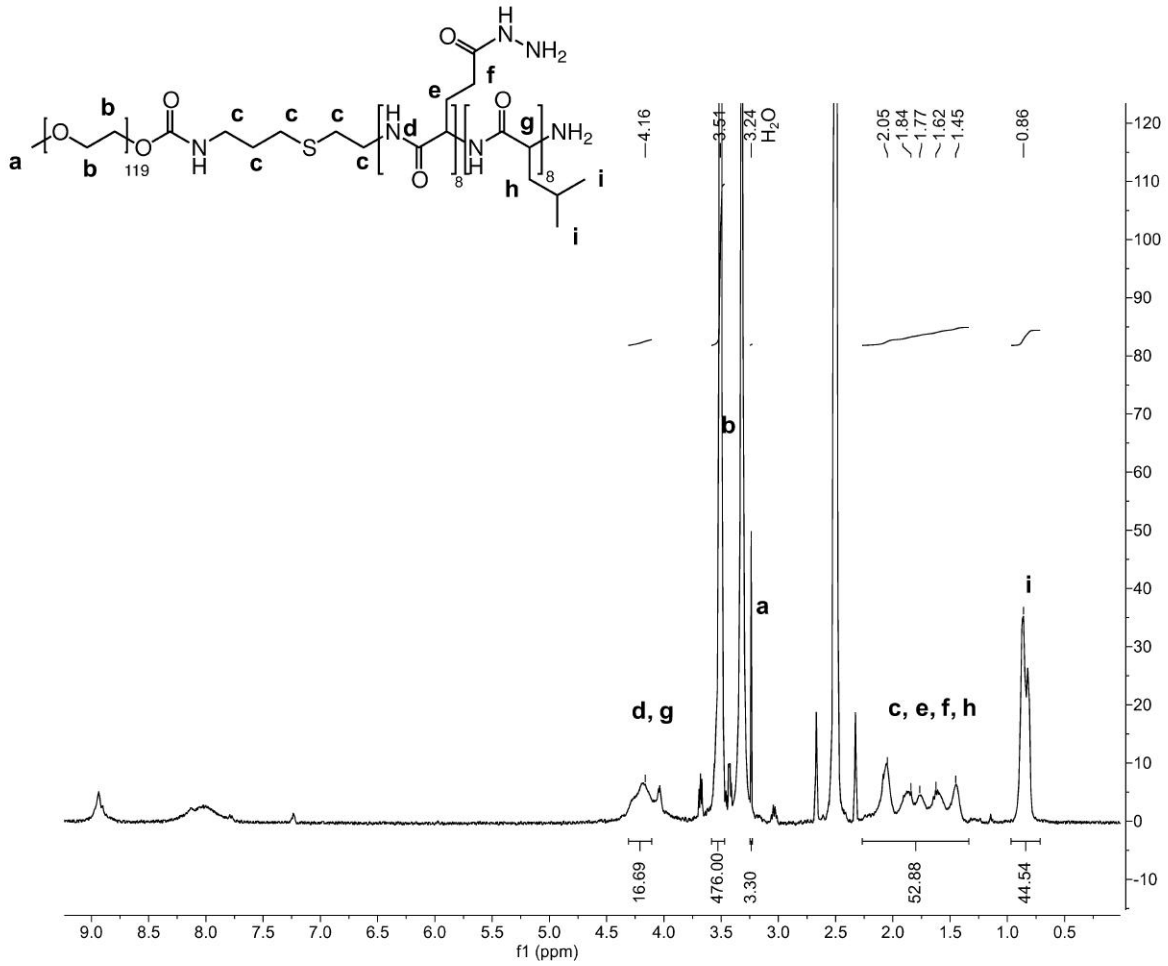

Figure 24. *^{1}H-NMR spectrum of mPEG$_{5kDa}$-b-(γ-hyd-Glu$_4$-r-Leu$_{12}$) in DMSO-d$_6$.*

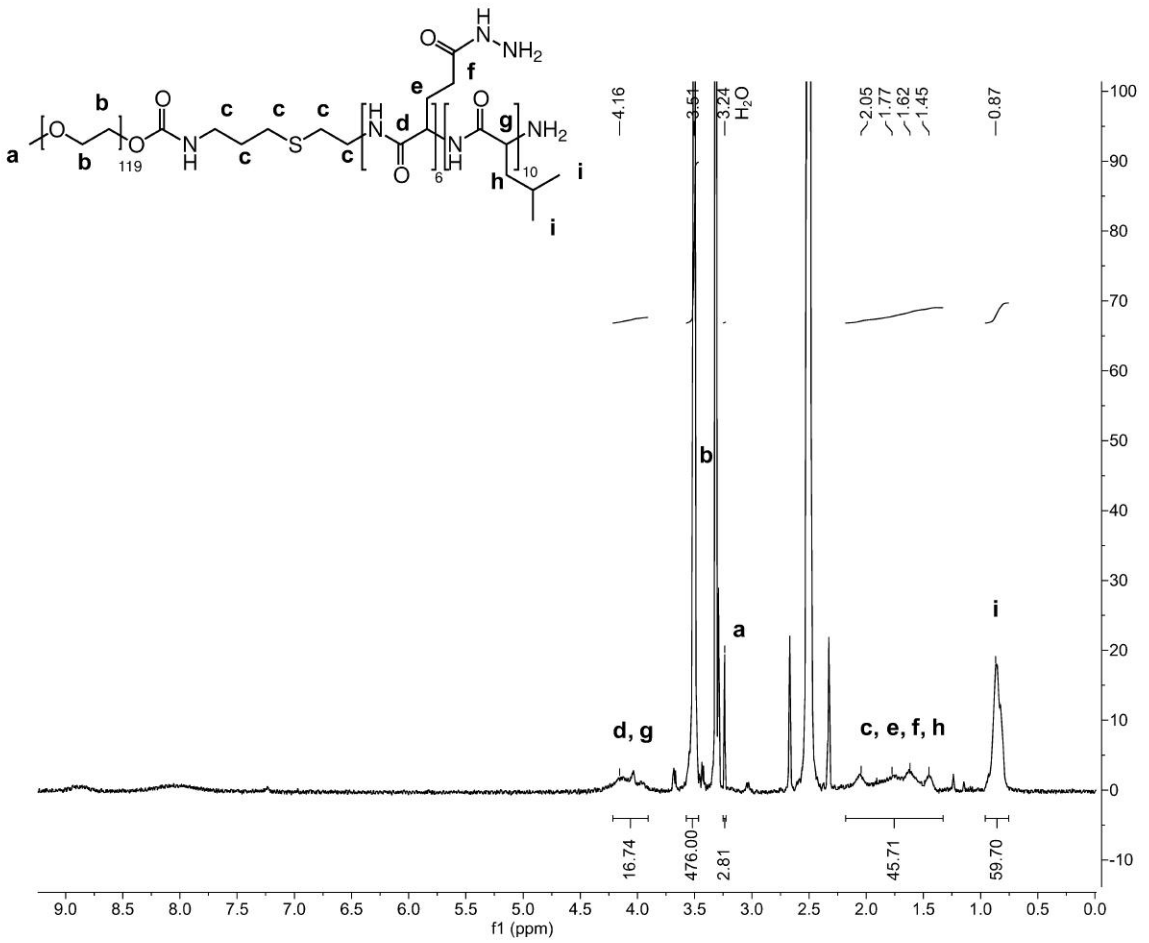

Figure 25. *^{1}H-NMR spectrum of $mPEG_{5kDa}$-b-(γ-hyd-Glu_4-r-Leu_{12}) in DMSO-d_6.*

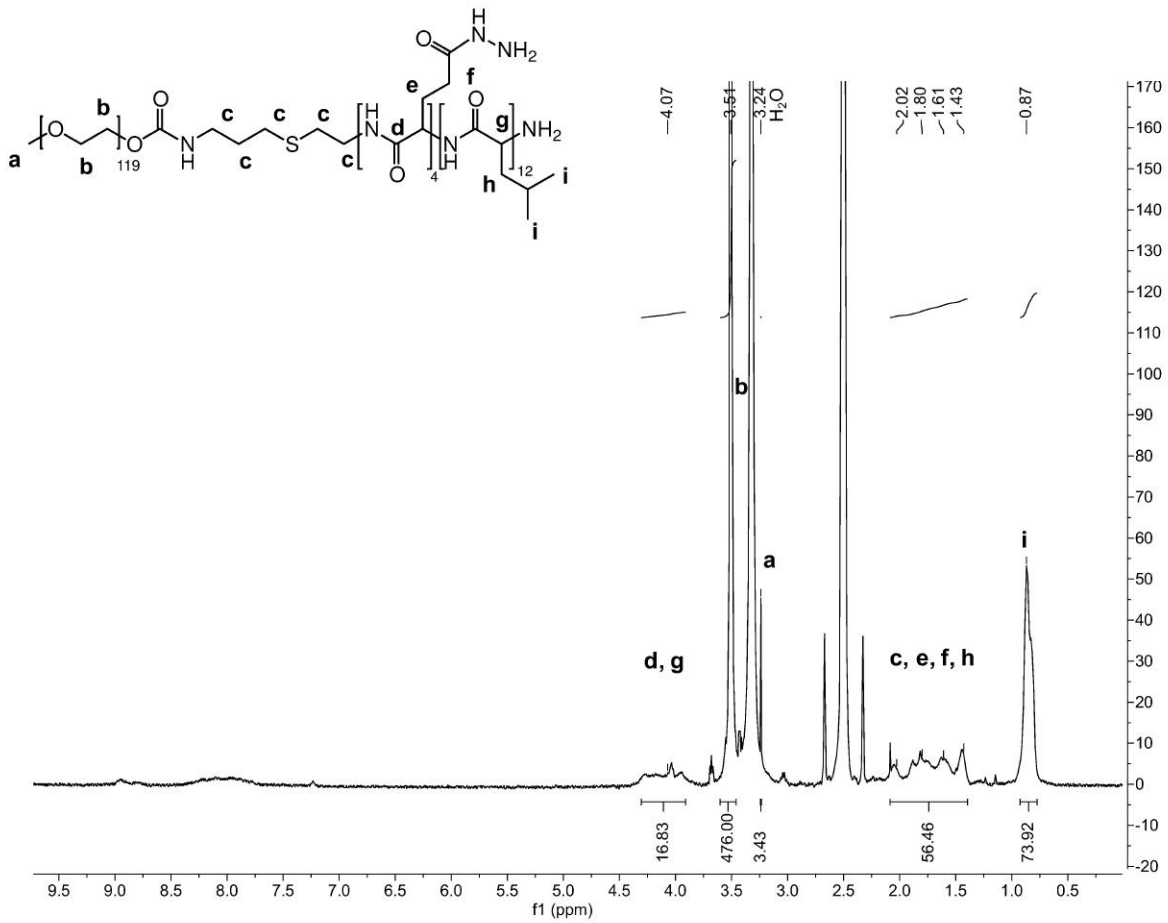

Figure 26. *^{1}H-NMR spectrum of mPEG$_{5kDa}$-b-(γ-hyd-Glu$_4$-r-Leu$_{12}$) in DMSO-d$_6$.*

Furthermore, Iodine assay and the modified protocol of the Snyder's assay[135] (paragraph 5.3.2.) were employed to confirm the number of γ-hydrazide moieties per polymer chain. The molar ratio between hydrazide group and PEG was found to be as expected and in agreement with the ^{1}H-NMR analysis.

6.4. Conjugation of Doxorubicin HCl to mPEG$_{5kDa}$-b-(γ-hydGlu$_n$-r-Leu$_m$) random copolymers

Doxorubicin was conjugated to the mPEG$_{5kDa}$-b-(γ-hyd-Glu$_n$-r-Leu$_m$) copolymers library through hydrazone bond formation, as reported in Scheme 9., involving a single step procedure where TFA was added as an acid catalyst.

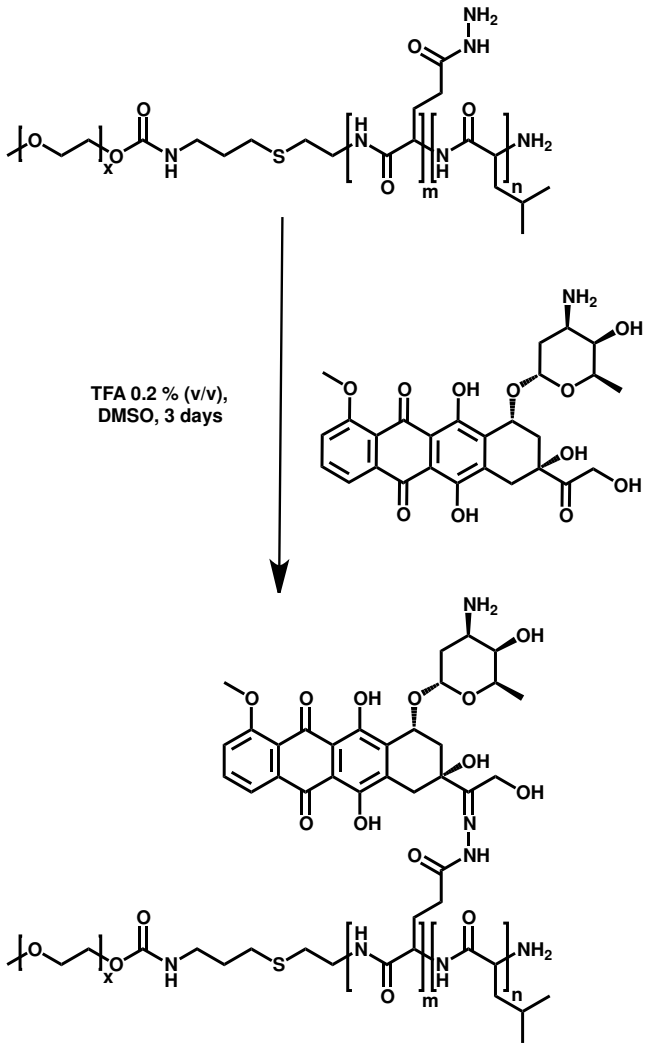

Scheme 9. *Doxorubicin conjugation to $mPEG_{5kDa}$-b-(γ-hyd-Glu_n-r-Leu_m) polymers.*

After the conjugation reaction a dialysis process was performed to purify the copolymer conjugates from the unreacted drug. The purification process was monitored by TLC in MeOH after pretreatment with 5% (v/v) TEA in MeOH, until disappearance of the unconjugated drug spot. The conjugation degree was then assessed by UV-Vis analysis at 488 nm and by Iodine assay, for the detection of Doxo and PEG, respectively, resulting in a drug content of 34% (w/w) for $mPEG_{5kDa}$-b-(γ-hyd[Doxo]-Glu_{16}), 30% (w/w) for $mPEG_{5kDa}$-b-(γ-hyd[Doxo]-Glu_8-r-Leu_8), 29% (w/w) for $mPEG_{5kDa}$-b-(γ-hyd[Doxo]-Glu_6-r-Leu_{10}) and 24% (w/w) for $mPEG_{5kDa}$-b-(γ-hyd[Doxo]-Glu_4-r-Leu_{12}).

The high conjugation degree achieved for $mPEG_{5kDa}$-b-(γ-hyd[Doxo]-Glu_4-r-Leu_{12}), $mPEG_{5kDa}$-b-(γ-hyd[Doxo]-Glu_6-r-Leu_{10}) and $mPEG_{5kDa}$-b-(γ-hyd[Doxo]-Glu_8-r-Leu_8), which were 100%, 87.5%, 70% respectively, highlighted the key role of Leucine as a spacer between Glutamic monomers, allowing a more efficient drug functionalization of the polymers with

respect to the $mPEG_{5kDa}$-b-(γ-hyd[Doxo]-Glu_{16}), that showed a low conjugation yield of 43.75%.

Previous studies revealed that a high Doxorubicin drug loading could induce the formation of insoluble products or macroaggregates[148]. The high drug conjugation achieved with DoxoMC-E_4L_{12}, combined with the high leucine content, which increases the hydrophobicity of the polyaminoacidic block, yielded to a poorly soluble bioconjugate, resulting in the tendency to generate aggregates. For these reasons, this formulation was considered not suitable for *in vitro* and *in vivo* applications, thus it was not included in further tests.

6.5. Characterization of the micellar drug delivery systems

The colloidal characterization of micelles assembled with $mPEG_{5kDa}$-b-(γ-hyd-Glu_n-r-Leu_m) and $mPEG_{5kDa}$-b-(γ-hyd[Doxo]-Glu_n-r-Leu_m), namely MC-E_nL_m and DoxoMC-E_nL_m, were performed by using dynamic light scattering (DLS), zeta potential (ZP) and transmission electron microscopy (TEM) to assess the size, morphology and charge of the polymeric systems. Data are summarized in Table 1.

Table 1. *Hydrodynamic diameter (d_H) and PDI obtained through DLS analysis, diameter determined by TEM analysis (d_{TEM}) and zeta potential (ZP) of DoxoMC-E_nL_m and MC-E_nL_m assemblies. (N.D. means Not Determined).*

	d_H (nm)	PDI	d_{TEM} (nm)	ZP (mV)
DoxoMC-E_{16}	41.6 ± 4.9	0.35 ± 0.08	38.4 ± 4.5	+3.20 ± 0.382
DoxoMC-E_8L_8	29.2 ± 1.1	0.46 ± 0.02	26.5 ± 3.0	+4.25 ± 0.246
DoxoMC-E_6L_{10}	33.3 ± 5.3	0.49 ±0.05	23.8 ± 3.0	+5.64 ± 0.349
MC-E_{16}	-	-	-	-1.65 ± 0.568
MC-E_8L_8	51.0 ± 4.2	0.46 ± 0.08	N.D.	-0.673 ± 0.210
MC-E_6L_{10}	50.2 ± 4.1	0.48 ± 0.05	N.D.	-0.946 ± 0.539
MC-E_4L_{12}	39.2 ± 5.6	0.41 ± 0.07	N.D.	-0.414 ± 0.202

DLS analyses were performed in PBS to estimate the colloidal features of the nanosystems under physiological conditions. As expected and shown in Table 1, the MC-E_{16} formulation did not yield any significant signal by DLS, which is ascribable to the negligible tendency to undergo self-assembling, because of the lack of the hydrophobic Leucine monomer. Notably,

only block copolymers displaying Leucine monomers along the backbone were endowed with sufficient hydrophobic features to induce the self-assembling process. Similar sizes were observed for the assemblies formed by MC-E_8L_8 and MC-E_6L_{10}, while a smaller diameter was observed for the particles formed by MC-E_4L_{12}, probably as a consequence of the different balance between the hydrophilic and hydrophobic monomers, which was markedly shifted towards the latter one. Thus a higher content of the hydrophobic monomer Leucine induce, at some extent, a more compact core of the micelles and thus a slight decrease in size.

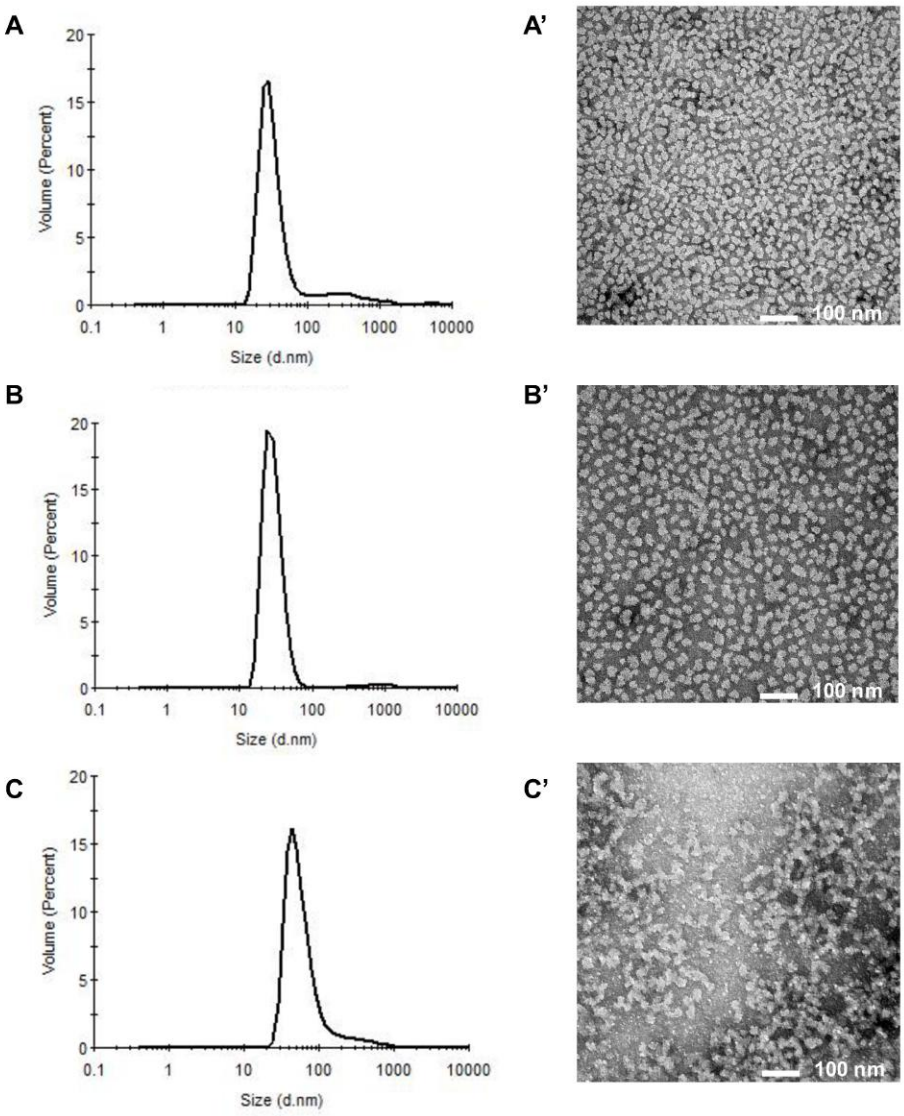

Figure 27. *Size analysis profiles by DLS (left) and TEM images (right) of DoxoMC-E_6L_{10} (panel A and A' respectively), DoxoMC-E_8L_8 (panel B and B', respectively) and DoxoMC-E_{16} (panel C and C', respectively).*

The size values detected by DLS showed that DoxoMC-E_6L_{10}, DoxoMC-E_8L_8 and DoxoMC-E_{16} have a size of 33.3 ± 5.3 nm, 29.2 ± 1.1 nm and 41.6 ± 4.9 nm, respectively (Figure 27., panel A, B, C). Moreover, considering the particle size of 39.2 ± 5.6 nm, 50.2 ± 4.1 nm and 51.0 ± 4.2 nm found for MC-E_4L_{12}, MC-E_6L_{10}, and MC-E_8L_8, respectively, it is noted that after Doxo conjugation the hydrodynamic diameter of the micellar formulations becomes smaller. This size decrease is due to the formation of a denser core in virtue of the stacking and hydrophobic interactions between Doxo and Leucine molecules that act as the driving force for the polymer conjugate self-assembling.

The zeta potential values obtained for the whole library revealed that all the micellar systems possessed an almost neutral charge. which can be ascribed to the shielding activity of the outer PEG corona.

TEM images of DoxoMCs formulations, reported in Figure 27., show that all the formulations containing Leucine in the polyaminoacidic block formed similar homogeneous nanostructures with a spherical shape and a size of 23.8 ± 3.0 nm for DoxoMC-E_6L_{10}, 26.5 ± 3.0 nm for DoxoMC-E_8L_8, and 38.4 ± 4.5 nm for DoxoMC-E_{16}, confirming the results obtained by DLS analyses.

This peculiar morphology was expected since spherically shaped micelles are generally favoured when the hydrophilic polymer block is longer than the hydrophobic polyaminoacidic portion[85]. DoxoMC-E_{16} formed micelles with the same morphology but with a larger size of nearly 40 nm. Indeed, while the presence of Leucine monomers promotes the formation of cohesive and smaller micelles in virtue of its hydrophobic behaviour, an increase in size is expected due to its absence in the polyaminoacidic block. Furthermore, Doxo conjugation increased the hydrophobicity of the systems promoting the self-assembling mechanism, as demonstrated, by contrast, by the non-assembling behaviour of MC-E_{16}, due to the absence of the hydrophobic components Leucine and Doxo.

The size of the self-assembling copolymers is an important feature that dictates the fate of the nanocarrier after injection in the bloodstream[149]. TEM and DLS results confirmed that the micellar nanosystem here obtained possess an suitable size for the selective tumor accumulation by the EPR effect[38,150,151].

The critical micelle concentration (CMC), which is the minimum concentration of polymer required for micelle spontaneous formation, was assessed by a fluorescent spectroscopic method using pyrene as a probe for the MC-E_nL_m formulations. It has been widely reported that the intensity ratio of the third (I_3) and first (I_1) peaks of the pyrene spectrum is correlated to the

probe's surrounding environment. An increase in the I_3/ I_1 ratio indicates a shift from a polar to a hydrophobic environment, which indicates the encapsulation of pyrene molecules in the micelle core generated by the self-assembling of the amphiphilic polymer chains[152].

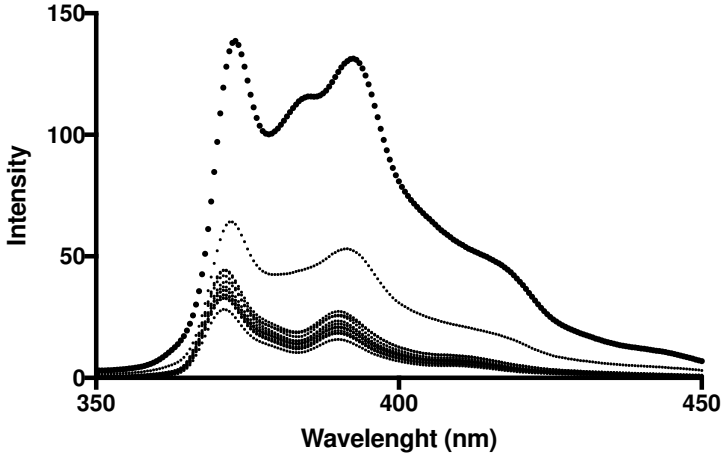

Figure 28. *Fluorescence spectra of pyrene at increasing MC-E_6L_{10} concentrations. The profiles refes to MC-E_6L_{10} as an example.*

The CMC of MC-E_nL_m formulations was assessed by the pyrene assay after dialysis process, in order to evaluate their ability to self-assemble in aqueous environment in virtue of the hydrophobicity provided by Leucine monomers. The I_3/I_1 ratio was plotted versus the logarithmic polymer concentration, as reported in Figure 29. The CMC was derived from the intercept of the two straight lines obtained.

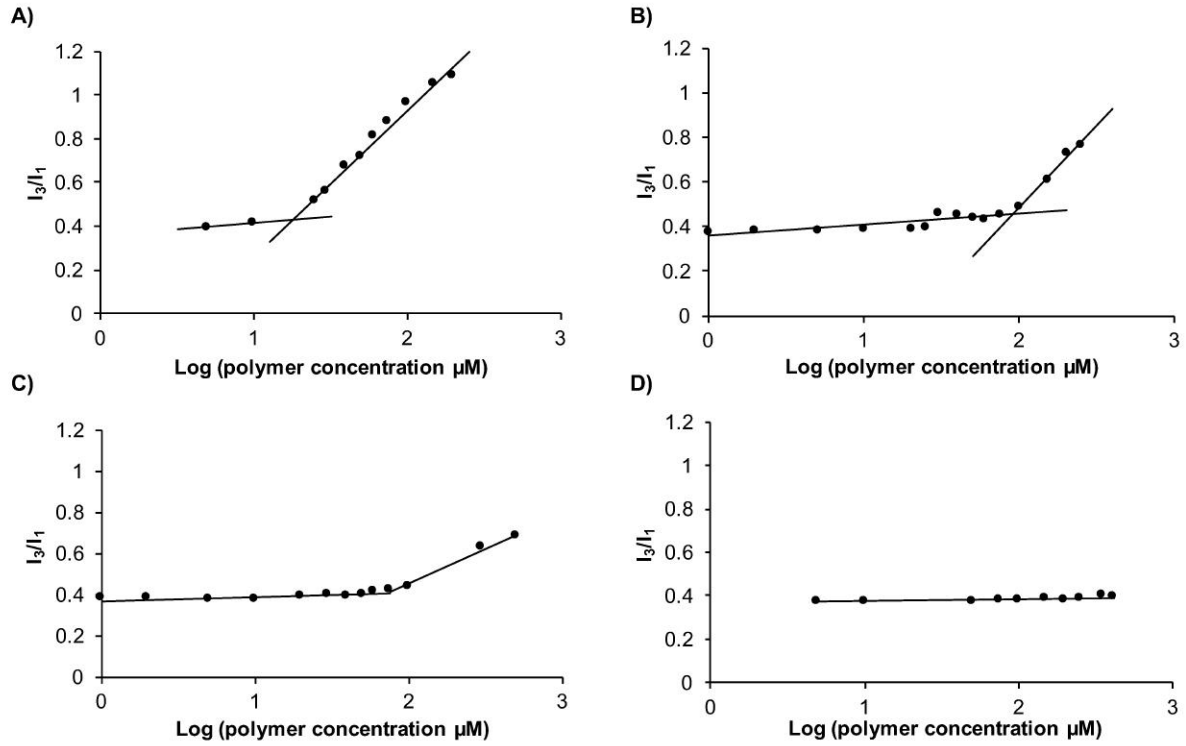

Figure 29. *I_3/I_1 ratio versus logarithmic concentration of (A) MC-E_4L_{12}, (B) MC-E_6L_{10}, (C) MC-E_8L_8 and (D) MC-E_{16}.*

As reported in Figure 28., when the polymer concentration increased, a shift in the pyrene emission spectra occurred, meaning that the environment surrounding the probe shifted from polar to hydrophobic, namely the aqueous medium and the micelles core, respectively.

The CMC values determined were 17.8± 13.1 µM, 92.2 ± 13.1 µM and 78.5 ± 8.6 µM for MC-E_4L_{12}, MC-E_6L_{10} and MC-E_8L_8, respectively. The higher the number of Leucine monomers included in the polyaminoacidic block, the lower the concentration of amphiphilic copolymer required to achieve self-assembling condition of the material. This could be ascribed to the hydrophobic character of Leucine monomers, which led to the self-association of the copolymers.

As previously reported by Vega *et al.*[153], the CMC for MC-E_{16} was not detectable, as it did not show self-assembling properties until its maximum solubility in aqueous solution.

Moreover, a novel strategy was set to assess the CMC values for DoxoMC-E_nL_m by using the conjugated Doxo as a fluorescent probe. To this aim, the ratio between the emission intensities of Doxo at 585 nm and 555 nm, namely $I_{585\ nm}/I_{555\ nm}$ (Figure 30.) was derived. This approach relies on the quenching of drug fluorescence when entrapped in hydrophobic micelle core due to the tight proximity of the drug molecules[119].

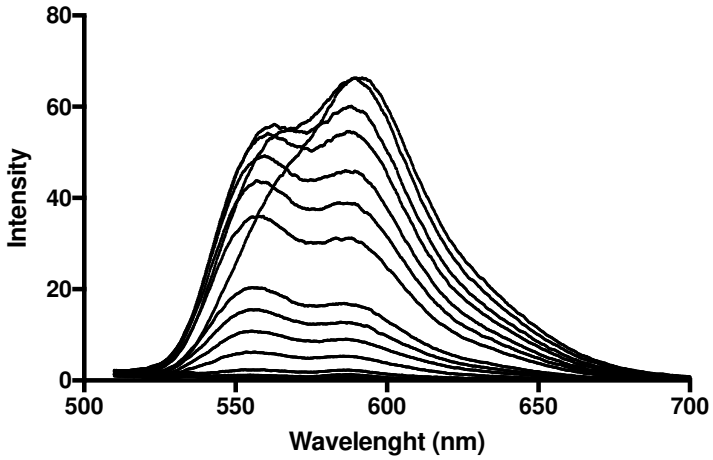

Figure 30. *Fluorescence spectra of Doxo at increasing DoxoMC-E_6L_{10} concentrations. The profiles refer to DoxoMC-E_6L_{10} as an example.*

As reported in Figure 31. left panels, increasing the polymer concentration in solution, as confirmed by Doxo absorbance at 488 nm, an important decrease in Doxo emission intensity at 555 nm was detected. The quenching of Doxo fluorescence was directly correlated with the self-assembling of the polymers. As Doxo molecules got closer into in the micelle core, the fluorescence quenching occurred, indicating micelles formation[99,154]. 9.5 ± 0.4 μM, 9.7 ± 0.3 μM and 21.1 ± 2.9 μM were the CMC values obtained for DoxoMC-E_6L_{10}, DoxoMC-E_8L_8, DoxoMC-E_{16}, respectively (Figure 31., panels on the right).

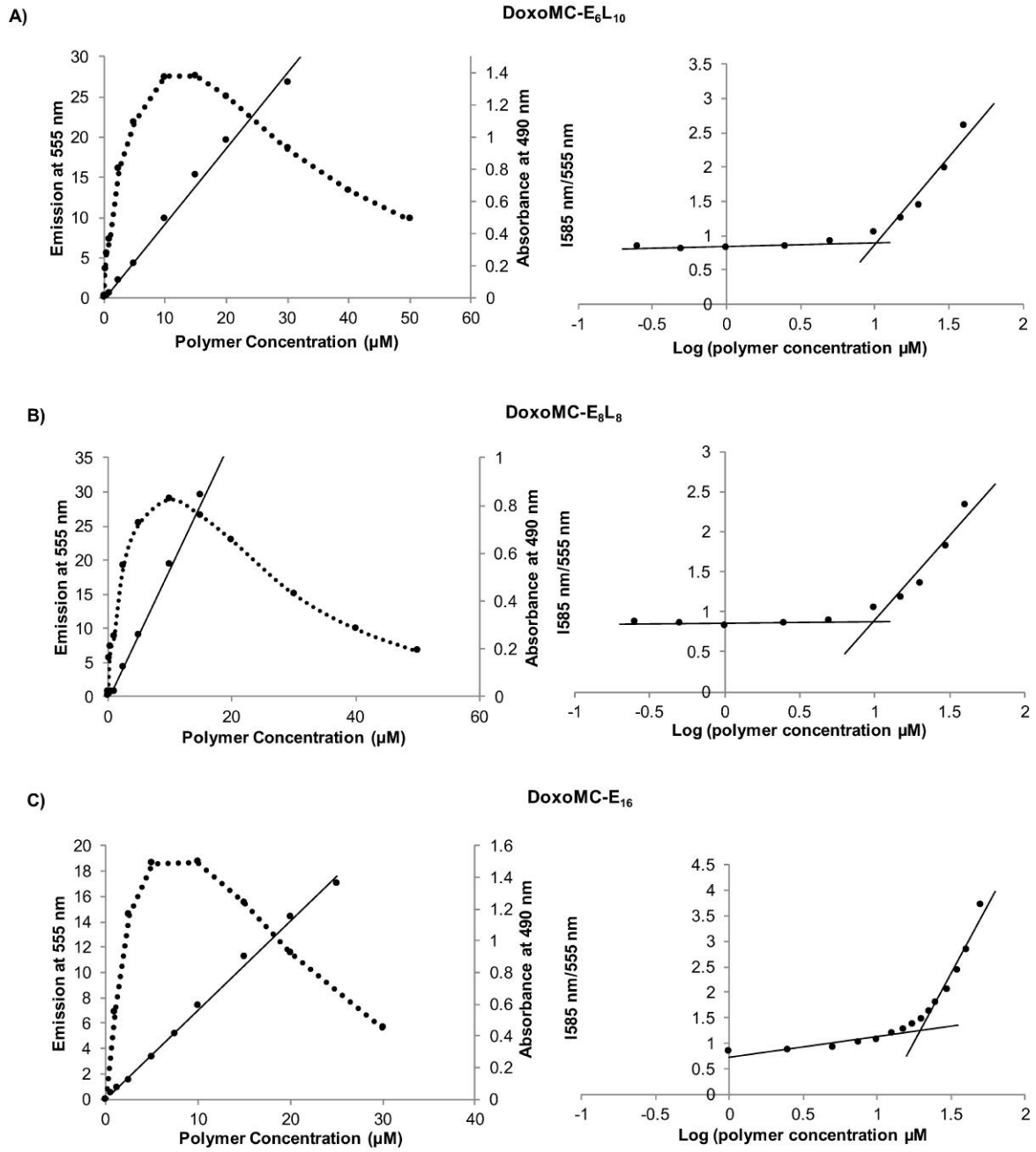

Figure 31. *Fluorimetric emission (•••) at 555.nm and UV-Vis absorbance intensity (—) at 488 nm of increasing Doxo conjugated polymer concentrations (left panels) and, $I_{585nm}/_{555nm}$ ratio versus logarithmic concentration of the polymers (Right panels). (A) DoxoMC-E_6L_{10}, (B) DoxoMC-E_8L_8, and (C) DoxoMC-EL_{16}.*

These data showed a nearly 10-fold decrease in CMC values of Doxo conjugated polymers with respect to non-drug conjugated polymers. Therefore, Doxo conjugation increased the polyaminoacidic block hydrophobicity, which significantly favour the polymeric chain cohesion to yield micelles and to a reduction of the concentration required to obtain the self-assembled systems.

The low CMC concentration obtained for DoxoMCs would provide a remarkable stability and prevent the dissociation of the nanosystems upon dilution occurring with intravenous administration.

6.6. Release studies

Doxorubicin release studies from the different micellar formulation were carried out in two different conditions, at pH 7.4 to mimic the bloodstream, and at pH 5.5 to simulate the lysosomal intracellular environment.

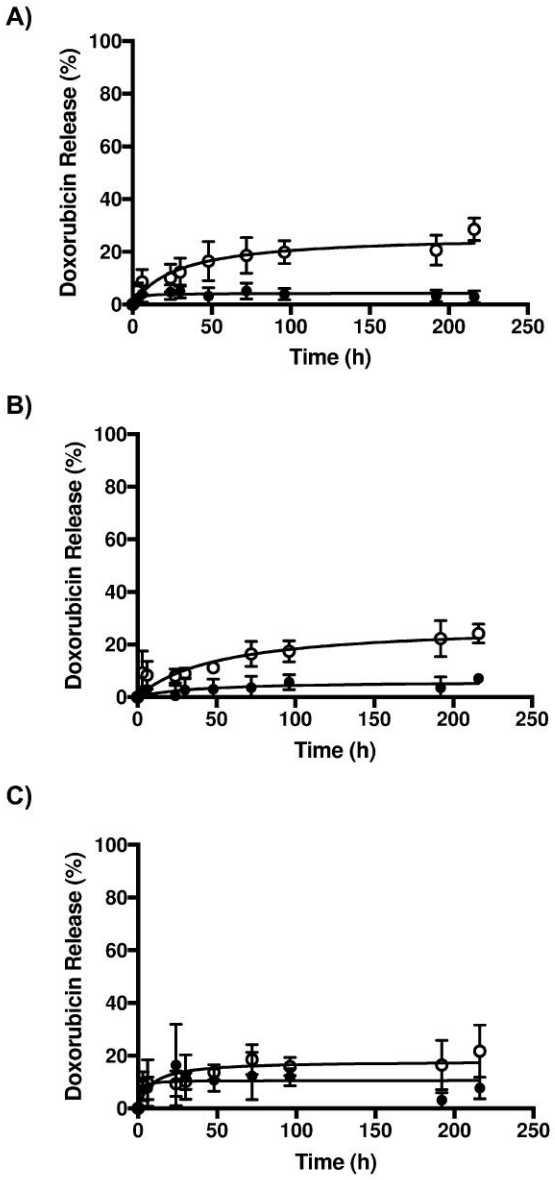

Figure 32. *Doxorubicin release profile of A) DoxoMC-E_6L_{10}, B) DoxoMC-E_8L_8, C) DoxoMC-E_{16} at pH 7.4 (●) and pH 5.5 (○).*

The release profiles reported in Figure 32. showed that Doxorubicin micellar formulations bearing leucine as a spacer in the backbone possess similar release profile at the two pH tested. Both DoxoMC-E_6L_{10} and DoxoMC-E_8L_8 formulations displayed a high stability at pH 7.4 with negligible drug release over time, while at pH 5.5 the drug release reached nearly 30% and 25%, respectively. This behaviour is due to the pH-sensitive character of the hydrazone bond through which doxorubicin is linked to the polymer backbone. This dictated a slightly faster release under acidic condition. On the contrary, DoxoMC-E_{16} exhibited a similar trend for both pH values, meaning that this formulation is fairly stable in both conditions.

These results may indicate that the micellar formulations present an extremely stable and dense core, that could initially prevent the solvent diffusion or restrain the release of the drug even after the bond hydrolysis[99]. Moreover, Markovsky *et al.*[155] and Arroyo-Crespo *et al.*[146] verified that a high Doxo loading in polymeric systems could prevent or significantly decrease drug release kinetics, which is in good accordance with the data here obtained. Nevertheless, leucine seemed to play an important role as a spacer among Doxo bearing units, facilitating the hydrazone bond cleavage under acidic environment, leading to a sustained and controlled release of Doxo from the micellar systems[119]. Hence, these nanocarriers features could be exploited not only to prevent drug dissociation and unspecific and undesired drug release in the bloodstream (pH 7.4) upon administration of the system, but also allow for a drug release mainly in the lysosomal subcellular compartments, thus reducing drug-related side effects due to its unspecific biodistribution[156,157].

6.7. *In vitro* studies

6.7.1. Cell viability studies

The cell viability was assessed on CT26 murine colorectal carcinoma cell line and 4T1 murine mammary carcinoma cell line by MTT assay, evaluating the cytotoxicity of the micellar formulations, namely DoxoMC-E_6L_{10}, DoxoMC-E_8L_8, DoxoMC-E_{16}, and using free Doxo as a positive control. Cells were incubated with different Doxo or micelles with Doxo equivalent concentration in the range of 0.1 nM - 100 μM for 48 hours or 72 hours.

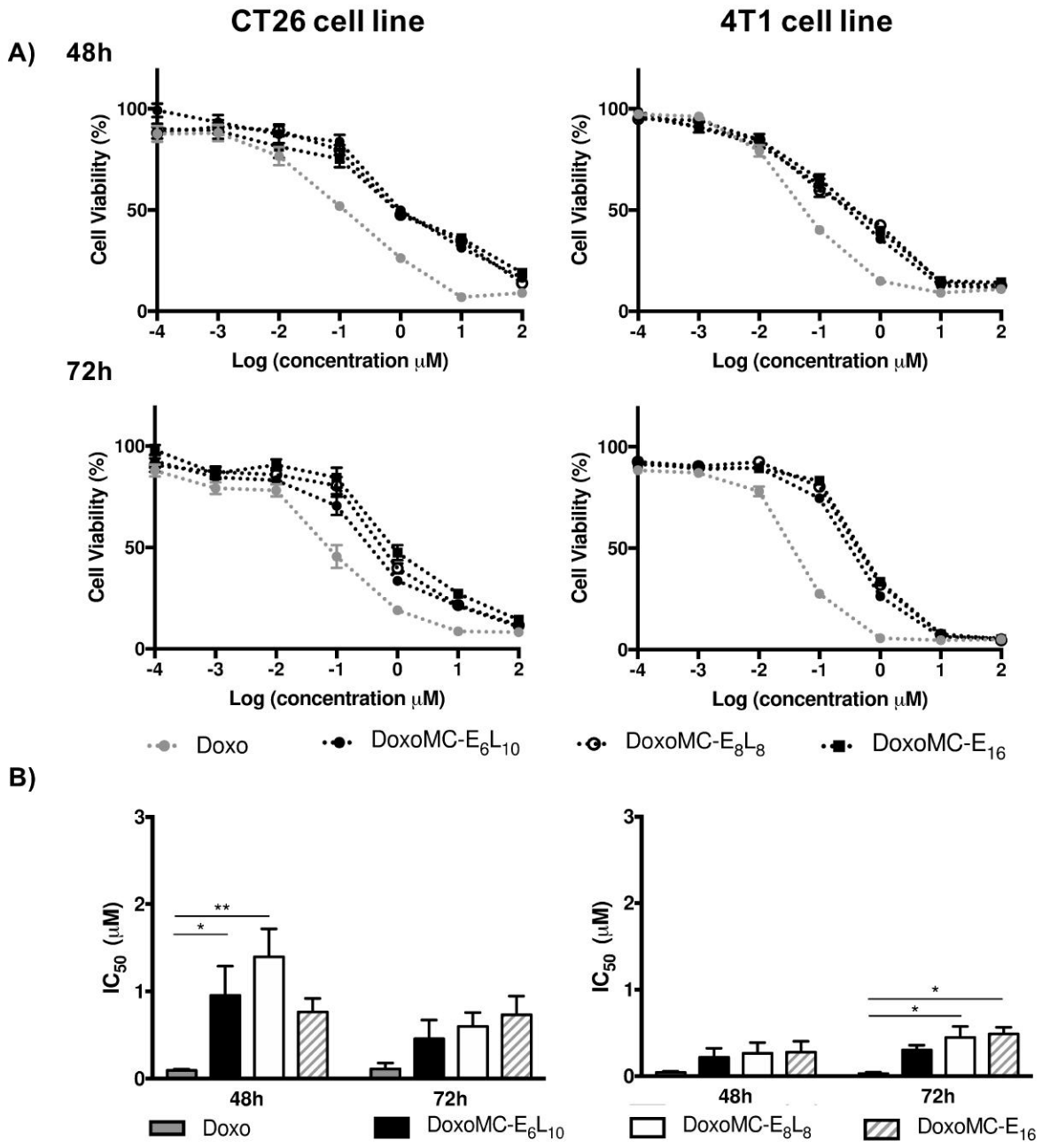

Figure 33. *Viability profiles of CT26 cell line (on the left) and 4T1 cell line (on the right) after A) 48 hours incubation and 72 hours incubation with Doxo or Doxo equivalent concentrations (●), DoxoMC-E_6L_{10} (●), DoxoMC-E_8L_8 (○), DoxoMC-E_{16} (■); B) IC_{50} values of Doxorubicin and micellar formulations (mean ± SEM, N=3, n=17) ***p< 0.001, **p< 0.01 *p<0.05.*

Concerning CT26 cell line, all micellar formulations showed cytotoxicity in a dose and time-dependent manner, as revealed by the IC_{50} values decrease from 48 hours to 72 hours, and their growth inhibition effects gradually approached those of free Doxo (Figure 33.A, panel on the left). No significant differences were observed at 72 hours incubation between the different

DoxoMCs formulations and, interestingly, the obtained IC_{50} values were comparable with the ones of the free drug.

The cytotoxicity studies performed on 4T1 cancer cells showed a similar behaviour at 48 hours incubation with the different treatments (Figure 33.B, panel on the right), and no significant differences between the micellar formulations and free Doxo were found. A slight increase in the IC_{50} values was detected at 72 hours with respect to 48 hours incubation time, and this might be ascribed to the rapid proliferation and aggressiveness of the cell line.
Nonetheless, the micellar formulations seemed to be more active in 4T1 cells, as the obtained IC_{50} values were lower than those found for the colorectal cancer cell line at 48 and 72 hours, in fact Doxo is one of the first-line treatments for mammary cancer disease[157–160].
To assess the cell biocompatibility of the self-assembling block copolymers in the absence of Doxo, MTT assays were performed on both cell lines, testing the maximum unconjugated nanocarrier concentrations used *in vitro*, namely 18 μM for MC-E_6L_{10} and MC-E_8L_8, and 13 μM for MC-E_{16}, respectively. At these concentrations, the CT26 cell viability was 85.5% (±4.5), while the 4T1 cell viability was 92.1% (±4.1).

Concerning Doxo micellar nanocarriers, all formulations have the equivalent drug content and no significant differences in terms of cytotoxicity were found. Despite this, DoxoMC-E_6L_{10} showed the lowest IC_{50} value in both cell lines, and this could be due to a more efficient release of Doxo inside the cell environment as previously shown by the *in vitro* studies. This could be ascribed to the fact that leucine spacer, in a 6:10 hydGlu:Leu molar ratio in the polyaminoacid block, is the most performing among the formulations tested in terms of efficient Doxo conjugation yield, hydrazone bond cleavage and diffusion of released drug from the micelles core. Therefore, it was selected for the further *in vitro* and *in vivo* investigations.

As reported in literature[119], the lower Doxo IC_{50} value with respect to nanocarriers can be explained by the different uptake mechanism involved for the small anticancer drug and the micellar carriers. Indeed, Doxo is a small molecule that is taken up by cells *via* passive diffusion through the cell membrane, while nanocarriers require an active mechanism of uptake, resulting in different drug concentration inside the cells. Furthermore, as a requisite for cell toxicity, the drug needs to be cleaved from the nanovectors backbone to be able to reach the nuclei and the DNA strands[99]. Interestingly, the obtained IC_{50} values for the micellar formulations stated that the drug exploited its cytotoxic action after 48h incubation time, meaning that Doxo into its

pharmacologically active form could be efficiently released from the polymeric backbone upon hydrazone bond cleavage.

Even if Doxorubicin has a higher cytotoxic activity, no significant differences with DoxoMCs were found. As already demonstrated by Balasso *et al.*[161] and Markovsky *et al.*[155], Doxo conjugated drug delivery systems could show less cytotoxic activity compared to the free drug. Despite this, the nanosystems offer advantages in terms of biodistribution and limited toxic side effects, since in principle these formulations could selectively accumulate in tumor tissues and allow multiple administrations.

6.7.2. Confocal studies

The intracellular fate of Doxo and DoxoMC-E_6L_{10} in the CT26 cell line was assessed by immunofluorescence analysis using confocal microscopy. Cell nuclei were marked with DAPI (blue), while lysosome were stained with a primary antibody against Lysosomal-associated membrane protein-1 (LAMP-1) and a secondary antibody labelled with Dylight® 488 fluorophore (green). Doxorubicin fluorescence (red) showed the accumulation of the free drug or the micellar nanocarrier within the cells.

Representative images are shown in Figure 34., where cells were imaged after 2 (Figure 34.A) and 24 (Figure 34.B) hours of incubation.

A)

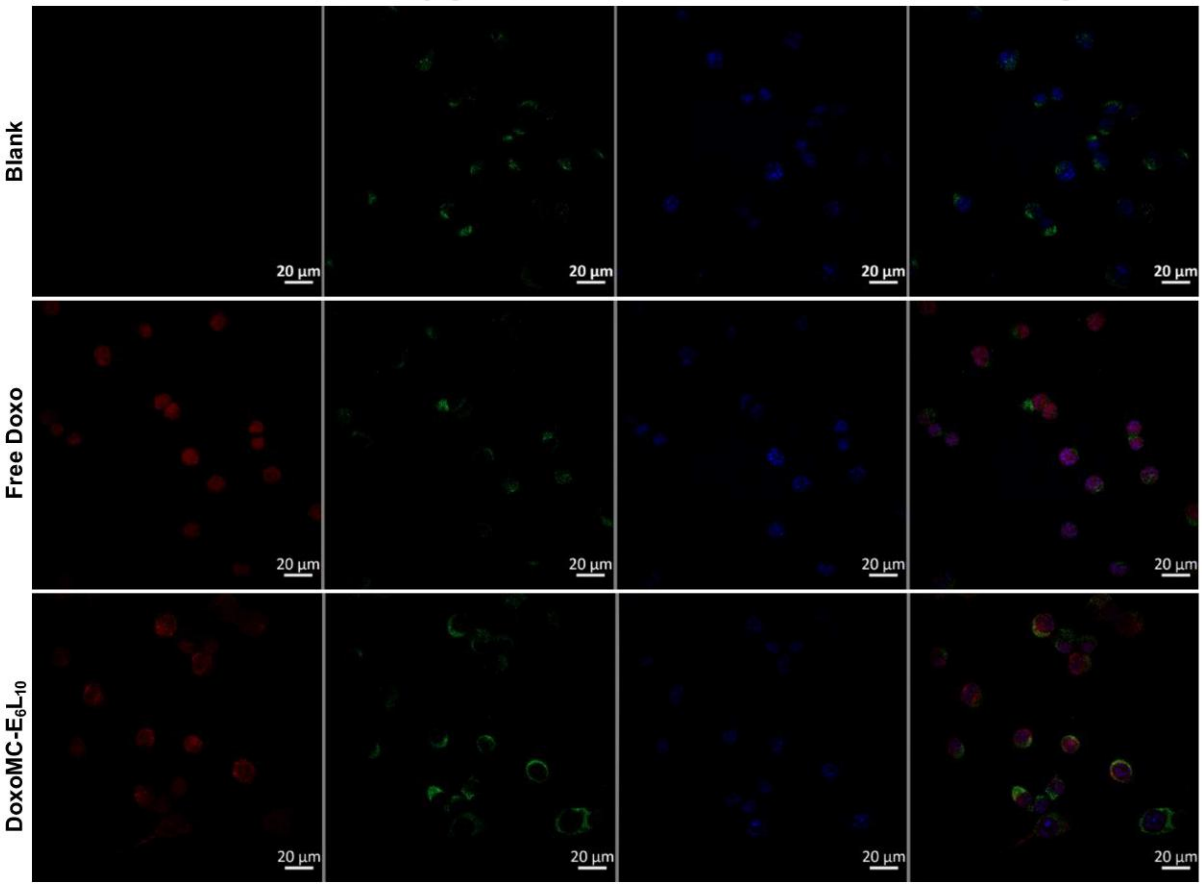
Doxorubicin
Dylight® 488
DAPI
Merge
Blank
Free Doxo
DoxoMC-E6L10
20 µm

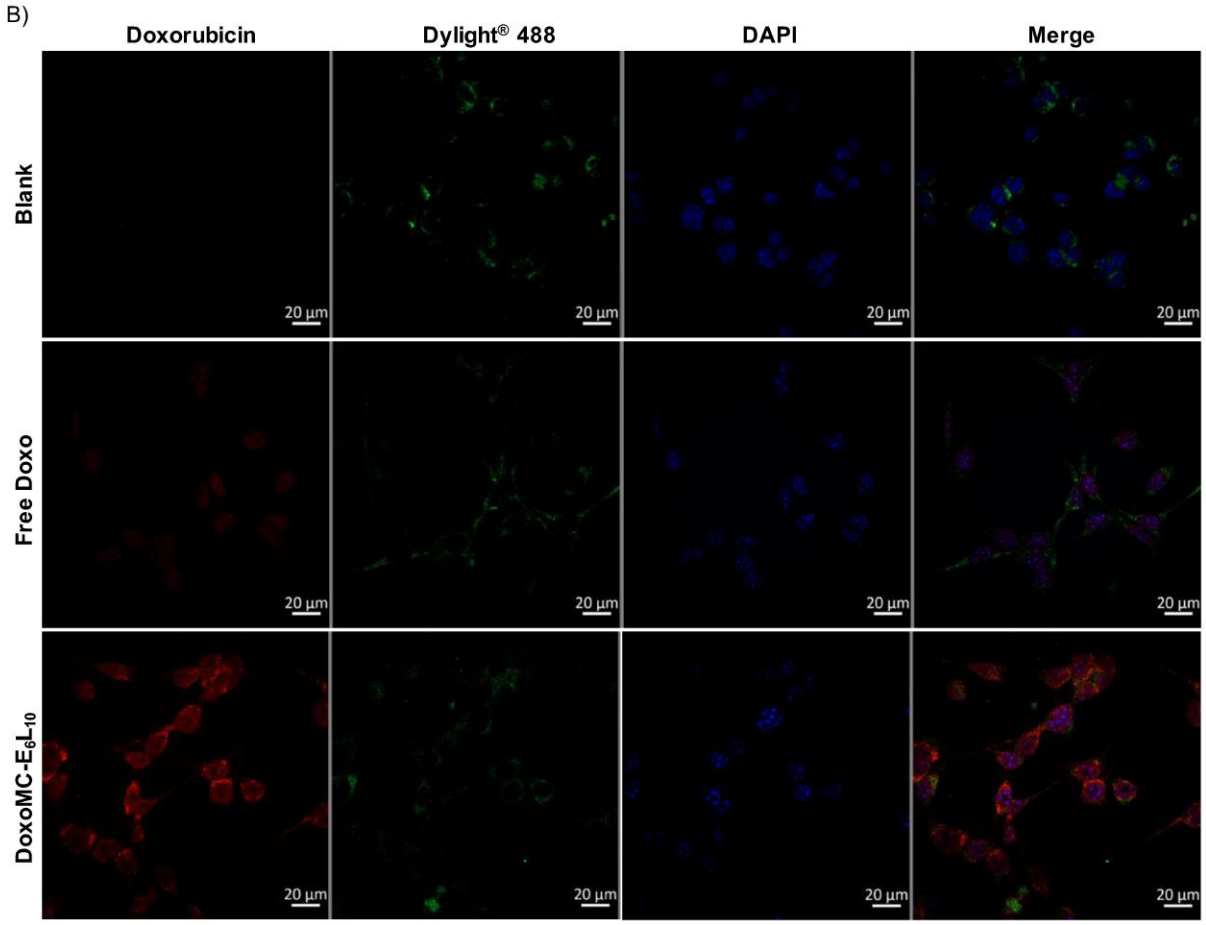

Figure 34. *Confocal microscopy images of CT26 cell incubated with Doxo and DoxoMC-E_6L_{10} for 2 (A) and 24 (B) hours. From the left, channel for Doxorubicin (red), lysosomal (green), and nuclei (blue) detection are presented, while the merged channels are shown on the right column. The scale bar is 20 µm.*

Upon cell incubation with free Doxo, the drug fluorescence was mostly distributed in the nuclei after 2 hours, while DoxoMC-E_6L_{10} was prevalently located in the lysosomal compartments, as indicated by the presence of brighter red spots co-localized with the lysosome staining, confirming the lysosomal entrapment and the selective intracellular delivery. The co-localization between DoxoMC-E_6L_{10} formulation and lysosomes raised after 24 hours incubation (Figure 34., panel B). In particular, the amount of Doxo that distributed the nuclei also increased, proving that the drug can be efficiently released from the polymeric backbone, through the hydrazone bond hydrolysis because of the subcellular compartment acidic pH. Indeed, after the uptake process, the polymeric based nanocarrier was confined in the lysosomal subcellular compartment, where the presence of the acidic environment could easily trigger the cleavage of the pH sensible hydrazone bond[102], resulting in Doxo release. Combined with this, the presence of enzymes, such as endopeptidases and cathepsins, in the lysosomal compartments might also provide for the enzymatic degradation of the polyaminoacidic block of the polymeric chain, participating in the release process[146,149]. In this way, the pH-sensitive

drug release would prevent unspecific drug loss in the bloodstream after nanocarrier administration.

According to the possible enzymatic degradation occurring intracellularly, we postulated that the slightly more pronounced cytotoxic activity observed in 4T1 cells with respect to CT26 cell line (see paragraph 6.7.1.) might be due to a higher level of Cathepsin B activity in this cell line, as previously reported by Arroyo-Crespo *et* al.[146]. However, dedicated studies are needed to confirm this hypothesis.

Due to time constraints, it was not possible to include in this thesis work more detailed studies of the micellar formulations intracellular trafficking. Further studies will be performed in order to improve the images quality and conduct a quantitative evaluation of micelles-lysosome colocalization at different time points.

6.8. In-vivo studies

Based on the *in vitro* results, the anticancer efficacy of DoxoMC-E_6L_{10} on CT26 and 4T1 subcutaneous tumor model in Balb/c mice was evaluated *in vivo*. These proof-of-concept studies were performed by evaluating both the intratumoral and intravenous routes of administration. The Doxo injected dose was selected according to Bae *et* al.[98] and Lv *et* al.[162], in which polyaminoacidic based micellar systems showed an anticancer activity dose ranging between 10 and 20 mg/kg. To evaluate the *in vivo* toxicity of DoxoMC-E_6L_{10}, a preliminary study was carried out in healthy mice, injecting through the tail vein a 12 mg/kg Doxo equivalent dose. The mice body weight and wellbeing were constantly monitored for 14 days and no significant alterations were observed, confirming the safety and the good tolerability of the systems at the selected dose.

Afterwards, the self-assembling system was firstly injected in CT26 tumour bearing mice to assess the efficacy of the system after local and systemic treatment. Doxo equivalent doses of 2.4 mg/kg and 12 mg/kg were tested for the intratumoral (IT) and intravenous (IV) administration, respectively.

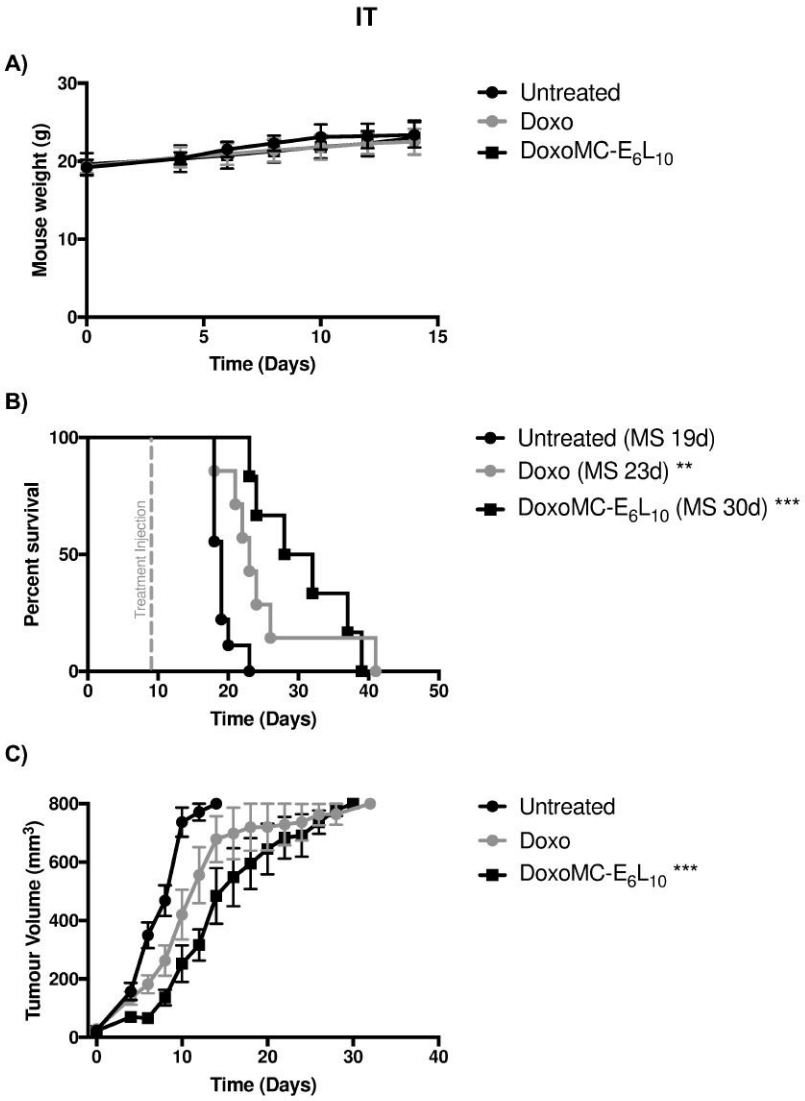

Figure 35. *In vivo antitumor efficacy of Doxo and DoxoMC-E_6L_{10} formulation in subcutaneous CT26 colorectal cancer model. The Doxo equivalent dose of 2.4 mg/kg was administered intratumorally. A) Animal body weight; B) Kaplan-Meier Survival curve; C) Tumor growth curves. Results are expressed in mean ± SEM, n=6-9, ***p< 0.001, **p< 0.01 *p<0.05, * is referred to the untreated group.*

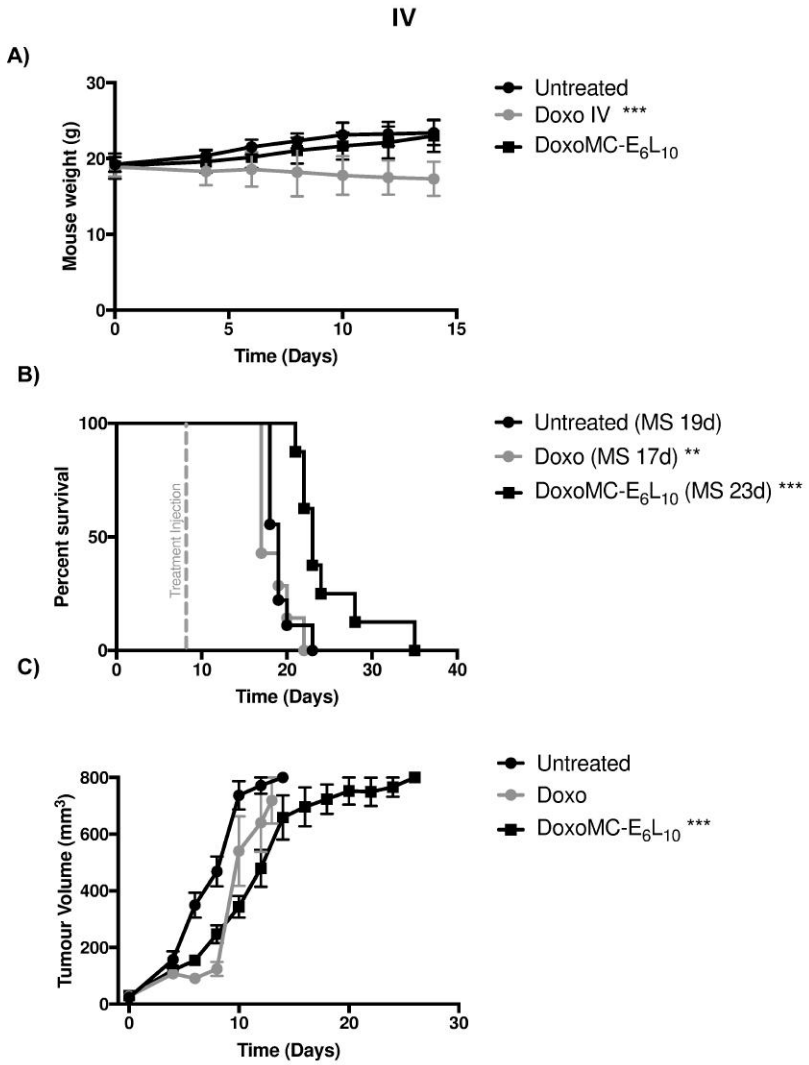

Figure 36. *In vivo antitumor efficacy of DoxoMC-E_6L_{10} formulation in subcutaneous CT26 colorectal cancer model. Doxo equivalent dose of 12 mg/kg for intravenous administration. A) Animal body weight; B) Kaplan-Meier Survival curve; C) Tumor growth curves. Results are expressed in mean ± SEM, n=6-9, ***p< 0.001, **p< 0.01 *p<0.05, * is referred to the untreated group.*

Interestingly, mice treated intravenously with DoxoMC-E_6L_{10} revealed no alteration in body weight and a significantly lower toxicity compared to the administered free drug. Subsequent analysis of the survival rates demonstrated that DoxoMC-E_6L_{10} treated mice survived longer than the controls, presenting a higher median survival time of 30 days and 23 days (Figures 35.B and 36.B) after intratumoral and intravenous administration, respectively.

The results showed a higher and significant regrowth delay with respect to the untreated group (p<0.001) after IT and IV injections of the micellar formulation, showing the antitumoral effect

of the system in both the administration routes tested, and no significant difference with Doxo was observed.
Moreover, it is worth noting that the dose here tested for the intratumoral treatment is lower than the commonly tested[163,164], highlighting the remarkable effect of these nanovectors even in low dose for a sustained time.

These evidences suggest that DoxoMC-E_6L_{10} could be an interesting formulation for intratumoral delivery of Doxo. On the other side, the tumor reduction after intravenous administration confirmed the ability of the nanosystems to reach the tumor mass exploiting EPR effect.

A further *in vivo* study was carried out using 4T1-bearing mice since this model was chosen for its wide use as a suitable experimental animal model for human mammary cancer[165]. Mice were randomly divided into groups and treated either locally with intratumoral injections of 3 mg/kg Doxo equivalent dose, or intravenously with single or multiple injections of 15 mg/kg. The aim of this study was to test the DoxoMC-E_6L_{10} toxicity and anticancer activity in a second solid tumor model and to verify its tolerability with a higher dose compared to the one tested in the CT26 subcutaneous tumor model.

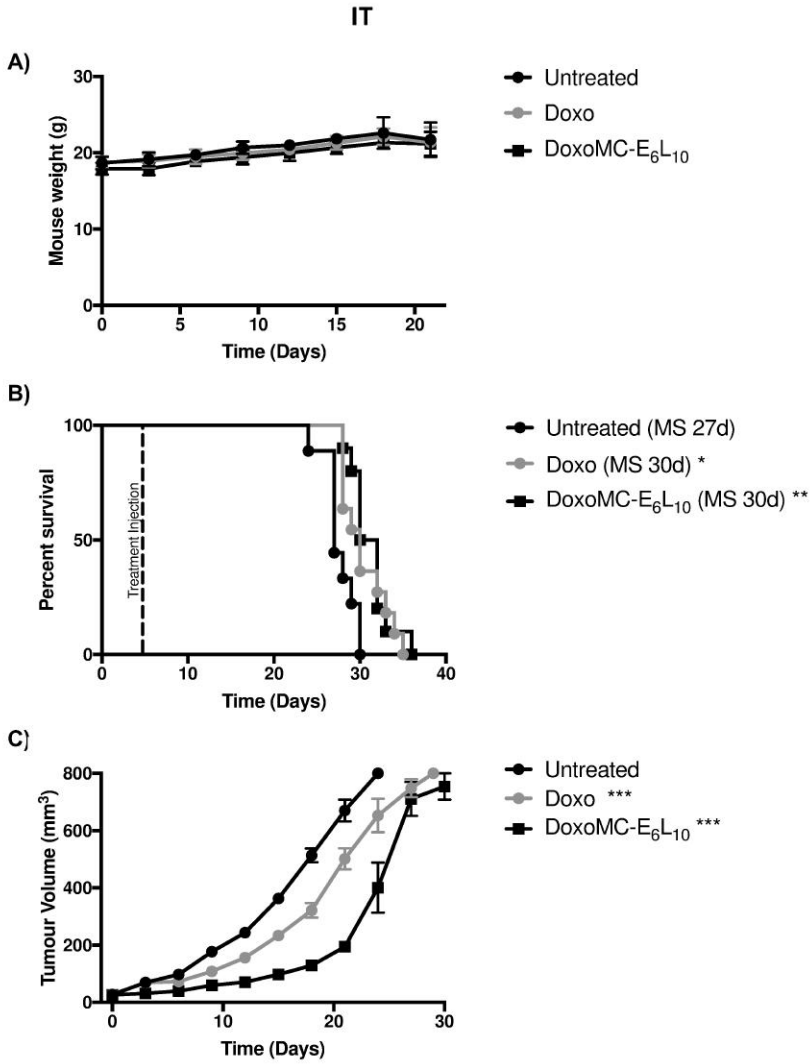

Figure 37. *In vivo antitumor efficacy of Doxo and DoxoMC-E_6L_{10} in subcutaneous 4T1 breast cancer model. Doxo equivalent dose of 3 mg/kg was administered via intratumoral injection. A) Animal body weigh; B) Kaplan-Meier Survival curve; C) tumor growth curves after local administration of Doxo and DoxoMC-E_6L_{10} formulations. Results are expressed in mean ± SEM, n=8-11, ***p< 0.001, **p< 0.01 *p<0.05.*

Concerning the intratumoral treatments, the Kaplan-Meier survival curves (Figure 37B) showed that Doxo and DoxoMC-E_6L_{10} treated mice presented the same median survival, that is significantly increased compared to the untreated group, namely 30 days for the treated groups and 27 for the control group. The equivalence of the median survival rates was caused by a spontaneous metastasis spreading from the primary tumor in all the groups ascribed to the highly tumorigenic and invasive behaviour of 4T1 tumor model. This led to the sacrifice of the mice for metastasis-related side effects and not for the tumour size[165]. As reported in Figure 37.A, an alteration in the body weight was noticed for untreated and treated groups starting

from day 18, and this was reasonably due to the metastasis onset. The presence of metastasis was confirmed by mice autopsies, demonstrating that lungs and spleen were the organs mainly affected. Both Doxo and DoxoMC-E_6L_{10} treated mice were significantly different as compared to the untreated group (p<0.001) and, moreover, mice treated locally with Doxo exhibited a lower regrowth delay with respect to the DoxoMC-E_6L_{10} injected ones (Figure 37.C). Based on the tumor volume values before metastasis onset, a significant difference (p<0.001) between Doxo treated group and DoxoMC-E_6L_{10} treated mice was detected, underlining the significant efficacy of the system after local administration.

Furthermore, the intravenous administration route was performed by single injection or multiple administrations every seven days. This treatment schedule was decided according to the increasing rate of the tumor volume. Free Doxo and Caelyx®, a trademark Doxorubicin liposomal formulation approved for the treatment of several cancers, such as breast, ovarian and multiple myeloma[166,167], were administered as controls. The high toxicity of Doxo, obtained after a single injection in the previous mice model and according to literature data[98,162], did not allow its use as a control for the multiple injection experiments.

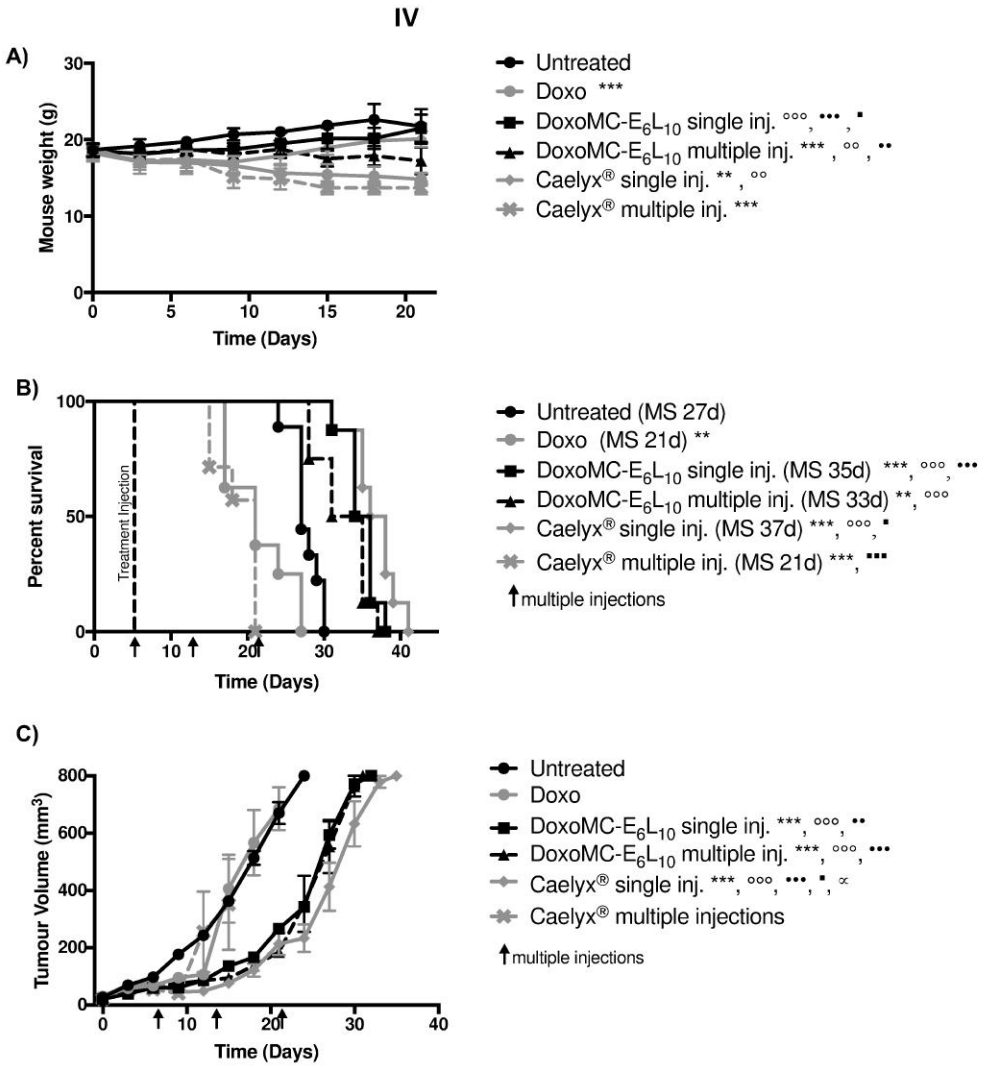

Figure 38. *In vivo antitumor efficacy of Doxo and DoxoMC-E_6L_{10} in subcutaneous 4T1 breast cancer model. Doxorubicin equivalent dose of 15 mg/kg was administered via intravenous injection. A) Animal body weight; B) Kaplan-Meier Survival curve; C) tumor growth curves after systemic administration of single or weekly administration of Doxo, DoxoMC-E_6L_{10} and Caelyx® formulations. Results are expressed as mean ± SEM, n=8-11, ***p< 0.001, **p< 0.01 *p<0.05. * is referred to the untreated group, ° is referred to Doxo, • is referred to Caelyx® multiple injections, ∝ is referred to DoxoMC-E_6L_{10} single injection, ■ is referred to DoxoMC-E_6L_{10} multiple injections.*

Interestingly, mice treated with DoxoMC-E_6L_{10} formulation exhibited negligible body weight loss after single administration with respect to untreated group (p<0.05), and significant lower toxicity compared to Doxo (p<0.001) (Figure 38.A). Furthermore, significant lower toxicity was found after multiple injection of the micellar formulation compared to the trademark liposomal formulation administered at the same Doxo concentration (p<0.01). As showed in Figure 38.B, a remarkable improvement in the median survival rate was observed after treatment with the micellar formulation in single or multiple administration, and it resulted significant compared to the control group (p<0.001), Doxo treated group (p<0.001) and

Caelyx® multiple administration treated group (p<0.001). The median survival rate was 35 and 37 days for DoxoMC-E_6L_{10} and Caelyx®, respectively, stressing a comparable efficacy of DoxoMC-E_6L_{10} with the liposomal formulation to prolong the mice survival.
Mice treated with DoxoMC-E_6L_{10} formulation exhibited a significant delay in tumor growth compared to untreated mice and, notably, the curves of micellar and liposomal formulation in Figure 38.C almost overlap, meaning that no significant differences between the two treatments were found. Overall, no significant difference was observed between single and weekly injections of micellar formulation in terms of survival, and this was mainly ascribable to the appearance of metastasis-related side effects which required the mice sacrifice independently from the tumor volumes. The data obtained for DoxoMC-E_6L_{10} multiple injections showed that the formulation can be safely administered to achieve high cumulative dose providing for a higher anticancer activity while limiting the toxicity. The opposite result was showed by the liposomal Caelyx® formulation since it caused a severe irreversible body weight loss.

These results confirmed the *in vivo* safety of the self-assembling block copolymer even at a high Doxo equivalent dose and multiple administrations. Indeed, this formulation allows to control drug release while reducing systemic side effects, retaining the anticancer activity and passively reaching solid tumors in virtue of the EPR effect. Additionally, a relevant feature that could contribute to the enhanced *in vivo* antitumor efficacy of the colloidal vehicle can be the enhanced blood circulation time of the formulation, due to the presence of the PEG shell on the micellar surface[11], which sustains the bioavailability and the accumulation in the tumor.

These encouraging outcomes suggest that DoxoMC-E_6L_{10} can enhance anticancer activity and limit toxic side-effects of anticancer drugs, leading to a remarkably prolonged survival.

7. CONCLUSIONS

In the last decades, nanocarriers have been widely investigated as drug delivery systems for the treatment of cancer, since they represent a promising strategy to overcome the limitations of the available chemotherapies. Indeed, smart nanocarriers offer advantages in terms of site-selective drug accumulation in the disease tissue, controlled drug release, reduction of systemic side effects and improvement of patient compliance.

In the light of this, the present thesis project involved the design and development of a "smart" drug delivery system based on amphiphilic di-block copolymers able to self-assemble in colloidal structures, namely polymeric micelles, and intended for anticancer therapeutic application.

The di-block copolymer backbone was composed by a hydrophilic block of polyethylene glycol and an amino acid-based block including different ratios of γ-hydrazinamide-glutamic acid (hydGlu) and Leucine. A library of amphiphilic di-block copolymers was successfully synthetized through Ring Opening Polymerization, leading to the formation of four $mPEG_{5kDa}$-b-(γ-hyd[Doxo]-Glu_n-r-Leu_m) copolymer derivatives. Doxorubicin was efficiently conjugated through hydrazone bond exploiting the γ-hydrazinamide pendant group of glutamic acid to obtain a pH-controlled release of the drug. We have demonstrated that Leucine was a key component that, by minimizing the steric hindrance of the drug, ensures a high drug conjugation yield.

Doxorubicin, together with Leucine, played a crucial role in the copolymer self-assembling step since both components increased the hydrophobic character of the polyaminoacidic block, thus ensuring high stability of the colloidal system.

The self-assembled nanovectors displayed optimal features in terms of size, charge, morphology, and critical micelle concentration for the selective tumor accumulation by EPR effect. The pH-cleavable hydrazone bond led to a controlled drug release in acidic condition, displaying relevant stability in physiological conditions. Moreover, the presence of Leucine in the polyaminoacidic block endorsed the pH-triggered release.

The cytotoxicity towards cancer cells of the colloidal formulations was tested *in vitro,* showing a dose dependent cytotoxicity comparable with that of the free Doxo cytotoxicity.

In vitro investigation confirmed lysosomal entrapment of the polymeric micellar formulation and the selective intracellular release of Doxo.
When administered *in vivo*, the drug loaded micellar nanocarriers displayed an excellent safety profile and led to an increased survival rate of subcutaneous tumor bearing mice. It is worth noting that the nanosystem demonstrated a high anticancer activity after local and systemic administration, while negligible toxicity was found.
The evidences we had in this PhD project confirm that engineered self-assembling polyaminoacidic micelles are a promising strategy to set up smart colloidal nanovectors for selective intracellular delivery of anticancer drugs.

Furthermore, an actively targeted system based on the functionalization of the copolymers with Folic Acid has been designed with the aim of improving the intracellular access of the nanocarriers by engaging the active uptake of cells, and ultimately the efficacy and potency of the nanosystem with respect to the untargeted formulation.

8. REFERENCES

1. Barenholz, Y. Doxil® - The first FDA-approved nano-drug: Lessons learned. *J. Control. Release* **160,** 117–134 (2012).

2. Drummond, D. C., Noble, C. O., Hayes, M. E., Park, J. W. & Kirpotin, D. B. Pharmacokinetics and in vivo drug release rates in liposomal nanocarrier development. *Journal of Pharmaceutical Sciences* (2008). doi:10.1002/jps.21358

3. Davis, M. E., Chen, Z. & Shin, D. M. Nanoparticle therapeutics: An emerging treatment modality for cancer. *Nat. Rev. Drug Discov.* **7,** 771–782 (2008).

4. Safra, T. *et al.* Original article patients reaching or exceeding cumulative doses of 500 mg / m 2. *Ann. Intern. Med.* **11,** 1029–1033 (2000).

5. Blanco, E., Shen, H. & Ferrari, M. Principles of nanoparticles design for overcoming biologica barriers for drug delivery. *Nat Biotechnol* **33,** 941–951 (2015).

6. Swaan, L. M. B. and P. W. ENDOCYTIC MECHANISMS FOR TARGETED DRUG DELIVERY Lisa. *Adv. Drug Deliv. Rev.* **59,** 748–758 (2007).

7. Mukherjee, S., Ghosh, R. N. & Maxfield, F. R. Endocytosis. *Physiol Rev* (1997).

8. Carrstensen, H., Müller, R. H. & Müller, B. W. Particle size, surface hydrophobicity and interaction with serum of parenteral fat emulsions and model drug carriers as parameters related to RES uptake. *Clin. Nutr.* **11,** 289–297 (1992).

9. Norman, M. E., Williams, P. & Illum, L. Human serum albumin as a probe for surface conditioning (opsonization) of block copolymer-coated microspheres. *Biomaterials* **13,** 841–849 (1992).

10. Salvati, A. *et al.* Transferrin-functionalized nanoparticles lose their targeting capabilities when a biomolecule corona adsorbs on the surface. *Nat. Nanotechnol.* **8,** 137–143 (2013).

11. Salmaso, S. & Caliceti, P. Stealth Properties to Improve Therapeutic Efficacy of Drug Nanocarriers. *J. Drug Deliv.* **2013,** 1–19 (2013).

12. Cabral, H. & Kataoka, K. Progress of drug-loaded polymeric micelles into clinical studies. *J. Control. Release* **190,** 465–476 (2014).

13. Dreaden, E. C., Austin, L. A., Mackey, M. A. & El-Sayed, M. A. Size matters: gold nanoparticles in targeted cancer drug delivery. *Ther. Deliv.* **3,** 457–478 (2012).

14. Release, P. Latest world cancer statistics Global cancer burden rises to 14 . 1 million new

cases in 2012 : Marked increase in breast cancers must be addressed. *Int. Agency Res. Cancer, World Heal. Organ.* 2012–2014 (2013). doi:223

15. Nigg, E. Cyclin-dependent protein kinases: key regulators of the eukaryotic cell cycle. *Bioessays* **17,** 471–480 (1995).

16. Hoeijmakers, J. H. J. Genome maintenance mechanisms for preventing cancer. *Nature* **411,** 366–374 (2001).

17. Xu, J., Lamouille, S. & Derynck, R. TGF-B-induced epithelial to mesenchymal transition. *Cell Res.* **19,** 156–172 (2009).

18. White, E. & DiPaola, R. S. The double-edged sword of autophagy modulation in cancer. *Clin. Cancer Res.* **15,** 5308–5316 (2009).

19. Kim, N. W. *et al.* Specific Association of Human Telomerase Activity with Immortal Cells and Cancer Published by : American Association for the Advancement of Science Stable URL : http://www.jstor.org/stable/2885288 JSTOR is a not-for-profit service that helps scholars , re. *Science (80-.).* **266,** 2011–2015 (1994).

20. Colotta, F., Allavena, P., Sica, A., Garlanda, C. & Mantovani, A. Cancer-related inflammation, the seventh hallmark of cancer: Links to genetic instability. *Carcinogenesis* **30,** 1073–1081 (2009).

21. Mantovani, A. Cancer: Inflaming metastasis. *Nature* **457,** 36–37 (2009).

22. Tsai, M., Chang, W., Huang, M. & Kuo, P. Tumor Microenvironment : A New Treatment Target for Cancer. **2014,** (2014).

23. Vaupel, P., Rallinoâ, F. & Okunieff, P. Blood Flow , Oxygen and Nutrient Supply , and Metabolic Microenvironment Human Tumors : A Review. *Cancer Res* **49,** 6449–6465 (1989).

24. Brown, N. S. & Bicknell, R. Hypoxia and oxidative stress in breast cancer: Oxidative stress - its effects on the growth, metastatic potential and response to therapy of breast cancer. *Breast Cancer Res* **3,** 1–5 (2001).

25. GRAY, L. H., CONGER, A. D., EBERT, M., HORNSEY, S. & SCOTT, O. C. The concentration of oxygen dissolved in tissues at the time of irradiation as a factor in radiotherapy. *Br. J. Radiol.* **26,** 638–648 (1953).

26. Kato, Y. *et al.* Acidic extracellular microenvironment and cancer. *Cancer Cell Int.* **13,** 1–8 (2013).

27. Yabu, M. *et al.* IL-23-dependent and -independent enhancement pathways of IL-17A production by lactic acid. *Int. Immunol.* **23,** 29–41 (2011).

28. Vogelstein, B. & Kinzler, K. W. Cancer genes and the pathways they control. *Nat. Med.* **10,** 789–799 (2004).

29. Van Sluis, R. *et al.* In vivo imaging of extracellular pH using 1H MRSI. *Magn. Reson. Med.* **41,** 743–750 (1999).

30. Griffiths, J. R. Are cancer cells acidic? *Br. J. Cancer* **64,** 425–427 (1991).

31. Khandrika, L., Kumar, B., Koul, S., Maroni, P. & Koul, H. K. Oxidative stress in prostate cancer. *Cancer Lett.* **282,** 125–136 (2009).

32. Bergers, G. & Benjamin, L. E. Tumorigenesis and the angiogenic switch. *Nat. Rev. Cancer* **3,** 401–410 (2003).

33. Gazit, Y. *et al.* Fractal characteristics of tumor vascular architecture during tumor growth and regression. *Microcirculation* **4,** 395–402 (1997).

34. Dameron, K. M., Volpert, O. V, Tainsky, M. S. & Bouck, N. Control of angiogenesis in fibroblast by p53 regulation of thrombospondin. *Science (80-.).* **265,** 1582–1584 (1994).

35. Nishida, N., Yano, H., Nishida, T., Kamura, T. & Kojiro, M. Angiogenesis in cancer. *Vasc. Health Risk Manag.* **2,** 213–219 (2006).

36. Allen, T. M. & Cullis, P. R. Drug Delivery Systems: Entering the Mainstream. *Science (80-.).* **303,** 1818–1822 (2004).

37. Jain, R. K. Normalization of tumor vasculature : An emerging concept in angiogenic therapy. *Science (80-.).* **307,** 58–62 (2005).

38. Matsumura, Y. & Maeda, H. A new concept for macromolecular therapeutics in cnacer chemotherapy: mechanism of tumoritropic accumulatio of proteins and the antitumor agents Smancs. *Cancer Res.* **46,** 6387–6392 (1986).

39. Dong, X. & Mumper, R. J. Nanomedicinal strategies to treat multidrug-resistant tumors: Current progress. *Nanomedicine* **5,** 597–615 (2010).

40. Moorthi, C., Manavalan, R. & Kathiresan, K. Nanotherapeutics to overcome conventional cancer chemotherapy limitations. *J. Pharm. Pharm. Sci.* **14,** 67–77 (2011).

41. Riddick, D. S. *et al.* Cancer Chemotherapy and Drug Metabolsim. *Drug Metab. Dispos.* **33,** 1083–1096 (2005).

42. Berardi, R. *et al.* State of the art for cardiotoxicity due to chemotherapy and to targeted therapies: A literature review. *Crit. Rev. Oncol. Hematol.* **88,** 75–86 (2013).

43. Strebhardt, K. & Ullrich, A. Paul Ehrlich ' s magic bullet concept : 100 years of progress. *Nat. Rev. cancer* **8,** 473–480 (2008).

44. Schwartz, R. S. Paul Ehrlich 's Magic Bullets. *Blood* 1079–1080 (2004). doi:10.1056/NEJMp048021

45. Kola, I. & Landis, J. Can the pharmaceutical industry reduce attrition rates? *Nat. Rev. Drug Discov.* **3,** 1–5 (2004).

46. Desai, N. Challenges in Development of Nanoparticle-Based Therapeutics. *AAPS J.* **14,** 282–295 (2012).

47. Nishiyama, N. & Kataoka, K. Current state, achievements, and future prospects of polymeric micelles as nanocarriers for drug and gene delivery. *Pharmacol. Ther.* **112,** 630–648 (2006).

48. Liechty, W. B. & Peppas, N. A. Expert opinion: Responsive polymer nanoparticles in cancer therapy. *Eur. J. Pharm. Biopharm.* **80,** 241–246 (2012).

49. Mosqueira, V. C. *et al.* Biodistribution of long-circulationg PEG-grafted nanocapsules in mice: effects of PEG chain length and density. *Pharm. Res.* **18,** 1411–1419 (2001).

50. Farokhzad, O. C. & Langer, R. Impact of Nanotechnology on Drug\nDelivery. *ACS Nano* **3,** 16–20 (2009).

51. Brinkhuis, R. P., Rutjes, F. P. J. T. & Van Hest, J. C. M. Polymeric vesicles in biomedical applications. *Polym. Chem.* **2,** 1449–1462 (2011).

52. Hauert, S. & Bhatia, S. N. Mechanisms of cooperation in cancer nanomedicine: Towards systems nanotechnology. *Trends Biotechnol.* **32,** 448–455 (2014).

53. Qi, W., Ghoroghchian, P. P., Li, G., Hammer, D. A. & Therien, M. J. Aqueous self-assembly of poly(ethylene oxide)-block-poly(ε- caprolactone) (PEO-b-PCL) copolymers: Disparate diblock copolymer compositions give rise to nano- and meso-scale bilayered vesicles. *Nanoscale* **5,** 10908–10915 (2013).

54. Gentile, F. *et al.* The effect of shape on the margination dynamics of non-neutrally buoyant particles in two-dimensional shear flows. *J. Biomech.* **41,** 2312–2318 (2008).

55. Christian, D. A. *et al.* Flexible filaments for in vivo imaging and delivery: Persistent circulation of filomicelles opens the dosage window for sustained tumor shrinkage. *Mol. Pharm.* **6,** 1343–1352 (2009).

56. Owens, D. E. & Peppas, N. A. Opsonization, biodistribution, and pharmacokinetics of polymeric nanoparticles. *Int. J. Pharm.* **307,** 93–102 (2006).

57. Nel, A. E. *et al.* Understanding biophysicochemical interactions at the nano-bio interface. *Nat. Mater.* **8,** 543–557 (2009).

58. Jeon, S. I., Lee, J. H., Andrade, J. D. & De Gennes, P. G. Protein-surface interactions in the presence of polyethylene oxide. I. Simplified theory. *J. Colloid Interface Sci.* **142,** 149–158 (1991).

59. Bertrand, N., Wu, J., Xu, X., Kamaly, N. & Farokhzad, O. C. HHS Public Access. 2–25 (2015). doi:10.1016/j.addr.2013.11.009.Cancer

60. Saha, R. N., Vasanthakumar, S., Bende, G. & Snehalatha, M. Nanoparticulate drug delivery systems for cancer chemotherapy. *Mol. Membr. Biol.* (2010).

doi:10.3109/09687688.2010.510804

61. Allen, T. M. Ligand-targeted therapeutics in anticancer therapy. *Nat. Rev. Cancer* **2,** 750–763 (2002).

62. Byrne, J. D., Betancourt, T. & Brannon-Peppas, L. Active targeting schemes for nanoparticle systems in cancer therapeutics. *Adv. Drug Deliv. Rev.* **60,** 1615–1626 (2008).

63. Seymour, L. W. *et al.* Hepatic Drug Targeting: Phase I Evaluation of Polymer-Bound Doxorubicin. *J. Clin. Oncol.* **20,** 1668–1676 (2002).

64. Bae, Y. H. & Park, K. Targeted drug delivery to tumors: Myths, reality and possibility. *J. Control. Release* **153,** 198–205 (2011).

65. Irvine, D. J. Drug delivery: One nanoparticle, one kill. *Nat. Mater.* **10,** 342–343 (2011).

66. Warenius, H. M., Galfre, G., Bleehen, N. M. & Milstein, C. Attempted targeting of a monoclonal antibody in a human tumour xenograft system. *Eur. J. Cancer Clin. Oncol.* **17,** 1009–1015 (1981).

67. Mellman, I. ENDOCYTOSIS AND MOLECULAR SORTING. *Annu. Rev. Cell Dev. Biol.* **12,** 575–625 (1996).

68. Onaca, O., Enea, R., Hughes, D. W. & Meier, W. Stimuli-responsive polymersomes as nanocarriers for drug and gene delivery. *Macromol. Biosci.* **9,** 129–139 (2009).

69. Pearson, R. T., Warren, N. J., Lewis, A. L., Armes, S. P. & Battaglia, G. Effect of pH and temperature on PMPC-PDPA copolymer self-assembly. *Macromolecules* **46,** 1400–1407 (2013).

70. Duncan, R. The dawning era of polymer therapeutics. *Nat. Rev. Drug Discov.* **2,** 347–360 (2003).

71. Li, Y. *et al.* Well-defined, reversible disulfide cross-linked micelles for on-demand paclitaxel delivery. *Biomaterials* **32,** 6633–6645 (2011).

72. Mabrouk, E., Cuvelier, D., Brochard-Wyart, F., Nassoy, P. & Li, M.-H. Bursting of sensitive polymersomes induced by curling. *Proc. Natl. Acad. Sci.* **106,** 7294–7298 (2009).

73. Soyez, H., Schacht, E. & Vanderkerken, S. The crucial role of spacer groups in macromolecular prodrug design. *Adv. Drug Deliv. Rev.* **21,** 81–106 (1996).

74. Jatzkewitz, H. An ein kolloidales Blutplasma-Ersatzmittel (Polyvinylpyrrolidon) gebundenes Peptamin (Glycyl-L-leucyl-mezcalin) als neuartige Depotform für biologisch aktive primäre Amine (Mezcalin). *Zeitschrift fur Naturforsch. - Sect. B J. Chem. Sci.* **10,** 27–31 (1955).

75. Ringsdorf, H. Structure and properties of pharmacologically active polymers. *J. Polym.*

Sci. Polym. Symp. **51,** 135–153 (2007).

76. Ulbrich, K. *et al.* Polymeric anticancer drugs with pH-controlled activation. *Int. J. Pharm.* **277,** 63–72 (2004).

77. Bell, C. L. & Peppas, N. A. Biomedical membranes from hydrogels and interpolymer complexes. in *Biopolymers II* (eds. Peppas, N. A. & Langer, R. S.) 125–175 (Springer Berlin Heidelberg, 1995).

78. Zhao, W., Gnanou, Y. & Hadjichristidis, N. Fast and Living Ring-Opening Polymerization of α-Amino Acid N-Carboxyanhydrides Triggered by an 'Alliance' of Primary and Secondary Amines at Room Temperature. *Biomacromolecules* **16,** 1352–1357 (2015).

79. Li, C. Poly(L-glutamic acid)-anticancer drug conjugates. *Adv. Drug Deliv. Rev.* **54,** 695–713 (2002).

80. Li, C. *et al.* Antitumor Activity of Poly (l-glutamic acid) -Paclitaxel on Syngeneic and Xenografted Tumors. *Clin. Cancer Res.* **5,** 891–897 (1999).

81. Uhrich, K. E., Cannizzaro, S. M., Langer, R. S. & Shakesheff, K. M. Polymeric Systems for Controlled Drug Release. *Chem. Rev.* **99,** 3181–3198 (1999).

82. Yoo, H. S., Lee, K. H., Oh, J. E. & Park, T. G. In vitro and in vivo anti-tumor activities of nanoparticles based on doxorubicin-PLGA conjugates. *J. Control. Release* **68,** 419–431 (2000).

83. Chen, B. *et al.* Synthesis and properties of star-comb polymers and their doxorubicin conjugates. *Bioconjug. Chem.* **22,** 617–624 (2011).

84. Lee, J., Cho, E. C. & Cho, K. Incorporation and release behavior of hydrophobic drug in functionalized poly(D,L-lactide)-block-poly(ethylene oxide) micelles. *J. Control. Release* **94,** 323–335 (2004).

85. Owen, S. C., Chan, D. P. Y. & Shoichet, M. S. Polymeric micelle stability. *Nano Today* **7,** 53–65 (2012).

86. Sezgin, Z., Yüksel, N. & Baykara, T. Preparation and characterization of polymeric micelles for solubilization of poorly soluble anticancer drugs. *Eur. J. Pharm. Biopharm.* **64,** 261–268 (2006).

87. Soussan, E., Cassel, S., Blanzat, M. & Rico-Lattes, I. Drug delivery by soft matter: Matrix and vesicular carriers. *Angew. Chemie - Int. Ed.* **48,** 274–288 (2009).

88. Gaucher, G. *et al.* Block copolymer micelles: Preparation, characterization and application in drug delivery. *J. Control. Release* **109,** 169–188 (2005).

89. Kataoka, K., Harada, A. & Nagasaki, Y. Block copolymer micelles for drug delivery: Design, characterization and biological significance. *Adv. Drug Deliv. Rev.* **47,** 113–131

(2001).

90. Dowling, K. C. & Thomas, J. K. A Novel Micellar Synthesis and Photophysical Characterization of Water-Soluble Acrylamide-Styrene Block Copolymers. *Macromolecules* **23,** 1059–1064 (1990).

91. Bash, E. Modeling of the Self-Assembly of Block Copolymers in Selective Solvent. *PhD Propos.* **1,** 13–40 (2015).

92. Riess, G. Micellization of block copolymers. *Prog. Polym. Sci.* **28,** 1107–1170 (2003).

93. Kalyanasundaram, K. & Thomas, J. K. Environmental Effects on Vibronic Band Intensities in Pyrene Monomer Fluorescence and Their Application in Studies of Micellar Systems. *J. Am. Chem. Soc.* **99,** 2039–2044 (1977).

94. Matsumura, Y. *et al.* Phase I clinical trial and pharmacokinetic evaluation of NK911, a micelle-encapsulated doxorubicin. *Br. J. Cancer* **91,** 1775–1781 (2004).

95. Nakanishi, T. *et al.* Development of the polymer micelle carrier system for doxorubicin. *J. Control. Release* **74,** 295–302 (2001).

96. Nishiyama, N., Kato, Y., Sugiyama, Y. & Kataoka, K. Complex Micelle with Time-Modulated Decaying Property as a Novel Drug Delivery System. *Pharm. Res.* **18,** 1035–1041 (2001).

97. Nishiyama, N., Bae, Y., Miyata, K., Fukushima, S. & Kataoka, K. Smart polymeric micelles for gene and drug delivery. *Drug Discov. Today Technol.* **2,** 21–26 (2005).

98. Bae, Y. *et al.* Preparation and Biological Characterization of Polymeric Micelle Drug Carriers with Intracellular pH-Triggered Drug Release Property: Tumor Permeability, Controlled Subcellular Drug Distribution, and Enhanced in Vivo Antitumor Efficacy. *Bioconjug. Chem.* **16,** 122–130 (2005).

99. Bae, Y., Jang, W. D., Nishiyama, N., Fukushima, S. & Kataoka, K. Multifunctional polymeric micelles with folate-mediated cancer cell targeting and pH-triggered drug releasing properties for active intracellular drug delivery. *Mol. Biosyst.* **1,** 242–250 (2005).

100. Kulthe, S. S. *et al.* Mixed micelle formation with hydrophobic and hydrophilic Pluronic block copolymers: Implications for controlled and targeted drug delivery. *Colloids Surfaces B Biointerfaces* **88,** 691–696 (2011).

101. Mura, S., Nicolas, J. & Couvreur, P. Stimuli-responsive nanocarriers for drug delivery. *Nature Materials* (2013). doi:10.1038/nmat3776

102. Beyer, U. *et al.* Synthesis and in vitro efficacy of transferrin conjugates of the anticancer drug chlorambucil. *J. Med. Chem.* (1998). doi:10.1021/jm9704661

103. Gillies, E. R., Jonsson, T. B. & Fréchet, J. M. J. Stimuli-responsive supramolecular

assemblies of linear-dendritic copolymers. *J. Am. Chem. Soc.* (2004). doi:10.1021/ja0463738

104. Toncheva, V., Schacht, E., Ng, S. Y., Barr, J. & Heller, J. Use of block copolymers of poly(ortho esters) and poly (ethylene glycol) micellar carriers as potential tumour targeting systems. *J. Drug Target.* (2003). doi:10.1080/10611860310001633839

105. Heffernan, M. J. & Murthy, N. Polyketal nanoparticles: A new pH-sensitive biodegradable drug delivery vehicle. *Bioconjug. Chem.* (2005). doi:10.1021/bc050176w

106. Patel, V. F. *et al.* Novel acid labile COL1 trityl-linked difluoronucleoside immunoconjugates: Synthesis, characterization, and biological activity. *Bioconjug. Chem.* (1996). doi:10.1021/bc960038u

107. Ling, J. & Huang, Y. Understanding the ring-opening reaction of ??-amino acid N-carboxyanhydride in an amine-mediated living polymerization: A DFT study. *Macromol. Chem. Phys.* **211,** 1708–1711 (2010).

108. Lu, H. & Cheng, J. Hexamethyldisilazane-mediated controlled polymerization of ??-amino acid N-carboxyanhydrides. *J. Am. Chem. Soc.* **129,** 14114–14115 (2007).

109. Deng, C. *et al.* Functional polypeptide and hybrid materials: Precision synthesis via α-amino acid N-carboxyanhydride polymerization and emerging biomedical applications. *Prog. Polym. Sci.* **39,** 330–364 (2014).

110. Kricheldorf, H. R. Polypeptides and 100 years of chemistry of α-amino acid N-carboxyanhydrides. *Angew. Chemie - Int. Ed.* **45,** 5752–5784 (2006).

111. Hadjichristidis, N., Iatrou, H., Pitsikalis, M. & Sakellariou, G. Synthesis of Well-Defined Polypeptide-Based Materials via the Ring-Opening Polymerization of r -Amino Acid N -Carboxyanhydrides. *Chem. Rev.* **109,** 5528–5578 (2009).

112. L-phenylalanine, D., L-lysine-, D., Cardinaux, F., Howard, J. C. & Taylor, G. T. Block Copolymers of Amino Acids . I . Synthesis. **16,** 2005–2028 (2005).

113. Lu, H. *et al.* Recent advances in amino acid N-carboxyanhydrides and synthetic polypeptides: Chemistry, self-assembly and biological applications. *Chem. Commun.* **50,** 139–155 (2014).

114. Weiss, R. B. The anthracyclines: will we ever find a better doxorubicin? *Semin. Oncol.* (1992). doi:10.5555/uri:pii:009377549290036Z

115. Minotti, G. Anthracyclines: Molecular Advances and Pharmacologic Developments in Antitumor Activity and Cardiotoxicity. *Pharmacol. Rev.* **56,** 185–229 (2004).

116. Cortés-Funes, H. & Coronado, C. Role of anthracyclines in the era of targeted therapy. *Cardiovasc. Toxicol.* **7,** 56–60 (2007).

117. Weiss, R. B., Sarosy, G., Clagett-Carr, K., Russo, M. & Leyland-Jones, B. Anthracycline

analogs The past, present, and future. *Cancer Chemother. Pharmacol.* **18,** 185–197 (1986).

118. Deng, S. & Wojnowski, L. Genotyping the risk of anthracycline-induced cardiotoxicity. *Cardiovasc. Toxicol.* **7,** 129–134 (2007).

119. Bae, Y. & Kataoka, K. Intelligent polymeric micelles from functional poly(ethylene glycol)-poly(amino acid) block copolymers. *Adv. Drug Deliv. Rev.* **61,** 768–784 (2009).

120. Deng, C., Jiang, Y., Cheng, R., Meng, F. & Zhong, Z. Biodegradable polymeric micelles for targeted and controlled anticancer drug delivery: Promises, progress and prospects. *Nano Today* (2012). doi:10.1016/j.nantod.2012.08.005

121. Kato, K. *et al.* Phase II study of NK105, a paclitaxel-incorporating micellar nanoparticle, for previously treated advanced or recurrent gastric cancer. *Invest. New Drugs* (2012). doi:10.1007/s10637-011-9709-2

122. Hamaguchi, T. *et al.* NK105, a paclitaxel-incorporating micellar nanoparticle formulation, can extend in vivo antitumour activity and reduce the neurotoxicity of paclitaxel. *Br. J. Cancer* (2005). doi:10.1038/sj.bjc.6602479

123. Burris, H. A. *et al.* A phase I dose escalation study of NK012, an SN-38 incorporating macromolecular polymeric micelle. *Cancer Chemother. Pharmacol.* (2016). doi:10.1007/s00280-016-2986-x

124. Matsumura, Y. Preclinical and clinical studies of NK012, an SN-38-incorporating polymeric micelles, which is designed based on EPR effect. *Advanced Drug Delivery Reviews* (2011). doi:10.1016/j.addr.2010.05.008

125. Saltz, L. B. *et al.* Irinotecan plus Fluorouracil and Leucovorin for Metastatic Colorectal Cancer. *N. Engl. J. Med.* (2000). doi:10.1056/NEJM200009283431302

126. Lavasanifar, A., Samuel, J. & Kwon, G. S. Poly(ethylene oxide)-block-poly(L-amino acid) micelles for drug delivery. *Adv. Drug Deliv. Rev.* (2002). doi:10.1016/S0169-409X(02)00015-7

127. Kim, T. Y. *et al.* Phase I and pharmacokinetic study of Genexol-PM, a Cremophor-free, polymeric micelle-formulated paclitaxel, in patients with advanced malignancies. *Clin. Cancer Res.* (2004). doi:10.1158/1078-0432.CCR-03-0655

128. Pillai, G. Nanomedicines for Cancer Therapy : An Update of FDA Approved and Those under Various Stages of Development. *SOJ Pharm Pharm Sci* (2014). doi:10.15226/2374-6866/1/2/00109

129. Knop, K., Hoogenboom, R., Fischer, D. & Schubert, U. S. Poly(ethylene glycol) in drug delivery: Pros and cons as well as potential alternatives. *Angewandte Chemie - International Edition* (2010). doi:10.1002/anie.200902672

130. Egusquiaguirre, S. P., Igartua, M., Hernández, R. M. & Pedraz, J. L. Nanoparticle

delivery systems for cancer therapy: Advances in clinical and preclinical research. *Clinical and Translational Oncology* (2012). doi:10.1007/s12094-012-0766-6

131. Bajaj, I. & Singhal, R. Poly (glutamic acid) - An emerging biopolymer of commercial interest. *Bioresource Technology* (2011). doi:10.1016/j.biortech.2011.02.047

132. Hoes, C. J. T. *et al.* Optimization of macromolecular prodrugs of the antitumor antibiotic adriamycin. *J. Control. Release* (1985). doi:10.1016/0168-3659(85)90046-X

133. van Heeswijk, W. A. R. *et al.* The synthesis and characterization of polypeptide-adriamycin conjugates and its complexes with adriamycin. Part I. *J. Control. Release* (1985). doi:10.1016/0168-3659(85)90006-9

134. Sims, G. E. C. & Snape, T. J. A Method for the Estimation of Polyethylene Glycol in Plasma Protein Fractions.pdf. *J. Anal. Biochem.* **107,** 60–63 (1980).

135. Snyder, S. L. & Sobocinski, P. Z. An improved 2,4,6-trinitrobenzenesulfonic acid method for the determination of amines. *Anal. Biochem.* **64,** 284–288 (1975).

136. Markland, P., Amidon, G. L. & Yang, V. C. Modified polypeptides containing γ-benzyl glutamic acid as drug delivery platforms. *Int. J. Pharm.* **178,** 183–192 (1999).

137. Williams, A. J. & Gupta, V. K. Self-assembly of a rodlike polypeptide on solid surfaces: Role of solvent, molecular weight, and time of assembly. *J. Phys. Chem. B* **105,** 5223–5230 (2001).

138. Smeets, N. M. B., Van Der Weide, P. L. J., Meuldijk, J., Vekemans, J. A. J. M. & Hulshof, L. A. A scalable synthesis of L-leucine-N-carboxyanhydride. *Org. Process Res. Dev.* **9,** 757–763 (2005).

139. Ambrosio, E. *et al.* A novel combined strategy for the physical PEGylation of polypeptides. *J. Control. Release* **226,** 35–46 (2016).

140. Piñeiro, L., Novo, M. & Al-Soufi, W. Fluorescence emission of pyrene in surfactant solutions. *Adv. Colloid Interface Sci.* **215,** 1–12 (2015).

141. Aguiar, J., Carpena, P., Molina-Bolívar, J. A. & Carnero Ruiz, C. On the determination of the critical micelle concentration by the pyrene 1:3 ratio method. *J. Colloid Interface Sci.* **258,** 116–122 (2003).

142. Hansen, M. B., Nielsen, S. E. & Berg, K. Re-examination and further development of a precise and rapid dye method for measuring cell growth/cell kill. *J. Immunol. Methods* **119,** 203–210 (1989).

143. Bastiancich, C. *et al.* Lauroyl-gemcitabine-loaded lipid nanocapsule hydrogel for the treatment of glioblastoma. *J. Control. Release* **225,** 283–293 (2016).

144. Dondoni, A. The emergence of thiol-ene coupling as a click process for materials and bioorganic chemistry. *Angew. Chemie - Int. Ed.* **47,** 8995–8997 (2008).

145. Mijangos, I. *et al.* Influence of initiator and different polymerisation conditions on performance of molecularly imprinted polymers. *Biosens. Bioelectron.* **22,** 381–387 (2006).

146. Arroyo-Crespo, J. J. *et al.* Anticancer Activity Driven by Drug Linker Modification in a Polyglutamic Acid-Based Combination-Drug Conjugate. *Adv. Funct. Mater.* **28,** (2018).

147. Lee, J. S. & Feijen, J. Polymersomes for drug delivery: Design, formation and characterization. *J. Control. Release* **161,** 473–483 (2012).

148. Scomparin, A., Salmaso, S., Bersani, S., Satchi-Fainaro, R. & Caliceti, P. Novel folated and non-folated pullulan bioconjugates for anticancer drug delivery. *Eur. J. Pharm. Sci.* **42,** 547–558 (2011).

149. Zagorodko, O., Arroyo-Crespo, J. J., Nebot, V. J. & Vicent, M. J. Polypeptide-Based Conjugates as Therapeutics: Opportunities and Challenges. *Macromol. Biosci.* **17,** 1–22 (2017).

150. Danhier, F., Feron, O. & Préat, V. To exploit the tumor microenvironment: Passive and active tumor targeting of nanocarriers for anti-cancer drug delivery. *J. Control. Release* **148,** 135–146 (2010).

151. Torchilin, V. Tumor delivery of macromolecular drugs based on the EPR effect. *Adv. Drug Deliv. Rev.* **63,** 131–135 (2011).

152. Nivaggioli, T., Alexandridis, P., Hatton, T. A., Yekta, A. & Winnik, M. A. Fluorescence Probe Studies of Pluronic Copolymer Solutions as a Function of Temperature. *Langmuir* **11,** 730–737 (1995).

153. Vega, J. *et al.* Targeting doxorubicin to epidermal growth factor receptors by site-specific conjugation of C225 to poly(L-glutamic acid) through a polyethylene glycol spacer. *Pharm. Res.* **20,** 826–832 (2003).

154. Wang, Y. *et al.* The effect of linkers on the self-assembling and anti-tumor efficacy of disulfide-linked doxorubicin drug-drug conjugate nanoparticles. *J. Control. Release* **279,** 136–146 (2018).

155. Markovsky, E., Baabur-Cohen, H. & Satchi-Fainaro, R. Anticancer polymeric nanomedicine bearing synergistic drug combination is superior to a mixture of individually-conjugated drugs. *J. Control. Release* **187,** 145–157 (2014).

156. Xu, H. *et al.* Amphiphilic poly(amino acid) based micelles applied to drug delivery: The in vitro and in vivo challenges and the corresponding potential strategies. *J. Control. Release* **199,** 84–97 (2015).

157. Li, M. *et al.* Nanoscaled poly(l-glutamic acid)/doxorubicin-amphiphile complex as pH-responsive drug delivery system for effective treatment of nonsmall cell lung cancer. *ACS Appl. Mater. Interfaces* **5,** 1781–1792 (2013).

158. Valero, V. *et al.* Phase II trial of docetaxel: a new, highly effective antineoplastic agent in the management of patients with anthracycline-resistant metastatic breast cancer. *J. Clin. Oncol.* **13,** 2886–2894 (1995).

159. Lao, J. *et al.* Liposomal Doxorubicin in the treatment of breast cancer patients: a review. *J. Drug Deliv.* **2013,** 456–409 (2013).

160. Lovitt, C. J., Shelper, T. B. & Avery, V. M. Doxorubicin resistance in breast cancer cells is mediated by extracellular matrix proteins. *BMC Cancer* **18,** 41 (2018).

161. Balasso, A. *et al.* Re-programming pullulan for targeting and controlled release of doxorubicin to the hepatocellular carcinoma cells. *Eur. J. Pharm. Sci.* **103,** 104–115 (2017).

162. Lv, S. *et al.* Doxorubicin-loaded amphiphilic polypeptide-based nanoparticles as an efficient drug delivery system for cancer therapy. *Acta Biomater.* **9,** 9330–9342 (2013).

163. Lammers, T. *et al.* Effect of Intratumoral Injection on the Biodistribution, the Therapeutic Potential of HPMA Copolymer-Based Drug Delivery Systems. *Neoplasia* **8,** 788–795 (2006).

164. Ren, S. *et al.* Comparison of pharmacokinetics, tissue distribution and pharmacodynamics of liposomal and free doxorubicin in tumour-bearing mice following intratumoral injection. *J. Pharm. Pharmacol.* **66,** 1231–1239 (2014).

165. Pulaski, B. a & Ostrand-Rosenberg, S. Mouse 4T1 breast tumor model. *Curr. Protoc. Immunol.* **Chapter 20,** Unit 20.2 (2001).

166. Tejada-Berges, T., Granai, C. O., Gordinier, M. & Gajewski, W. Caelyx/Doxil for the treatment of metastatic ovarian and breast cancer. *Expert Rev. Anticancer Ther.* **2,** 143–150 (2002).

167. O'Brien, M. E. R. *et al.* Reduced cardiotoxicity and comparable efficacy in a phase III trial of pegylated liposomal doxorubicin HCl (CAELYX^{TM}/Doxil®) versus conventional doxorubicin for first-line treatment of metastatic breast cancer. *Ann. Oncol.* **15,** 440–449 (2004).